UNCLASSIFIED

WAPD-127
Part III

Metallurgy and Ceramics
(M-3679, 18th Edition)

CLASSIFICATION CANCELLED
DATE 3/7/57
For The Atomic Energy Commission
H. A. Carell
Chief, Declassification Branch

DEVELOPMENT AND PROPERTIES OF URANIUM-BASE ALLOYS CORROSION RESISTANT IN HIGH TEMPERATURE WATER

Part III - Corrosion Mechanism of Uranium-Base Alloys in High Temperature Water

Edited
by

M. W. Burkart

Contract AT-11-1-GEN-14

LEGAL NOTICE

This report was prepared as an account of Government sponsored work. Neither the United States, nor the Commission, nor any person acting on behalf of the Commission:

A. Makes any warranty or representation, express or implied, with respect to the accuracy, completeness, or usefulness of the information contained in this report, or that the use of any information, apparatus, method, or process disclosed in this report may not infringe privately owned rights; or

B. Assumes any liabilities with respect to the use of, or for damages resulting from the use of any information, apparatus, method, or process disclosed in this report.

As used in the above, "person acting on behalf of the Commission" includes any employee or contractor of the Commission to the extent that such employee or contractor prepares, handles or distributes, or provides access to, any information pursuant to his employment or contract with the Commission.

Price $ 0.70

Available from the
Office of Technical Services
Department of Commerce
Washington 25, D. C.

BETTIS PLANT PITTSBURGH, PA.
Operated for the U. S. Atomic Energy Commission by
Westinghouse Electric Corporation

UNCLASSIFIED

DISCLAIMER

This report was prepared as an account of work sponsored by an agency of the United States Government. Neither the United States Government nor any agency Thereof, nor any of their employees, makes any warranty, express or implied, or assumes any legal liability or responsibility for the accuracy, completeness, or usefulness of any information, apparatus, product, or process disclosed, or represents that its use would not infringe privately owned rights. Reference herein to any specific commercial product, process, or service by trade name, trademark, manufacturer, or otherwise does not necessarily constitute or imply its endorsement, recommendation, or favoring by the United States Government or any agency thereof. The views and opinions of authors expressed herein do not necessarily state or reflect those of the United States Government or any agency thereof.

DISCLAIMER

Portions of this document may be illegible in electronic image products. Images are produced from the best available original document.

The experimental work described in this report was performed by

W. E. Bond
W. A. Bostrom
R. F. Boyle
M. W. Burkart
F. M. Cain, Jr.
I. Cohen
E. K. Halteman
R. D. Leggett
T. R. Padden
A. B. Rothman
R. A. Wolfe

TABLE OF CONTENTS

Page

PREFACE 0

I. INTRODUCTION 11

II. CORROSION TESTING OF BARE SAMPLES 13

A. Physical Changes During Corrosion 13

B. Identification of the Corrosion-Induced Precipitate 15
1. Evidence in Support of a UH_3 Precipitate 15
a. X-ray Diffraction 16
b. Electron Diffraction 16
c. Magnetic Measurements 16
d. Thermodynamic Evidence 16
2. Evidence in Conflict with a UH_3 Precipitate 18
a. Neutron Diffraction 18
b. Chemical Analysis and Density 18
c. X-ray Diffraction 19
d. Dissociation Pressure 19
e. Phase Distribution 20
3. Other Properties of the Precipitated Phase 20
a. Metallography and Hardness 20
b. Reaction with Molecular Hydrogen 21
c. Behavior on Annealing 22
d. Effect of Stress 22
4. Corrosion Mechanism of Uranium-Base Alloys 22

C. Fuel Life in Terms of Factors Affecting Corrosion-Induced Precipitation 25
1. Thermodynamic Phase of the Alloy 26
a. Alpha 26
b. Alpha Plus Epsilon 26
c. Gamma 26
d. Epsilon 26
e. Distorted Alpha 27
2. Heat Treatment 27
a. Homogenization 27
b. Low Temperature Annealing of Uranium-Molybdenum Alloys 29
c. Grain Size 31
d. Atmosphere 31
3. Effect of Alloy Composition 31
a. Effects of Small Alloy Additions of Cu, W, and Zr 32
b. Influence of Small Additions of Cr and Ti on the Corrosion Properties of U-Mo Binary Alloys 32
c. Influence of Platinum Additions to U-Mo Alloys 34
4. Corrosion Medium 35
a. Effect of Hydrogen and Oxygen Additions to the Test Water 35
b. Effect of Platinum and Nickel Ion Additions 36

Page

5. Effect of Temperature 37
6. Effect of Stress 37

D. Summary of Corrosion Testing of Bare Specimens 38

III. CORROSION TESTING OF ZIRCALOY-CLAD SPECIMENS 39

IV. CALCULATED LIFE OF A ZIRCALOY-CLAD URANIUM ALLOY FUEL ELEMENT 41

V. SUMMARY AND CONCLUSIONS 44

VI. REFERENCES 46

APPENDIX 47

TABLES 49

FIGURES 59

DECLASSIFIED

PART III - CORROSION MECHANISM OF URANIUM-BASE ALLOYS IN HIGH TEMPERATURE WATER

PREFACE

This report is Part III of a series describing the development program of a fuel alloy for the Pressurized Water Reactor at Bettis Plant. Parts I and II dealt with the physical properties, effect of fabrication, and corrosion resistance of bare and clad uranium-base alloys, respectively. This report supplements the previous two in the series and describes in more detail the various factors influencing the mechanism of corrosion of uranium-base alloys. The fourth and final report of the series, Part IV - Radiation Stability of Uranium-Base Alloys, will be concerned with irradiation-induced effects observed in the most promising alloys described in the first three parts of this series.

In addition to the above series of four reports, several topical reports or scientific papers were issued describing separate phases of the development work performed at Bettis Plant. Also, as indicated in Part I, it was necessary to enlist the aid of other laboratories to expedite completion of selected phases of the development work. This was done either through subcontracts sponsored by Bettis Plant or through research sponsored directly by the Reactor Development and Engineering Divisions of the Atomic Energy Commission. The work performed by these laboratories is covered in separate topical and final reports, referred to but not discussed in detail in Parts I through III. For the sake of completeness and for easy reference, these reports are listed as an appendix to this report.

I. INTRODUCTION

An attempt will be made in this report to provide some insight into the corrosion mechanism of uranium-base alloys in high temperature water--the intent being to explain the observed corrosion behavior of Zircaloy-clad, uranium alloy fuel elements. For this purpose, however, it is necessary to consider the corrosion of both bare and clad specimens. The first half of this report describes the experiments conducted with bare samples and is concerned with the corrosion of uranium alloys in high temperature water. The effect of cladding is then considered and, finally, this information is correlated with the behavior of clad fuel rods.

During corrosion of bare gamma-phase uranium specimens, two distinct processes are observed. In the first process a smooth oxide scale is formed on the metal surface which continually flakes off during exposure and results in a uniform weight loss of the specimen. The protective oxide is present as a thin, adherent layer whose thickness remains approximately constant throughout the corrosion test. As the metal oxidizes during corrosion, a nonadherent layer is built up on this film and continually sloughs off.

Coincident with the uniform corrosion just mentioned, another process occurs which eventually leads to failure of the metal by cracking and general disintegration. The failure takes place during a relatively short period of time compared to the total exposure. To distinguish this type of failure from the uniform corrosion, the cracking or disintegration of the metal will be referred to as "discontinuous failure."

Metallographic examination of corrosion specimens reveals that the onset of discontinuous failure is always preceded by the formation of a plate-like second phase in the gamma uranium matrix. It is believed that discontinuous failure is intimately associated with this precipitated plate-like phase. The U-3.8 w/o Si alloys consisting wholly of the epsilon phase and the low alloy-content alpha prime alloys do not exhibit the corrosion-induced precipitation and are not subject to this type of failure. During the course of this investigation it was found that the discontinuous failure is sensitive to heat treatment, alloying additions, and water additions. These effects will be described in the section on the corrosion testing of bare specimens.

Clad specimens produced by the co-extrusion of the fuel alloy with Zircaloy are also susceptible to discontinuous failure when tested with intentional cladding defects. It appears that, apart from its role as a barrier between fuel and water, zirconium cladding provides an additional benefit as a consequence of the hydrogen-gettering property of the zirconium which inhibits precipitation of the second phase.

The corrosion life of the clad alloys is also very sensitive to the quality of the bond between the fuel and cladding. Poor quality may be a result of incomplete bonding or the formation of a corrosion-susceptible diffusion layer. In the case of incomplete bonding, the presence of an extensive unbonded interface plus a cladding defect renders the fuel susceptible to attack over a large area. The subsequent formation of UO_2 with its accompanying increase in volume causes the cladding to rupture. A similar but more rapid mode of failure would occur if a corrosion-susceptible layer were present. The layer may form by diffusion between the Zircaloy and the fuel during heat treatment or, in the case of U_3Si, during

extrusion. Failures of this type have already been discussed in WAPD-127, Part II. Section III of this report assumes a well bonded cladding with no corrodible diffusion layer and will be concerned only with the discontinuous failure of clad fuel rods.

DECLASSIFIED

II. THE CORROSION TESTING OF BARE SAMPLES

As stated previously, the corrosion behavior of bare uranium alloys will be described in order to formulate a mechanism that may be applied to clad fuel rods. Many uranium-base alloys were investigated during the course of this program, but, in view of the favorable properties described in Part I, most of the work has been concerned with the corrosion of gamma-phase uranium alloys containing molybdenum or niobium as the main alloying constitutent. The corrosion experiments with these alloys are described in the following sections.

A. Physical Changes During Corrosion

The corrosion behavior typical of a bare gamma uranium alloy is shown in Fig. 1. This specimen was a U-12 w/o Mo alloy tested in pressurized degassed water at 650°F. The corrosion rate was practically constant at 0.28 mg/cm^2-hr or increased slightly until about 15 to 20 days of exposure. At this point the onset of discontinuous failure occurred in this particular sample, and the specimen soon began to crack and disintegrate, increasing the exposed surface area which resulted in an increased rate of weight loss. The observed changes in corrosion rate may be either gradual or sudden. For the specimen sizes and geometry used in the experiments reported in Part I, about 10% of the specimen was consumed by general attack before discontinuous failure occurred. Macroscopic and microscopic photographs of a U-9 w/o Mo specimen that failed by cracking are shown in Figs. 2, 3, and 4. In Fig. 4 the presence of a plate-like precipitate can readily be seen. Metallographic examination of corrosion specimens reveals that the onset of discontinuous failure is always preceded by the formation of a plate-like second phase in the gamma uranium matrix. The microstructure of a corrosion specimen removed from test before discontinuous failure is illustrated in Fig. 5 and may be compared to its structure prior to testing in Fig. 6. The microstructures show the existence of continuous paths of precipitate through the metal.

Hydrogen analyses of specimens periodically withdrawn from corrosion test reveal that the hydrogen concentration of the alloy increases with exposure to the high temperature water as shown in Fig. 7. The hydrogen is available as a corrosion product resulting from the formation of UO_2 by the reaction of the alloy with water. As will be shown later, about 20% of the hydrogen released by this reaction is absorbed in the gamma-phase matrix. Specimens analyzed just prior to discontinuous failure contained as much as 1200 ppm of hydrogen, whereas the plate-like phase appears to precipitate out at a hydrogen concentration between 10 and 25 ppm. The pickup of hydrogen is fairly uniform throughout the specimen, although after short exposures enrichment of the hydride phase may be observed at the surface. In Fig. 7 it can be seen that the rate of hydrogen pickup is unaffected by removal of the surface layer after each test period, indicating that the absorption of hydrogen is not controlled by the solution of a surface hydride film but, rather, that it occurs by direct solution of hydrogen. The observed increase in hydrogen content prior to and during the formation of the plate-like precipitate suggests that this constituent may be a hydride of uranium. Additional evidence linking the identity of this phase to a hydride is that it can be removed by vacuum annealing at temperatures of 300°C and above. Decomposition products of the gamma transformation would certainly not dissolve at such temperatures, nor could other likely products of corrosion such as oxides be dissipated at any of the test temperatures.

UNCLASSIFIED

The precipitation and growth of the second phase during corrosion are accompanied by an increase in hardness as shown in Fig. 8. The hardness increase results from the dispersion of the harder precipitated phase and also from the strain hardening of the gamma-phase matrix due to the lower density of the precipitate.

The hydrogen-rich phase appears to precipitate first in the grain boundaries. Subsequently the plates form at the grain boundary and grow edgewise into the grain, eventually traversing it. Precipitation within a grain occurs on the {100} planes of the gamma uranium matrix. The plates may also originate within a grain or on a plate already formed. Such behavior is probably a function of the concentration and rate of diffusion of hydrogen. In this manner a continuous path of the hydrogen-rich material is formed throughout the metal. In those cases where growth of the plates has been inhibited by heat treatment or alloying an appreciable increase in life has been observed before the onset of discontinuous failure. A similar increase in life is observed when the hydrogen-rich phase is caused to precipitate, or combine with the alpha phase in a spheroidal form, so that it does not form a continuous network.

The corrosion susceptibility of the hydrogen-rich phase is somewhat greater than that of the gamma matrix, and the corrosive attack occurs preferentially along the continuous paths of precipitate. The attack is then both transgranular and intergranular. In addition to providing a corrosion susceptible path through the metal, the growth of the hydrogen-rich phase accelerates the corrosion process. Because of the lower density of the precipitate, the surrounding matrix is highly stressed and subject to the formation and propagation of cracks at the ends of the precipitated plates. Thus the metal is both embrittled and rendered susceptible to stress corrosion. Subsequent corrosion of the hydrogen-rich phase results in the formation of uranium dioxide of even lower density. Apparently the formation of the hydrogen-rich phase is not sufficient in itself to cause cracking of the metal since continuous networks of the precipitated phase have been observed both in cathodically hydrided and corroded specimens that were not cracked. However, oxidation of the hydrogen-rich phase through corrosion undoubtedly results in crack propagation. There also exists the possibility of stress-accelerated decomposition of the gamma phase at the edges of the growing plates or cracks, resulting in the formation of more corrodible phases. The structure appearing at the leading edges of the cracks in Fig. 3 may be evidence of such an effect. Stress-accelerated decomposition of the gamma phase may be noted in the serrated stress-strain curve of the U-12% w/o Mo alloy at 500°F as shown in Fig. 9. The corrosion of the hydrogen-rich phase has the appearance of "oxide fingers" growing into the metal along the paths of precipitate. Microstructures illustrating this phase of the corrosion process are shown in Figs. 3 and 10. The growth of these "fingers" results in cracking and failure of the metal.

Extrapolation of the uniform weight loss curves during general corrosion indicates that these alloys would have a satisfactory corrosion life for use in the reactor were it not for the occurrence of discontinuous failure. Since that failure is of vital significance, this report on the mechanism of corrosion will be concerned primarily with the discontinuous type of failure.

B. Identification of the Corrosion-Induced Precipitate

The observed increase in hydrogen content prior to and during the formation of the plate-like precipitate suggests that the precipitate may be a hydride of uranium and that it may be duplicated outside of the corrosion process by the introduction of hydrogen into uranium metal.

Thus far it has been found that this phase can be produced in gamma-phase alloys in at least three different ways: (1) by corrosion testing in high temperature pressurized water, (2) by making the specimen the cathode of an electrolytic cell, and (3) by ionic bombardment. It is equally significant that it cannot be produced by heating in molecular hydrogen, at least at pressures up to one atmosphere.

In the cathodic hydriding method the alloy was made the cathode in an electrolytic cell with an electrolyte of 0.1 N phosphate solution of Na_2HPO_4 and NaH_2PO_4 buffered to a pH of 7.0. Platinum was used as the anode and to make electrical contact with the alloy. A current density of 15 ma/cm^2 was found to be satisfactory. The depth of hydriding in a given sample depends on both temperature and time.

Hydrogen has also been introduced into a U-12 w/o Mo alloy by means of a glow discharge of hydrogen. A sample was subjected to a hydrogen glow discharge for 1 1/4 hr at a current density of 7 ma/cm^2 and a potential difference of 2800v. Under these conditions the precipitated plate-like phase was produced to a depth of approximately 0.01 in.

In both of these methods of introducing hydrogen the microstructure and distribution of the plate-like phase are similar to those produced during corrosion, and the resulting phase is assumed to be the same hydrogen-rich phase. The hydrogen required to form the precipitate in the corrosion process is presumably made available by the oxidation of uranium in water according to the following reaction:

$$2\,H_2O + U \rightarrow UO_2 + 4H.$$

Note that the hydride phase is formed in gamma-phase alloys only under conditions such that atomic or ionized hydrogen is released at the metal surface.

The experimental evidence concerning the nature of the precipitated phase conflicts in many respects with the concept that the precipitate is UH_3, the only stable U-H compound as yet established.[1] There is, however, considerable evidence for the presence of UH_3 in a corroded specimen. To present a more coherent picture, the material in this section of the report has been arranged according to whether it is in agreement or disagreement with the concept of a UH_3 precipitate. In addition to presenting a brief summary of other physical properties, the section concludes with an attempted rationale of the data.

1. Evidence in Support of a UH_3 Precipitate

Uranium hydride exists in two allotropic forms: alpha UH_3, a recently discovered low temperature form[2]; and beta UH_3.[1] The crystal structure of beta UH_3 is cubic with a_o = 6.620 A and eight molecules per unit cell. The hydrogen atoms occupy the interstices between the uranium atoms so that each

UNCLASSIFIED

metal atom is surrounded by 12 hydrogen atoms at a distance of 2.32 A. The low temperature form, alpha UH_3, has been detected when hydrogen was allowed to react slowly with uranium powder at temperatures below 25°C. The crystal structure of this form of UH_3, is simple cubic with a_o = 4.160 A and two molecules per unit cell. The interatomic distances, U-12 H = 2.32 A, are identical with those in beta UH_3.

a. X-ray Diffraction. - Examination of hydrided polycrystalline samples of U-12 w/o Mo by X-ray diffraction methods has given inconclusive evidence for the presence of either alpha or beta UH_3. The best patterns obtained show only four weak and very broad peaks at the predicted location of beta UH_3 in spite of the fact that the precipitated phase constitutes at least 20% of the bulk specimen volume. A typical pattern is shown in Fig. 11. A measurement of the line breadth of the strongest peak gave a particle size of 25 to 50 A for the diffracting crystallites. Annealing of hydrided samples for 24 hr at 300°C in a helium atmosphere sharpened the X-ray lines to the point where six or seven peaks were observed in the correct positions for beta UH_3. However, this is believed to be a surface effect only, as discussed below. The same results were obtained whether the specimens were hydrided cathodically or by corrosion testing.

b. Electron Diffraction. - The electron diffraction technique was also utilized in an attempt to identify the plate-like phase. The electron beam was adjusted to a diameter of about 1 mil and the sample was aligned so that the platelets were parallel to the beam. A fresh surface of metal was prepared, and special precautions were taken to prevent surface oxidation prior to insertion of the sample into the diffraction camera. An electron diffraction pattern was obtained showing the first 14 lines of beta UH_3. The pattern consisted of sharp, uniformly darkened rings which indicated polycrystalline material with a random orientation and a particle size larger than 1000 A. Several additional weak lines were observed that would fit the beta UH_3 unit cell and would correspond to multiple reflections from the strong lines.

c. Magnetic Measurements. - The magnetic properties of UH_3 were first observed by Rundle, who reported that the hydride is more strongly paramagnetic than metallic uranium.[1] Susceptibility measurements at low temperature revealed that the hydride became ferromagnetic at a Curie temperature of about 175°K. This is the first known case of ferromagnetism in an actinide compound. Above the Curie point the hydride is paramagnetic.

Gamma-phase U-Mo alloys containing the hydrogen-rich plate-like phase are also observed to be ferromagnetic at low temperatures, regardless of whether the second phase is produced by corrosion testing, cathodic hydriding, or hydrogen glow discharge. The magnetic properties of these alloys as a function of temperature are shown in Fig. 12. The Curie temperature of the ferromagnetic constituent was found to range from 175° to 155°K. The variation in Curie temperature over a range of values may be due to the presence of molybdenum alloyed with the hydride.

d. Thermodynamic Evidence. - The use of the U-H phase diagram as evidence for a UH_3 precipitate is a negative form of support since no other hydrogen-uranium compounds are known. Furthermore, it is unlikely that the presence of Mo or Nb would have much of an effect, at least insofar as forming an actual U-Mo-H compound. Formation of such a compound would require diffusion

UNCLASSIFIED

of the Mo or Nb, which should be negligible at the cathodic hydriding temperatures employed, namely up to 100°C. The Mo or Nb could exert its influence through the stabilization of the gamma phase, for which no meta-stable equilibrium diagram with hydrogen has been published.

Thermodynamic evidence supports the conclusion that UH_3 should form as a result of the reaction of gamma uranium-molybdenum (or niobium) alloys with hydrogen. For the reaction

$$\alpha U + 3/2\ H_2 \rightarrow UH_3 \ ,$$

the free energy change is[3]

$$\Delta F = -30{,}100 + 42.6T \ . \qquad (1)$$

For the $\gamma \rightarrow \alpha$ equilibrium[4]

$$\Delta F = -2485 - 10.6T + 2.1T \log T + 4 \times 10^{-3} T^2 - 8 \times 10^4 T^{-1} \ ;$$

thus for the reaction

$$\gamma U + 3/2\ H_2 \rightarrow UH_3 \ ,$$

$$\Delta F = -32{,}585 + 25.25T + 4.4T \log T + 4 \times 10^{-3} T^2 - 8 \times 10^4 T^{-1} \ . \qquad (2)$$

At a temperature of 650°F, the free energy change for alpha uranium reacting to form UH_3 is

$$\Delta F_{\alpha U \rightarrow UH_3} = -4110 \text{ cal/mol} \ ,$$

whereas for gamma uranium it is

$$\Delta F_{\gamma U \rightarrow UH_3} = -8132 \text{ cal/mol} \ .$$

If the uranium in the gamma phase (in a 12 w/o Mo alloy) is considered to be an ideal solution and the free energy is corrected for its dilution (assuming that the molybdenum is inert to hydrogen);

$$\Delta F_{12 \text{ w/o Mo-}\gamma U \rightarrow UH_3} = -8406 \text{ cal/mol} \ .$$

Thus, thermodynamically, gamma-phase alloys should react to form UH_3.

2. Evidence in Conflict with a UH_3 Precipitate

a. Neutron Diffraction. - The precipitated hydrogen-rich platelets are distributed throughout the volume of a sample; therefore, the best diffraction results should be obtained by using a radiation that would penetrate the thickness of the specimen. Electron diffraction gives information from only a very thin layer of the sample surface, perhaps 50 A at most. The depth of penetration of Cu-K radiation is only about 1 mil in U-Mo alloys; thus the surface reflection X-ray technique employed also gives information from only a thin surface layer. The relative ease of penetration by neutrons indicates that neutron diffraction would be an ideal method for obtaining information about volume effects in uranium alloys.

Because the coherent scattering cross section of deuterium is greater than that of hydrogen, samples to be examined by neutron diffraction were cathodically hydrided in heavy water to form a deuterium-rich phase. Comparison samples were also prepared in ordinary water, forming the hydrogen-rich phase. Lineal analysis of the microstructures indicated that 5 to 8 v/o of these samples consisted of platelets. The samples were examined in the neutron diffractometer of the Brookhaven National Laboratory by Dr. L. M. Corliss.

The results obtained upon an untreated sample indicated some preferred orientation was produced during the cooling of the ingot. No extra lines were observed on the hydrided sample. The background was high, indicating a random distribution of hydrogen. The deuterided sample showed a slight increase in intensity in the neighborhood of the strongest UD_3 peak. The volume of UD_3 would have to be less than 1% to give a peak of this intensity. If the particle size of the UD_3 was less than 50 A, the diffraction peak would be very broad, and accurate measurements of intensity would be impossible. Neutron diffraction thus gave no clear evidence for the presence of crystalline deuteride and set an upper limit upon the amount of the deuterium-rich phase present, which was much less than that observed by metallography. Neutron diffraction results confirmed the X-ray diffraction observation in bulk samples in showing no extra reflections that could be ascribed either to UH_3 or phases other than the gamma phase. In addition, these results indicate that the UH_3 phase found by electron and X-ray diffraction is confined to the surface of the specimens.

b. Chemical Analysis and Density. - An experiment was conducted to correlate the hydrogen content of a U-10 w/o Mo alloy with changes in microstructure, lattice parameter, and density. The results indicate that the lattice parameter of the gamma-phase alloys increases to a maximum of approximately 0.5% after cathodic hydriding. An increase in the lattice parameter was noted prior to the appearance of the plate-like phase. After the first appearance of this second phase the lattice parameter seems to remain at a constant value. The solubility limit of hydrogen in the alloy, determined by the first appearance of the second phase and the discontinuity in the lattice parameter as a function of hydrogen content, is between 11 and 25 ppm of hydrogen, as shown in Fig. 13.

The density of the gamma-phase material decreases with increasing hydrogen content. The density of a U-10 w/o Mo specimen hydrided 4 days at 100°C was observed to change from 17.23 to 17.17 g/cc. The volume of the hydrogen-rich phase was determined by lineal analysis be to 2.4%; chemical analysis gave a hydrogen content of 120 ppm. The hydrogen content of the specimen may then be

DECLASSIFIED

described as

$$\text{total H} = f_m \rho_m s + f_p \rho_p [H]_p = \rho_{alloy} [H]_{alloy}$$

where f_m and f_p are the volume fractions of the matrix and plates, respectively; ρ_m and ρ_p are their densities; s corresponds to the solubility of hydrogen in the matrix; and $[H]_p$ is the hydrogen concentration in the plates in ppm. The density of the gamma uranium matrix at a hydrogen concentration of 20 ppm was assumed proportional to the hydrogen concentration and is 17.22 g/cm^3. The value of $\rho_p [H]_p$ was calculated to be 6.44×10^{-2} g of hydrogen. From the fact that the density of the alloy $D = f_m \rho_m + f_p \rho_p$, the density of the plates was determined to be approximately 15 g/cc and their concentration to be 4300 ppm. This corresponds to a composition $UH_{1.02}$. These values are not too accurate because of the inability to obtain a uniform distribution of the hydrogen-rich phase throughout the specimen. When the cathodic hydriding technique is used, the volume percentage of the precipitated phase is very high at the surface and falls off sharply towards the interior of the specimen.

c. X-ray Diffraction. - Careful measurements were made on a large grained, hydrided specimen with an X-ray spectrometer. When the orientation of the specimen was such as to provide reflection from only one grain, it was possible to resolve the (110) gamma diffraction peak into two separate ones corresponding to gamma structures of slightly different lattice parameters. Use of the specimen integrator obliterated this resolution. After hydriding, back-reflection Laue patterns from the same large grained specimen show the presence of additional spots slightly displaced from those present before hydriding, which indicates a second phase of the same structure and a slightly altered orientation. This evidence suggests that the hydrogen-rich phase may consist of gamma uranium with an increased cell size due to dissolved hydrogen and which may, of course, constitute a distinct separate phase.

d. Dissociation Pressure. - The dissociation pressure of the precipitated second phase was determined in order to compare it with the published values for UH_3. In this experiment a U-12 w/o Mo specimen was annealed at 900°C for 24 hr, and water quenched to retain the gamma phase, then electropolished and exposed to degassed water at 343°C. After the corrosion treatment the specimen was again electropolished and then sealed in a constant volume system in which the dissociation pressure was determined as a function of temperature. Equilibrium conditions were usually attained within 24 hr, even at temperatures as low as 150°C. The equilibrium pressures were reproducible either upon heating or cooling to the desired temperature. Thus molecular hydrogen could be introduced into the metal through the medium of the plate-like second phase although, as will be shown, it cannot be introduced in samples that do not contain this phase.

The values obtained for the equilibrium pressures of specimens with different initial concentrations of hydrogen are shown in Fig. 14. From this figure it can be seen that the dissociation pressure and the heat of dissociation for the hydrogen-rich phase are different from those of UH_3 in equilibrium with either alpha uranium or gamma uranium. The slope of the curve for UH_3 in equilibrium

UNCLASSIFIED

with gamma uranium would differ from that for alpha uranium by approximately 10%. The heat of dissociation of the hydrogen-rich phase in gamma uranium was found to be 5.65 kcal/mol H_2. By differentiating the values of $\Delta F/T$ in Eq (1) and (2) with respect to temperature, the heat of formation of UH_3 from alpha uranium is found to be 20.5 kcal/mol H_2 and that for its formation from gamma uranium is 23.4 kcal/mol H_2. Thus, not only is the pressure above the hydrided samples higher than that over equilibrium UH_3, but also its heat of formation is much less. Both of these observations confirm the belief that the phase is not UH_3 and that it is a nonequilibrium phase. Were this phase some yet unidentified stable hydride of composition UH as already estimated, its vapor pressure at corresponding temperatures would be less than that of UH_3.

e. Phase Distribution. - Another aspect of the hydrogen-rich phase requiring clarification is its distribution throughout the matrix at sufficiently long corrosion or cathodic hydriding periods. Consider the gamma phase as a single component; attack by hydrogen should then follow the activity gradient of hydrogen through the specimen. In other words, an external hydrogen-rich layer should form, and no internal precipitation of a second phase should occur in a single component matrix other than that which occurs on cooling from the reaction temperature due to change in solubility with temperature. It has been verified that the platelets are not appreciably more soluble at corrosion temperature than at room temperature; consequently they precipitate during the reaction with hydrogen. The formation of the stable UH_3 as an external hydride is observed in the case of cathodic hydriding or water corrosion of alpha uranium, U_3Si, or alpha prime alloys, none of which exhibit precipitation of the hydrogen-rich platelets. It is concluded, therefore, that precipitation of the platelets is due to a relaxation of the phase rule which permits another degree of freedom resulting from the presence of another variable believed to be the state of stress in the system.

3. Other Properties of the Precipitated Phase

a. Metallography and Hardness. - A metallographic study was made of the hydrogen-rich platelets in each of two gamma-quenched U-12 w/o Mo samples, one having been cathodically hydrided and the other corrosion tested in 650°F water for 28 days. The platelets in both samples were similar in appearance and, as shown in Fig. 15, they apparently consist of two parts: an inner, well defined plate, surrounded by an irregular gray border. The possibility of this structure being an artifact was investigated by subjecting the samples to mechanical, acid, and electrolytic polishing and etching, all of which revealed a duplex structure. Additional evidence for the duplex structure is provided by the fact that the inner and outer parts of the platelets oxidized at different rates when a polished sample was heat-tinted.

Differences in the platelet components are revealed by scratch hardness as shown in Fig. 16. When a Knoop indenter under a constant load is moved across a polished sample surface parallel to the 172° included angle, the scratch width is made by the 130° included angle of the diamond. A series of such scratches made with a 10-g load resulted in a matrix scratch width of 2.2μ, tapering to a width of 1.2μ in the inner part of the platelet. The tapering decrease in width is explicable if the center part of the platelet is harder than the matrix and the outer part only slightly different in hardness. Interference microscope measurements showed that the particular scratched platelet was less than 0.1 below the matrix. This is insufficient to account for the observed difference

in scratch width. Thus it appears that the center portion of the platelet is appreciably harder than the matrix while the outer rim hardness differs only slightly, if at all, from the matrix hardness.

Finite layers of known total thickness were carefully removed from the metal by polishing. Subsequent examination revealed that the hydrogen-rich phase was precipitated in the form of platelets rather than the needles appearing on the two-dimensional surface.

It has also been observed that there exists an etching effect at the gamma grain boundaries of corrosion-tested or cathodically hydrided specimens prior to the appearance of the hydrogen-rich plate. With the metallographic technique normally employed, grain boundaries can be revealed only with difficulty in gamma-quenched specimens, whereas they are evident after very short etching treatments in samples corrosion tested for a short time prior to metallographic examination. The cause for this effect is believed to arise from the hydrogen enrichment of the grain boundaries or possibly from the precipitation of a hydrogen-rich phase in the grain boundaries.

This grain boundary effect is clearly shown in Fig. 17, which is a cross section of a 12 w/o Mo specimen cathodically hydrided at 100°C for 40 hr. Note that the penetration of the grain boundary etching effect far exceeds that of the plate-like precipitate visible only at the very outer surface. If the greater penetration of the grain boundary effect is evidence of a faster diffusion rate at grain boundaries than in the bulk of the matrix, it may be estimated that at 100°C grain boundary diffusion rates of hydrogen are about 200 times as great as volume diffusion rates, a not unlikely factor.

b. Reaction With Molecular Hydrogen. - The following experiment was performed to determine the rates of reaction of molecular hydrogen with uranium in various crystalline states. Samples of quenched U-9 w/o Mo, U-12 w/o Mo, U-4 w/o Nb, and epsilonized U-4 w/o Si were placed in a calibrated manometric system and annealed at 500°C for 16 days in hydrogen at a pressure of 1 atm. This thermal treatment was intended to promote the decomposition of the gamma phase and should result in a transformation product having about 45% alpha in the case of the 9 w/o alloy, 25% for the 12 w/o Mo alloy, and 90% for the 4 w/o Nb alloy. The U_3Si alloy will remain in the epsilon condition. At this temperature, which is well above the decomposition temperature of UH_3, no reaction of the alloys with hydrogen would be expected and none was observed. An additional gamma-quenched U-12 w/o Mo specimen similarly annealed in hydrogen at 400°C showed no reaction after 32 days, although the alpha phase would form UH_3 at such a temperature in contact with 1 atm of hydrogen.

After the 500°C anneal the temperature was lowered to 300°C at which a reaction was observed between hydrogen and the gamma decomposition products. After 1 wk at 300°C the temperature was lowered to 250°C where an increased reaction rate was observed as shown in Fig. 18. At 250°C the gamma-quenched U-4 w/o Nb alloy reacted very quickly at a rate similar to that expected for unalloyed uranium. The amount of hydrogen pickup in each case appears to be proportional to the amount of alpha present. The epsilon decomposition product of U-Mo, like the epsilon U_3Si phase, does not appear to pick up hydrogen. No reaction was observed in a U-12 w/o Mo gamma-quenched specimen after 5 mo at 300°C. From these experiments it was concluded that molecular hydrogen cannot be introduced into a gamma-phase uranium alloy, the epsilon phase in the U-Mo

DECLASSIFIED

system, or an epsilonized U-Si alloy, whereas it will combine with metal in the alpha or alpha-plus-epsilon state.

Some of the work just described has recently been repeated.[5] It was found that the gamma-phase U-12 w/o Mo alloys in 1 atm of molecular hydrogen will absorb hydrogen to the extent of 12 ppm at 343°C. This value represents the solubility limit of hydrogen in gamma uranium at 343°C at 1 atm external hydrogen pressure. The 12 ppm observed value coincides with the value extrapolated from the uranium-hydrogen equilibrium diagram.[6]

c. Behavior on Annealing. - Once the precipitate has been formed, either by corrosion or by cathodic hydriding, it may be removed by vacuum annealing at temperatures as low as 100°C. Subsequent exposure to a molecular hydrogen atmosphere results in the formation of the hydrogen-rich phase as plates of the same size and in the same locations as prior to the vacuum annealing. No growth of the plates was observed nor were any new plates formed. Thus, the formation of the plates must produce some configuration of imperfection or internal strain in the metal which is retained even after all the hydrogen has been removed. This concept is also confirmed by metallographic examination which, as shown in Fig. 19, reveals the former location of the plates as ghosts resulting from an increased rate of attack during electropolishing.

d. Effect of Stress. - The presence of the "ghosts" described above is indicative of a stress effect which is probably connected with the reduced density of the hydrogen-rich phase. The large increase in volume upon formation of the hydride undoubtedly strains the surrounding matrix and is responsible for the imperfections remaining in the metal as "ghosts" after removal of the hydrogen. As will be described later, the application of stress affects the distribution and orientation of the precipitated platelets. This too is ascribed to the reduced density of the plates and the concommitant stresses, which explain the retarded growth of the plates in regions under compressive stress. The strains accompanying formation of the plates are also believed to be responsible for the hardening observed during hydrogen absorption (Fig. 8). It has also been found that uranium hydrided under high pressures forms a phase of density 15 g/cm^3 which spontaneously transforms to UH_3 upon release of the pressure or constraint.[7]

4. Corrosion Mechanism of Uranium-Base Alloys

Although considerably more evidence bearing on the corrosion mechanism and nature of the hydrided phase will be presented later, it is considered pertinent at this point to review the data already presented and to propose a mechanism for the corrosion reaction that may be useful in interpreting the data that follow.

Consider first the corrosion of alpha uranium in water at 650°F. When the uranium surface is exposed to water, it oxidizes and liberates hydrogen.

UNCLASSIFIED

according to the reaction previously discussed. A certain fraction of the hydrogen* dissolves in the bare metal. As shown in Fig. 14, UH_3 decomposes at a pressure of 88 mm at 650°F. By assuming Sievert's law behavior for the solubility of hydrogen in alpha uranium, and referring to Fig. 8.1 of reference (3) it may be calculated that when the hydrogen content of the surface of the sample reaches 0.34 ppm UH_3 will form at the surface. Subsequent corrosion will then occur by oxidation of UH_3 by the water, further liberation of hydrogen, formation of additional UH_3, etc. It is characteristic of oxide films formed indirectly by oxidation of previously formed films that they are not protective; the rusting of iron in moist atmosphere is an example of this behavior. Thus the corrosion rate of alpha uranium would be expected to be quite high in water, appreciably faster than the rate of oxidation by air or oxygen, and similar to its rate of attack by hydrogen. Reference to Fig. 20 (derived from data in Ref. 8 and in WAPD-127, Part I), a plot of the rate of corrosion as a function of temperature of alpha uranium by air, water, and hydrogen and of U_3Si and gamma U-Mo alloys by water, shows that this expectation is indeed confirmed and that the attack of alpha uranium by water is much more rapid than that by air and similar to the rate of attack by hydrogen.

Consider next the corrosion of uranium-base alloys that form no hydride, such as epsilon U_3Si. It is believed that the free energy of the reaction

$$3U + Si \rightarrow U_3Si$$

is sufficiently more negative than that of

$$U_{(\text{in } U_3Si)} + 3/2\ H_2 \rightarrow UH_3$$

so that, unlike the case of gamma U-Mo previously considered, no stable hydride is favored thermodynamically. The corrosion rate in this case would be expected to be similar to that of alpha uranium in air (modified somewhat by the difference in crystal structure of the bare metal and the tendency for this reaction to be controlled by the internal oxidation of uranium and the diffusion of uranium through a silicide film as described in Ref. 9). Again Fig. 20 confirms this expectation. Note that no hydride formation is observed in the water corrosion of U_3Si.

---

*It is important to recall again that 20 to 25% of the hydrogen liberated in the corrosion reaction dissolves in gamma-phase alloys. Almost the same percentage dissolves in zirconium in the course of its hot water corrosion. The percentage dissolved must be a function of the recombination velocity of hydrogen atoms in the water, rate of solution and solubility in the base metal, etc. An investigation of such behavior is considered very important in the further development of corrosion resistant alloys in general, both uranium, zirconium, and ferrous-base. As will be shown later, the amount of hydrogen that dissolves in gamma-phase alloys can be varied by additions to the water or to the alloy.

UNCLASSIFIED

Consider briefly the corrosion of a gamma-phase U-Mo (or U-Nb) sample. Because of the higher solubility of hydrogen in the gamma phase of uranium than in the alpha phase, the hydrogen content of gamma in equilibrium with UH_3 should be 4.1 ppm. As corrosion proceeds, a surface coating of UH_3 would be expected to form when the hydrogen content of the surface of the uranium reaches this value. Suppose, however, that for some reason UH_3 cannot form and the hydrogen content at the surface continues to build up beyond its equilibrium value of 4.1 ppm to that value represented by extrapolation of the dissociation pressure over hydrided gamma U-Mo at 650°F in Fig. 14, namely 2000 mm. From Fig. 8.1 in reference (3) this would correspond to a value of 19.7 ppm of hydrogen in solution in the metal. Assume further that at these hydrogen contents in gamma uranium a metastable U-H phase diagram is valid. These various assumptions are analyzed below.

First, the assumption of a metastable U-H phase diagram should not be surprising, particularly since it is noted under conditions of release of atomic hydrogen. Indeed, the commercial process of nitriding steels is based on the existence of the metastable Fe-N phase diagram, and nitriding occurs in the dissociation of NH_3 under nonequilibrium conditions. If such a metastable phase diagram is formed, note that considerable information is available concerning it. It has been estimated that at 650°F the limit of solubility of the hydride phase in gamma uranium occurs at about 20 ppm. The first hydride in the metastable system has a composition $UH_{1.02}$ (probably UH). The difference in hardness across a hydride platelet indicates either that this phase has a considerable existence range and that its hardness increases markedly with increasing hydrogen content or that a still higher hydrogen content metastable phase exists. The uranium atoms in this phase exist in a body-centered cubic array, and the U-H distances are presumably sufficiently close to those in UH_3 that the ferromagnetic behavior of this phase is similar to that of UH_3. Its density is about 15 g/cc as compared to 10.9 g/cc for UH_3.

Consider next the reasons why the UH_3 equilibrium phase does not form in contact with gamma U-Mo but does with alpha uranium. It is suggested that in the case of alpha uranium the differences in crystal structure and density between the metal and hydride phase are such that the latter forms with no coherency with the matrix. The extremely fine crystallite size of the hydride and the lack of adherence between external hydride and metal during the reaction of alpha uranium and hydrogen attest to this lack of coherency. However, in the case of gamma uranium sufficient similitude of crystal structure exists to cause the formation of a hydride oriented coherently with the matrix. Because of the large lattice strains involved in matching a phase of density 10.9 g/cc with one of density 17 g/cc, further transformation of UH_3 is prohibited. This argument is, of course, highly speculative but does point up the effect of lattice strain discussed below.

One feature of the formation of hydride during the corrosion of gamma-phase alloys remains unaccounted for by the preceding explanation, namely its formation as a two-phase structure uniformly through the body of the specimen. Normally in the diffusion of hydrogen into a single phase matrix, a surface coating of the hydride (stable or metastable) would be expected to form at the surface, and this phase layer would grow into the matrix. If a two-phase metal-plus-hydride structure should form at the surface, it should not progress into the metal, since from the phase rule in a two component condensed system the compositions of the phases in a two-phase zone cannot change at constant

DECLASSIFIED

temperature. It is suggested that, thermodynamically, the metastable U-H system does not behave like a normal condensed system, but that in addition to the usual degrees of freedom of composition and temperature another degree of freedom, namely stress, is active. Thus an activity gradient, and hence diffusion, can occur between two-phase regions of different gross composition.

The effect of stress and the evidence for a stressed condition accompanying the formation of hydride have already been discussed; further experimental evidence will follow. The marked hardening during corrosion testing is sufficient evidence for the presence of such stress. The appearance of UH_3 at the free surface of hydrided samples where lattice strain cannot operate to maintain the metastable hydride further vouches for the importance of lattice strain. Fig. 19 showing "ghosts" of the original platelets after removal of hydrogen at low temperatures may be interpreted as evidence of the existence of such strains. It is significant that samples heated long enough to remove all metallographic evidence of the platelets can not absorb hydrogen. It would be expected that, if the hydrogen activity changed with stress and with the amount of the hydride phase, different decomposition pressures (depending upon the composition of the sample within the two-phase region) would exist and a single decomposition pressure (as shown in Fig. 14) would not apply over the entire two-phase region. Some evidence of such effects was in fact observed; however the experimental data are as yet too fragmentary to permit any conclusions.

The corrosion of gamma-phase alloys may be visualized as follows. As hydrogen is released by the corrosion process and dissolves in the bare metal, concentrations of 19.7 ppm are built up. When the hydrogen content at the surface exceeds this value, the metastable hydride precipitates; diffusion of hydrogen then occurs between this highly stressed two-phase zone and less highly stressed regions, precipitating hydride in such regions when their composition also exceeds 19.7 ppm. As described previously, the hardening and accelerated corrosion of the hydride phase eventually lead to cracking and discontinuous failure. Note that in the corrosion of these alloys, the oxide forms directly on the metal and not by oxidation of a hydride. Therefore this oxide is more protective than that found on alpha uranium during water corrosion, and, as may be seen in Fig. 20, the corrosion parallels more closely the air oxidation behavior of alpha uranium than it does its hydrogen corrosion behavior.

The corrosion behavior of uranium alloys may be generalized as follows. A uranium alloy of maximum hot water corrosion resistance must not react with hydrogen. To prevent discontinuous failure, absorption of hydrogen may be controlled by contact with hydrogen-gettering agents, by suitably hydrogen depolarizers, or by heat-treatment to render more innocuous the precipitation of the hydride. Examples of each of these effects will be cited. Thus although the discontinuous failure of gamma-phase alloys is a harmful corrosion effect, it is evident that without such an effect the corrosion resistance would markedly deteriorate.

C. Fuel Life in Terms of Factors Affecting Corrosion-Induced Precipitation

Many of the factors affecting the rate and mode of corrosion have already been presented in WAPD-127, Parts I and II, dealing with the corrosion resistance of unclad and clad alloys, respectively. However they were reported in terms of the corrosion life of the specimen rather than as an interpretation of the corrosion mechanism. These factors will be reconsidered in the following

UNCLASSIFIED

section; and the effects of such variables as heat treatment, alloy composition, and corrosion medium will be described in terms of their effect upon the formation and growth of the hydrogen-rich precipitate which determines discontinuous failure.

1. Thermodynamic Phase of the Alloy

The rate and mode of corrosion failure of the U-Mo alloys have been determined as a function of the thermodynamic phase in contact with the corrosion medium. Furthermore, the behavior of these phases during cathodic hydriding has also been examined and is described in the following.

a. Alpha. - The alpha phase corrodes extremely fast in comparison to the gamma phase (Fig. 20) and at such a rate that it could not be considered as a core material. This phase fails by a uniform corrosive attack wherein the resultant oxide material is continually sloughed off the surface until the entire metal is consumed. The alpha phase readily absorbs molecular hydrogen as shown in Fig. 14. During cathodic hydriding a sludge forms in the hydriding solution indicating that hydride forms continuously on the surface and is removed or reacts with water to form oxides which slough away. There is no evidence of a plate-like, hydrogen-rich phase present in the alpha phase.

b. Alpha Plus Epsilon. - The alpha-epsilon pearlitic mixture appears to fail through the corrosion of the alpha phase. During cathodic hydriding the alpha lamellae are hydrided in place leaving the epsilon unaltered. The interface showing the extent of hydrogen penetration into the pearlitic structure is shown in Fig. 22b for a U-7 w/o Mo alloy annealed 7 days at 550°C. When this adherent layer reaches a certain thickness, expansive forces cause cracking of the layer at the corners of the samples and in the case of rectangular specimens results in a Maltese cross appearance similar to that observed upon oxidation of such metals as tungsten, which forms a nonprotective oxide whose specific volume is much less than that of the metal. The appearance of cathodically hydrided specimens of 9, 10, and 12 w/o Mo after 21 days annealing at 400°C is shown in Figs. 21a and b and 22a, respectively. Note again the tendency for hydriding to occur in the transformed regions.

c. Gamma. - The gamma-phase alloys, as has already been stated, have a relatively low rate of uniform corrosive attack and fail by sudden cracking and disintegration long before the general attack attains any proportion of consequence, the so-called discontinuous type of failure. This type of failure is always preceded by the formation of a dense network of a hydrogen-rich second phase as shown in Fig. 2. It is the corrosion behavior of the gamma-phase alloys as a whole with which this report is primarily concerned.

d. Epsilon. - The mode of corrosion in the epsilon phase has not been well established. In all epsilon alloys tested small amounts of the alpha phase have been found. In some cases the alpha was present before corrosion testing, and in others it appears to have precipitated during corrosion at the 343°C test temperature. The data indicate that the epsilon phase has a corrosion life at least as long as that of the gamma phase, although it is not known whether discontinuous failure will occur. A sample of 15 w/o U was annealed at 500°C for 3 wk to produce the epsilon structure and then cathodically hydrided. The resulting microstructure showed no precipitation of the hydrogen-rich plates found in gamma alloys and was nonmagnetic at liquid nitrogen temperatures. It is

DECLASSIFIED

concluded that the metastable U-H system does not exist for alloys of the U_2Mo (epsilon) structure.

e. Distorted Alpha. - As-quenched U-4 w/o Nb alloys having the distorted alpha structure contained a sparse distribution of the platelet phase after cathodic hydriding for 3 days at 100°C. The plates were not found in hydrided specimens previously annealed for 1 wk at 200°, 300°, or 400°C. A rather heavy film observed on this material during cathodic hydriding indicates formation of a hydrogen-rich layer at the metal surface similar to that observed in the alpha phase material. Similarly this structure does not absorb hydrogen during corrosion testing.[8] It is concluded, therefore, that this structure also does not form the metastable U-H system.

2. Heat Treatment

The corrosion behavior of the more favorable appearing alloys was studied as a function of their heat treatment to determine the heat treatment that would produce a homogeneous structure of the desired phase to render the metal most corrosion resistant. With this in mind various low temperature annealing treatments have been performed to determine their effect upon corrosion resistance. An effort was also made to determine the optimum homogenizing treatment for these alloys. In the following sections the results of these experiments are described along with the effects of grain size and annealing atmosphere.

a. Homogenization. - The solidification of these alloys is not an equilibrium process and results in coring of the cast structure. Fig. 23a shows an example of this type of microsegregation or coring in an induction melted, chill cast heat of U-12 w/o Mo. Subsequent extrusion of the cast structure elongates the zones of segregation and results in structures similar to that shown in Fig. 23b. The corrosion resistance of unclad specimens from these extruded alloys is adversely affected by the presence of this type of coring.

As seen in Fig. 23c, the continuous, longitudinal regions with lowest molybdenum content are rapidly hydrided during corrosion in high temperature water. The hydrided zones corrode preferentially producing uranium oxide fingers which penetrate into the sample along the stringers. Fig. 23d shows this preferential form of attack. The formation of the oxide, whose density is much lower than that of the metal, produces high internal stresses in the metal which lead to an early cracking failure of a fibrous or wood-splintering type.

The microsegregation can be eliminated and the corrosion resistance greatly improved by high temperature annealing in the range of 900° to 1000°C. An homogenizing treatment used for the laboratory preparation of uranium-molybdenum alloy samples consists of annealing for 24 hr at 900°C in a helium-filled Vycor bulb, followed by a water quench without breaking the bulb. The data in Table I show that this treatment almost doubled the corrosion life of unclad samples in the case of eight different extrusions of U-12 w/o Mo alloys. The effect upon the rate of corrosion is shown in Fig. 24 for various homogenizing treatments. Note that the 700°C anneal had little effect, but corrosion resistance was appreciably improved as the annealing temperature was increased to 900° and 1000°C.

Because of the increased corrosion resistance resulting from the elimination of segregation, a program was undertaken to determine the homogenizing treatment

DECLASSIFIED

yielding the optimum corrosion resistance. For this purpose two duplex melted heats of uranium-molybdenum were extruded. One was an 11.2 w/o Mo alloy (Extrusion No. 1101-1-13) which was extrusion-clad with Zircaloy-2 to 0.437 in. diam, a reduction of 25 to 1. The other was a 12 w/o Mo alloy Extrusion No. (J959) which was extruded without cladding to 2 in. diam, a 4 to 1 reduction. Unclad corrosion specimens from both of the extrusions were annealed in helium-filled Vycor bulbs for various periods of time at 600°, 700°, 800°, 900°, and 1000°C and quenched to retain the gamma structure. The samples were electropolished and then corrosion tested in 650°F degassed water. Metallographic specimens were obtained for each annealed condition.

The corrosion results are presented in Table II. Extrusion No. J959 has an as-extruded corrosion life 2 wk longer than the life for the other extrusion. This increased life is to be expected since the amount of reduction during the extrusion of J959 was small (4 to 1) compared to the reduction (25 to 1) of the reference fuel element. The small reduction did not distort the segregated areas appreciably; thus there were no elongated stringers of segregated alloy to provide an almost continuous path for corrosion through the specimen. Figs. 25 and 27a show the extruded structures of the two alloys.

Annealing at 600° and 700°C does not improve the corrosion resistance of these materials, and in many cases such annealing actually decreases the corrosion life. The time of annealing has little effect at these temperatures. It is apparent from the corrosion tested sample of Fig. 26 that 168 hr at 600°C is not sufficient for homogenization of Extrusion No. 1101-1-13. Actually the diffusion rates at these temperatures were found to be too low to attain homogeneity within 504 hr of annealing for either material. Some improvement in corrosion life occurred when the samples were annealed at 800°C. Again there is no definite effect of the time of annealing. From these results it was concluded that no benefit results from annealing extruded uranium-molybdenum alloys at temperatures below 800°C.

The best resistance to corrosion was obtained by homogenizing at 900° and 1000°C. For these temperatures the time of annealing is an important factor. It was found that the shorter annealing times resulted in longer corrosion lives. The minimum time at temperature required for this effect is unknown since no times shorter than 30 min were studied. Within the 30-min period it appears that homogenization of the alloy was achieved. The effect of short annealing times is apparently related to the nature and distribution of impurities in the metal. In Figs. 27 a, b, c, d the microstructures of specimens annealed for progressively longer times at 1000°C are shown. It is apparent that the increased annealing times have resulted in the agglomeration of the residual impurities in the metal. Possibly some solution of impurities may also have occurred.

It is believed that the agglomeration of the impurities alters the distribution and morphology of the hydrogen-rich precipitate. A fine uniform dispersion of impurity particles would inhibit growth of the plate-like precipitate and thus alter its distribution throughout the gamma matrix. This viewpoint is supported by the plot of hydrogen concentration versus corrosion weight loss shown in Fig. 28. The amount of hydrogen absorbed is a linear function of the weight loss for the first 14 days in test and is independent of the homogenizing treatment. Since the amount of hydrogen absorbed is the same, the effect of the different homogenizing treatments

DECLASSIFIED

must be to alter the distribution or morphology of the precipitate. This effect is considered further in the next section.

The reason for the exceptional corrosion resistance of Extrusion No. 1101-1-13 is related to the presence of small quantities of Cu, W, and Zr and is discussed in the section on alloy additions.

From the results plotted in Fig. 24 it appears that the corrosion rate of the metal is affected by the rate of cooling from the homogenizing temperature, although the life to discontinuous failure is unaffected. In an experiment to determine the effect of cooling rate, two identical U-12 w/o Mo rods were annealed for 24 hr in vacuum at 900°C. One sample was allowed to cool by radiation, and the other was quenched with a helium blast. The results are shown in Table III. The corrosion rate of the slow cooled sample is higher than that of the quenched sample, although their lives are unaffected. This behavior is again attributed to the nature and distribution of precipitated impurities which alter the corrosion behavior of the metal. The effect of cooling rate, however, is minor compared with those of temperature and time of annealing.

b. Low Temperature Annealing of Uranium-Molybdenum Alloys. - It has been reported in Part I that the annealing of gamma uranium-molybdenum alloys at low temperatures in the range of 300° to 500°C results in a marked improvement in the corrosion resistance. The optimum corrosion resistance obtained depends upon the molybdenum content and the temperature and time of annealing. Maximum corrosion resistance for induction melted and chill cast alloys was obtained by annealing a U-11.5 w/o Mo alloy for 35 days at 400°C. This treatment increased the corrosion life from 35 days in the gamma-quenched condition to 105 days as annealed. Subsequently an investigation was undertaken in order to determine the mechanism of this annealing effect and whether duplex-melted and extruded alloys behaved like the induction-melted alloys.

A series of binary uranium alloys with compositions of 7, 9, 10.5, 11.3, and 12 w/o Mo were prepared by the duplex-melting process and extruded without cladding to 0.5 in. diam rods. Specimens for metallographic examination and corrosion testing were machined from these rods and annealed in helium-filled Vycor bulbs for various times at 300° and 400°C.

Hardness measurements were made on samples from all conditions of heat treatment. The hardness of the various alloys is plotted as a function of annealing time in Figs. 29, 30, and 31. As expected, the gamma-quenched hardness increases as the molybdenum concentration increases. The hardness of annealed samples depends upon the molybdenum content, the temperature, and the time of annealing. Note that at least for the 10 to 12 w/o Mo alloys these temperatures are much too low to produce transformation to the alpha-plus-epsilon phases at the annealing times used. The alloys with lower molybdenum content attain higher annealed hardnesses and have a higher initial rate of hardening. The corrosion testing was done in 650°F water, and the tests were continued until the samples failed either by complete oxidation or by discontinuous failure. The test results are presented in Fig. 32.

It is apparent that each of these gamma-quenched alloys can be improved by the proper treatment. The greatest improvement and the maximum corrosion life were obtained by annealing U-12 w/o Mo for 3 to 5 wk at 400°C. The anomalous behavior of the 10.5 w/o Mo samples annealed for 15 wk at 343°C is unexplained.

Samples from a duplex-melted, extruded U-12 w/o Mo rod were annealed at 343°C and at 400°C and then corrosion tested in 650°F degassed water. Periodically specimens were removed from test for the determination of hydrogen content, metallographic appearance, and hardness. These results are shown in Table IV.

Unlike the majority of uranium-molybdenum extrusions, this material in the as-extruded condition was only slightly segregated, and consequently the as-extruded corrosion life is as good as that after homogenization. In agreement with Fig. 32 the 343°C anneal has had little effect upon the corrosion characteristics whereas the 5-wk anneal at 400°C has appreciably increased corrosion life. It should be noted that, in general, the 400°C anneal is not effective unless it is preceded by the gamma-quenching treatment probably because phase transformation occurs in the segregated low molybdenum regions during low temperature annealing.

The effect of annealing upon corrosion rates can be described by a graphical plot of the corrosion weight loss per unit of initial surface area versus the corrosion time. The data from Table IV are plotted in this manner in Fig. 33. It should be noted that the samples annealed at 400°C for 5 wk have a low initial rate which is linear for 28 days and then begins increasing towards discontinuous failure at 70 to 77 days. The other conditions show an increase in corrosion rate after the first period with all samples failing in 35 to 42 days. Another example of the effect of annealing is shown in Fig. 37 where the corrosion data for the U-12 w/o Mo alloys of Fig. 32 have been plotted.

Examination of the microstructures in Figs. 34 a, b, c, d reveal that the distribution of the hydrogen-rich phase is markedly altered in the samples annealed at 400°C subsequent to the gamma-quenching treatment. The plates are shorter, thinner, and more numerous than those found in the gamma-quenched samples. The boundaries of these plates are highly oriented, in contrast to the quenched samples in which the boundaries of the plates appear less dependent upon crystallographic orientation.

These effects may be correlated with the mechanism for corrosion of gamma-phase alloys already proposed. The aging treatments applied to the 12 w/o Mo alloys are believed primarily to cause precipitation of impurities such as carbides, nitrides, and oxides. The aging times at 400°C are insufficient to cause any X-ray evidence of phase transformation to alpha plus epsilon, although resistivity measurements indicate that some transformation may occur.[9] In any case, as shown in Fig. 31, considerable hardening occurs during this aging treatment; the hardening and impurity precipitation are considered most important. Many more platelets of the hydrogen-rich phase are presumed to nucleate and grow with the precipitated impurities acting as nucleation sites. Thus, for the same hydrogen content, more platelets are produced in the aged alloys than in cleaner, as-quenched alloys. Similarly the growth of the hydrogen-rich phase is inhibited in the aged samples because of the higher hardness of matrix and the consequent attainment of a saturation stress at a smaller platelet dimension than in the as-quenched alloys. The decrease in the number of platelets with increased aging time is attributed to agglomeration of the precipitated impurities and, hence, a decreased number of nucleation sites.

The effect of the small platelet size upon discontinuous failure may result from the generation of lower stresses by the platelet which could be relieved by

plastic deformation at the ends rather than by splitting, such as would occur when a much larger plate oxidizes. In addition, the fine dispersion of short thin platelets results in a much more continuous gamma matrix and does not offer a connected network of the hydrogen-rich phase along which the corrosion might occur.

c. Grain Size. - The grain size of the gamma phase appears to have some effect upon the corrosion of these alloys. Fig. 35 illustrates the structure of a gamma-quenched U-12 w/o Mo alloy corrosion tested for 14 days in 650°F water. This sample has a duplex grain structure, and the amount of the hydrogen-rich phase precipitated is greater in the fine grained portions than in the coarser grained. Furthermore, the individual plates are coarser in the fine grained material. The difference between the two grain sizes is apparently due to the greater volume of grain boundary material in the fine grain region through which hydrogen can diffuse more readily than through the bulk gamma volume. This effect, which is of minor significance, was not investigated further because of the difficulty in obtaining large grained material without a duplex structure.

d. Atmosphere. - It was considered at one time that corrosion failure may be associated with gaseous impurities. Therefore the effect of annealing atmosphere was determined by using U-12 w/o Mo specimens annealed 24 hr at 900°C in vacuum, helium, oxygen, tank hydrogen, and hydrogen from the decomposition of UH_3. In the case of the oxygen atmosphere the specimens were annealed in oxygen until a heavy scale formed (approximately 1/2 hr) and then annealed for the remainder of the 24 hr in vacuum. The results of these treatments are summarized in Table V. There is some indication that the corrosion rate may be improved in samples annealed in helium or tank hydrogen. Both of these gases contained some oxygen and water vapor since no effect was made to dry the gases. The samples annealed in oxygen have approximately the same corrosion rate as the samples annealed in hydrogen produced by the decomposition of UH_3.

Apparently the different annealing atmospheres have no significant effect upon the subsequent corrosion behavior of the alloy. This conclusion is further borne out in Fig. 36 which shows that the amount of hydrogen present is independent of the pre-corrosion treatment.

3. Effect of Alloy Composition

The effect of gross alloy additions to uranium metal has already been presented in Parts I and II and will receive no further emphasis in terms of corrosion mechanism. Increasing additions of Mo or Nb decrease the rate of corrosion, prolong the time for discontinuous failure, and stabilize the gamma phase. The effect of Mo concentration on the corrosion of U-Mo alloys is shown in Fig. 22, WAPD-127 Part I. The minimum weight loss occurs at a Mo concentration of 12 w/o Mo. This composition also has the longest life before discontinuous failure.

Additional testing of U-Nb and U-Nb-Pt ternaries did not provide any significant contribution to an understanding of the corrosion mechanism of the uranium alloys. In general, the corrosion rate and corrosion life of as-extruded U-Nb alloys are improved with increasing amounts of Nb or by adding Pt. The extruded plus gamma-quenched U-Nb alloys derived no particular benefit from the addition of Pt. Increasing the Nb content of U-Nb binaries in the range 8 to 12 w/o Nb improved corrosion resistance to 343°C water and improved the stability of the gamma phase at 400°C. Platinum additions improved the thermal stability at 500°C, and during

UNCLASSIFIED

400°C annealing appears to have promoted the formation of a submicroscopic precipitate throughout the gamma matrix.

a. Effects of Small Alloy Additions Of Cu, W, and Zr. - During the homogenization experiments mentioned in section II-C-2, it was discovered that an extruded rod (No. 1101-1-13) of U-11.2 w/o Mo had exceptionally good corrosion resistance in 650°F water. Unclad specimens annealed for 30 min at 900°C had a corrosion life of 105 to 119 days. The alloy was analyzed and found to contain from 0.01 to 1.0 w/o each of copper, tungsten, and zirconium. One or more of these impurity elements is believed to be the source of the improved corrosion resistance since, the only difference between this alloy and other alloys similarly tested is the presence of these additional elements. The carbon content was found to be 0.042%.

Specimens from this extrusion were annealed for 24 hr at 900°C, quenched to retain the gamma structure, and then corrosion tested in 650°F water. The corrosion results are shown in Fig. 37 along with the corrosion curves for a typical U-11.3 w/o Mo alloy, a U-12 w/o Mo alloy in the gamma-quenched condition, and the same U-12 w/o Mo alloy after a 3 wk anneal at 400°C. The effect of the impurity elements may be seen by comparing the U-11.2 w/o Mo specimen with the U-11.3 w/o Mo specimens. The corrosion behavior of the specimen containing the impurities approached that of the aged U-12 w/o Mo alloy. The microstructure of this specimen after 28 days in 650°F water is shown in Fig. 38. The effect of the impurities is seen to have limited lateral growth of the hydrogen-rich phase and to have resulted in a much larger number of plates than found in alloys without the impurities. No micrographs were taken of the structure during the corrosion process of this same alloy annealed 30 min at 900°C, but it is presumed that a finer impurity distribution was present and that its microstructure would approach more closely those of Figs. 34 a, b, c, d.

Other evidence for the effect of impurities upon corrosion resistance may be found in the corrosion characteristics of high purity U-12 w/o Mo. The high purity alloy was prepared by remelting a duplex-melted alloy in a urania crucible under vacuum. The material was held at 1300°C for 8 hr under a vacuum of 10^{-6} mm of mercury, annealed 24 hr at 900°C in vacuum, water quenched, then corrosion tested in 650°F water. It was found to have an extremely short corrosion life; all specimens tested disintegrated within 21 days. Thus, reducing the residual impurities of the alloy decreases corrosion life. The observed corrosion rates are presented in Table VI.

b. Influence of Small Additions of Cr and Ti on the Corrosion Properties of U-Mo Binary Alloys. - It was reported in Part I that small additions of Cr and Ti significantly extend the corrosion life of low molybdenum (7 to 9 w/o) U-Mo alloys in the gamma condition. Subsequent corrosion testing has verified that the corrosion properties of alloys with these additions are improved by several orders of magnitude over those of the binary alloys. Specimens containing Cr and Ti additions prepared in the form of arc-melted buttons by the Armour Research Foundation were corrosion tested 650°F water. The corrosion rates at various stages during the test and the failure times of the ternary specimens are summarized in Table VII. Also included are the corresponding data for U-7 and U-9 w/o Mo binary specimens fabricated and tested at the same time.

It is apparent that without exception the ternary alloys are as good as or better than the equivalent binary alloys. In some instances the ternary alloys

UNCLASSIFIED

are phenomenally superior to the binaries. No correlation exists between the corrosion behavior and the amount or type of ternary addition, the alloy level, or, for that matter, between supposedly duplicate specimens. Certain of these ternary specimens exhibited extremely long lives and low rates, but the behavior was entirely random.

After 154 days of testing those specimens indicated in Table VII as discontinued were examined for microstructure, hardness, and hydrogen content. The hardness and hydrogen content of the specimens removed are tabulated in Table VIII. Also included are the weight loss incurred by the specimens up to the time of removal and the percentage of hydrogen released during corrosion that was absorbed by the specimens. The weight losses are small for specimens tested this length of time, varying from 150 to 300 mg/cm^2. The hydrogen concentration roughly corresponds to the weight loss, varying from 100 to 200 ppm. If the reaction $U + 2\ H_2O \rightarrow UO_2 + 4H$ is assumed, it is possible to calculate from the weight loss and hydrogen concentration the fraction of hydrogen produced that was absorbed by the specimen. These values range from 7 to 9% for the specimens in Table VIII. The value repeatedly observed for binary alloys is about 20%.

From Table VIII it may be concluded that the ternary additions serve to reduce the rate of corrosion by more than a factor of two and to inhibit hydrogen pickup by a factor of two. Metallographic examination revealed that the ternary specimens contained practically no hydrogen-rich plates. Similar binary alloys containing 200 ppm of hydrogen would show a dense precipitation of the plate-like phase. The microstructure consisted primarily of islands of a second phase in the gamma matrix. Figs. 39 to 41 depict the appearance of a representative specimen both before and after corrosion testing. Fig. 42 is a high magnification micrograph of the post-test microstructure. From Figs. 40 to 41 it is seen that a few plates are present but not enough to account for the 200 ppm of hydrogen contained in the material. The salient structural change during corrosion is the precipitation of a fine spheroidal phase well dispersed throughout the matrix.

In order to determine the nature of the spheroidal precipitate a single grain was isolated from the bulk specimen and subjected to X-ray analysis. The X-ray diffraction pattern revealed the presence of a partially oriented alpha uranium precipitate in a gamma matrix. No uranium hydride was detected by X-ray diffraction, although the specimen was ferromagnetic at liquid nitrogen temperature.

It is believed that the chromium and titanium additions have produced the very important effect of altering the mode of decomposition of the gamma phase. Instead of the lamellar alpha-plus-epsilon structure, the precipitated alpha occurs as isolated spheres in the gamma matrix. The epsilon decomposition product is not detected but may appear at a later stage. Consequently the gamma matrix is continuous, and the isolated dispersion of easily hydrided, corrodible alpha provides no connected path for corrosion. Furthermore, the gamma matrix has undoubtedly been enriched in Mo as a result of alpha precipitation and its corrosion resistance thereby increased.

Since the few hydrogen-rich plates present are insufficient to account for the observed hydrogen concentration of 200 ppm and the limit of solubility of hydrogen in the gamma phase in equilibrium with UH_3 has been shown to be 4.1 ppm, it must be assumed that the hydrogen is concentrated in the alpha phase. The alpha particles must then act as sinks for the hydrogen, otherwise the precipitated hydrogen-rich plates would be present in the matrix. Those few plates present

DECLASSIFIED

originate at the grain boundaries which are readily etched. Hence bulk diffusion in the gamma matrix cannot keep pace with grain boundary diffusion of hydrogen, and the plate-like phase is precipitated in the regions of high hydrogen concentration along the grain boundaries. Although the effect of the chromium and titanium additions results in a spheroidal decomposition product acting as a sink for hydrogen, the origin of this effect is not known. Examination of the U-Cr and U-Ti phase diagrams may give some clue to this effect. In the U-Ti system the alpha phase is a peritectoid decomposition product. Thus in the U-Mo-Ti system the initial gamma decomposition product may be peritectoid alpha which would most likely precipitate in a spheroidal form. It is unlikely that a lamellar alpha-epsilon decomposition product would form as a result of this reaction.

c. Influence of Platinum Additions to U-Mo Alloys. - In the initial stages of the alloy development program it was believed that discontinuous failure during corrosion resulted from the decomposition of the gamma phase. Examination of the phase diagrams of the alloys of Zr, Nb, and Mo with uranium shows that the gamma-phase field of these alloys contracts progressively in the order mentioned. The contraction was greatest in the U-Mo alloy and is believed to result from an increase in the electron-atom ratio as the valence of the alloying element increases. From this observation and other information on the crystal structures and ionic radii it was postulated that platinum would be soluble in gamma uranium and should reduce the electron-atom ratio, thereby extending the gamma-phase field and increasing the stability of the gamma phase.

Subsequent testing of U-Mo-Pt ternary alloys soon indicated that, although the Pt additions increased the thermal stability of the gamma phase, its effect upon the corrosion rate of these alloys was of far greater consequence. The effect of the platinum addition may be seen in Tables IX and X which summarize the corrosion data of ternary specimens made from arc-melted buttons prepared by the Armour Research Foundation. It is apparent that the addition of platinum decreases the corrosion rate and extends the corrosion life of U-Mo alloys in practically all conditions.

Hydrogen analyses of the ternary specimens removed from corrosion test before failure reveal that hydrogen absorption in the U-Mo-Pt alloys is much less in a given period of exposure than for the U-Mo binaries. The U-Mo alloys absorb about 20% of the hydrogen liberated during the oxidation of uranium, whereas the U-12 w/o Mo ternaries containing platinum absorb less than 1%. Thus a U-12 w/o Mo-0.6 w/o Pt alloy showed no precipitation of the hydrogen-rich plates after 154 days in 650°F water. Platinum additives to the U-9 w/o Mo alloys were somewhat less effective; these specimens absorbed 2 to 5% of the hydrogen released and showed extensive precipitation of the hydrogen-rich plates after 168 days in 650°F water. The platinum additions do not appear to affect the solubility of hydrogen in the gamma phase or the mode of formation of the plates. The primary effect of the platinum additions appears to be the reduction of the amount of hydrogen absorbed by the specimen relative to that produced by the corrosion reaction.

The mechanism by which platinum additions reduce the hydrogen pickup is not clearly understood, but either of two factors or a combination of both is possible. The platinum may become incorporated in the lattice of the oxide that forms on the specimen surface and improve its effectiveness as a barrier to the diffusion of hydrogen, or it could become incorporated in the oxide as inert particles which act as nuclei for the recombination of hydrogen atoms. Whether the

UNCLASSIFIED

oxidation process is one of cation diffusion or anion diffusion, the hydrogen must diffuse through the oxide to be absorbed by the sample. The second possibility is more likely because platinum is known to be a hydrogen depolarizer; that is, it acts as a catalyst in the formation of molecular hydrogen from atomic hydrogen. This possibility would have an important effect upon the corrosion life of the alloys in light of the findings that the uranium gamma phase does not absorb more than 12 ppm of molecular hydrogen at 1 atm. In other words, the hydrogen-rich precipitate is not found in gamma uranium specimens exposed to an atmosphere of molecular hydrogen. Presumably the platinum bearing alloys owe their increased corrosion lives to the formation of molecular hydrogen at the specimen surface which reduces the amount of nascent hydrogen available to the metal.

A low temperature annealing treatment of 7 days at 400°C was found to increase both the corrosion resistance and corrosion life of the platinum ternary alloys. The corrosion rate of 0.003 mg/cm^2-hr obtained in the annealed U-9 w/o Mo-1.2 w/o Pt alloy is the lowest observed for any uranium alloy and, on the basis of the number of atoms consumed, is a rate of the same order of magnitude as that of stainless steel under similar conditions.

Annealing for longer times or at higher temperatures reduced the corrosion life of the ternary alloys. The effect of the 7-day anneal at 400°C is believed to be similar to that observed in the U-Mo binary alloys wherein the size and growth of the hydrogen-rich platelets are inhibited by the presence of precipitated impurity particles or possibly by an intermediate transformation product in the decomposition of the gamma phase. The effect of precipitated impurities upon the growth of the hydrogen-rich plates has already been discussed. The ability of the platinum to stabilize the gamma phase may be seen in the microstructures of the U-9 w/o Mo alloys after annealing for 35 days at 400°C, shown in Figs. 43, 44, 45, and 46. In addition to the gamma decomposition products at the grain boundaries, a very fine dispersion of precipitate may be discerned throughout the matrix of the grains.

4. Corrosion Medium

a. Effect of Hydrogen and Oxygen Additions to the Test Water. - The influence of hydrogen and oxygen additions to the corrosion test water was studied using gamma-quenched U-12 w/o Mo specimens. The gas additions to the test water were made by passing the gas under pressure directly to the autoclave after it had been degassed by venting to the atmosphere. The amount of gas added corresponded to an equilibrium concentration of 10 cc gas/g H_2O. Past experience has indicated, however, that tests of this type seldom attain greater than 50% of the equilibrium concentration. Thus the gas concentration was probably about 5 cc gas/g H_2O. No gas analyses of the water were made. One series of tests was conducted using argon as a blank.

The weight losses during corrosion in the different media are shown in Fig. 47, and the hydrogen concentration of the corroded specimens is plotted in Fig. 48. The gaseous additions do not appear to influence the rate of corrosion, though the hydrogen pickup by samples exposed to oxygenated water is reduced. This reduced hydrogen pickup is also reflected in an increase in corrosion lives. Figs. 49 to 53 illustrate the microstructures of the specimens after 15-days exposure to the various media. From these structures it may be concluded that in U-Mo alloys the addition of hydrogen to the test water does not influence hydrogen absorption by the specimens, whereas oxygen additions

are effective in inhibiting hydrogen absorption. It is believed that the effect of the excess oxygen addition is to depolarize the nascent hydrogen formed upon oxidation of the alloy in water. However complete depolarization does not occur since the specimens eventually fail discontinuously.

A similar test with hydrogen added to the test water was conducted on the "strained alpha" structure of a U-4 w/o Nb alloy. This structure is capable of absorbing molecular hydrogen. The results of a 5-day corrosion test with and without the addition of hydrogen are shown in Fig. 54. Failure of the "strained alpha" structure appears sensitive to the presence of hydrogen in the test water. These results indicate that "strained alpha" alloys corrode by the formation of UH_3.

b. Effect of Platinum and Nickel Ion Additions. - From the investigation of the corrosion behavior of the U-Mo-Pt ternaries and from the knowledge that the gamma phase does not absorb molecular hydrogen beyond 12 ppm it was concluded that the reduced hydrogen pickup and corrosion rate of the alloys resulted from the low hydrogen overvoltage of the platinum believed to be present in the oxide layer as hydrogen depolarizing particles.

Aside from the use of alloying additions, another method for reducing hydrogen absorption during corrosion may be the use of hydrogen depolarizers in the corrosion medium. The effectiveness of these water additions was evaluated by comparing the corrosion behavior of U-12 w/o Mo alloy in degassed water with similar specimens in water containing 50 ppm of Ni as $NiSO_4$, 50 ppm of Pt as H_2PtCl_6, and in water containing about 10 ppm of Pt as colloidal platinum.

The corrosion behavior in these media is shown in Fig. 55. The corrosion of the specimens exposed to water containing colloidal platinum was identical to that of the specimen tested in degassed water. However the corrosion behavior of specimens tested in water containing Ni and Pt ions was altered. From these experiments it is concluded that the addition of nickel sulphate or platinic chloride to the test water extends the corrosion life of U-12 w/o Mo, whereas the addition of colloidal platinum in the amounts studied has no effect on the life. Figs. 56 a, b, c, d illustrate the microstructures of the specimens tested in the various media after 25 days at 650°F. Note the reduced pickup of hydrogen in the specimens tested in solutions containing Ni and Pt ions.

These experiments were repeated with another set of specimens similarly tested in water containing a nickel chloride addition to determine whether the anion addition played any role in the extension of corrosion life. There was no significant difference in corrosion life between the chloride and sulphate additions; it is concluded that the effect is due to the nickel and platinum ions.

Hydrogen analyses of the specimens confirmed that the effect of the nickel and platinum additions is to reduce the hydrogen absorbed by the specimens. The fraction of available hydrogen absorbed by the specimens tested in degassed water or in water containing colloidal platinum varied from an initial value of 15% to a final value of 25% during the later stages of corrosion. The specimens tested in water containing the Ni or Pt additions absorbed only 5% of the total available hydrogen.

From these results it is concluded that the Ni and Pt act as hydrogen depolarizers. The mechanism is probably one where the Ni and Pt are plated out on the specimen as fine particles which act as centers of hydrogen molecule formation effectively reducing the amount of hydrogen absorbed by the specimen.

5. Effect of Temperature

The effect of water temperature upon corrosion rate and corrosion life is shown in Figs. 28 and 29 in WAPD-127 Part I. Gamma-quenched U-9 to 12 w/o Mo alloys approximately double their corrosion rate and halve their corrosion life for every 50°F increase in test water temperature in the range 600° to 750°F. The effect of temperature in the cathodic hydriding process is shown in the following table which presents the depth of penetration of the hydrogen-rich plates as a function of the temperature of the electrolyte.

Temperature, °C	20	100	200
depth, in.	0.003	0.045	0.050

This increase in penetration is presumably due to the increase in diffusion rate of the hydrogen with increasing temperature. The decrease in corrosion life is probably due to the increased rate of oxidation with temperature and possibly to the increased rate of hydrogen diffusion.

6. Effect of Stress

The corrosion of the gamma-phase alloys is markedly affected by the state of stress to which the specimens are subjected. The role of stress in corrosion appears to be determined by its effect upon the formation of the hydrogen-rich plates. Cathodic hydriding experiments were conducted on gamma-quenched U-10 w/o Mo strips held in a constant moment bending jig. The microstructure of specimens cathodically hydrided under stress are shown in Figs. 57 and 58. It is evident that the plates first form in the region under tension and align themselves perpendicular to the direction of the tensile force. After longer hydriding times the plates appear on the compression side and are parallel to the compression direction. Thus the formation of the hydrogen-rich plates appears to be accelerated by tensile stresses and inhibited by compressive stress.

The effect of stress is understandable if the density of the hydrogen-rich phase is less than that of the gamma uranium as experimental results have already indicated. Because of its decreased density, the formation of the hydrogen-rich plates would relieve the applied tensile stress or, in other words, the energy of formation of this phase would be decreased. This would be especially true when the plates are aligned perpendicular to the direction of the tensile stress whereby maximum growth occurs parallel to the applied tensile direction. In order to form the new phase in a region under compression, work must be done against the compressive forces resisting expansion in regions of the newly formed lower density phase. This work would be at a minimum perpendicular to the direction of compression by a factor proportional to the Poisson ratio. Thus the formation of the new phase would be inhibited in regions of compression, and the plates would form parallel to the direction of compression because the maximum growth or widening of the plates occurs in the perpendicular direction. The stress relief provided by the preferential mode of growth was observed to produce a permanent set in the specimen.

UNCLASSIFIED

The effect of stress upon the corrosion of a U-Mo alloy is shown in Figs. 59 and 60. In this case the specimens were clad with Zircaloy-2 which had been defected by drilling a 0.040 in. hole through the cladding and into the fuel element. One of the stressed specimens was tested with the defect in the side under tension and another with the defect in the compression side. The specimens were initially stressed in a bending jig to 95,000 psi. Cracking occurred in the specimen susceptible to corrosion under tension, whereas no cracking or hydrogen-rich platelets were observed in the specimen susceptible to corrosion under compression.

D. Summary of Corrosion Testing of Bare Specimens

The corrosion of the alpha, gamma, epsilon, and strained alpha phases of uranium base alloys occurs by a uniform general attack resulting from oxidation of the metal by the high temperature water. Of these phases the gamma, epsilon, and possibly "strained alpha" are satisfactory from the standpoint of corrosion resistance in a pressurized water reactor.

The gamma phase, however, is subject to premature failure by cracking or general disintegration of the metal, which would render it unsuitable. This type of failure, termed "discontinuous failure," results from the precipitation of a highly corrodible hydrogen-rich phase which forms a continuous network through the material. The subsequent corrosion of this phase leads to discontinuous failure.

The exact nature of the precipitated phase is unknown. Electron diffraction patterns reveal the presence of UH_3. X-ray patterns yield diffuse peaks corresponding to the first few lines of UH_3, and neutron diffraction results give no indication of UH_3. The precipitated phase is ferromagnetic with a Curie point over a range of temperatures which includes that for UH_3. Approximate density determinations and chemical analyses indicate that the material is $UH_{1.02}$ with a density of 15 g/cm^3. The hydrogen-rich material precipitates out in the form of plates on the {100} planes of the gamma phase when a hydrogen concentration between 11 to 25 ppm is exceeded. Metallographic examination reveals that many of the plates consist of a hard, well defined center of finite width surrounded by a softer irregular material. The decomposition pressures of the precipitated phase have been determined and found to be higher than those of UH_3. Although the structure and composition of the phase are unknown, the evidence indicates that it is not UH_3.

The gamma and epsilon phases do not absorb molecular hydrogen, whereas the alpha and strained alpha do so readily. Precipitation is believed to originate from the absorption of atomic hydrogen released upon oxidation of the uranium in high temperature water.

The addition of Mo and Nb to uranium increases the time required for discontinuous failure. The use of platinum as an alloying element reduces the absorption of atomic hydrogen, probably by means of its catalytic behavior to promote the formation of molecular hydrogen. Small additions of chromium, titanium, and vanadium prolong corrosion life by altering the mode of formation of the alpha phases upon decomposition of gamma so that the alpha phase precipitates as isolated spheres in the gamma matrix to which the dissolved hydrogen diffuses. Thus the alpha phase and the hydrogen associated with it are rendered innocuous from the viewpoint of discontinuous failure.

RELEASED

Copper, tungsten, and zirconium as impurities were found to inhibit growth of the hydrogen-rich phase when combined with the proper heat treatment. This effect is believed to result from the precipitation of the impurities as intermetallics which obstruct growth of the plates. Very short homogenizing treatments at 1000°C were also found to inhibit growth because of the resulting fine dispersion of precipitated impurities.

The addition of nickel ions to the corrosion medium reduced the absorption of atomic hydrogen by the gamma phase, probably because of the low hydrogen overvoltage of nickel promoting formation of molecular hydrogen. Hydrogen and argon additions to the water had no effect on discontinuous failure, whereas the addition of oxygen appears to retard pickup of hydrogen.

Compressive stress in the alloy inhibited precipitation of the hydrogen-rich phase, as a consequence of the increase in free energy for the formation of this lower density phase.

All of the factors affecting the corrosion life of the uranium base alloys considered may be described in terms of their effect upon the formation of the hydrogen-rich plates or upon phase transformations in the alloy. The factors retarding precipitation or growth of the plate-like phase are also found to increase corrosion life. Similarly those factors that inhibit transformation in the alloy or render the transformation products innocuous are compatible with long corrosion test lives. However the controlling effects upon corrosion life prior to discontinuous failure are the precipitation and growth of the hydrogen-rich phase.

These experimental results were reconciled on the basis of a corrosion mechanism involving precipitation of a metastable uranium hydride and its propagation through the test samples under the action of stress.

III. CORROSION TESTING OF ZIRCALOY-CLAD SPECIMENS

In the previous section on the corrosion testing of bare specimens various experiments were described in terms of their effect upon the corrosion life of gamma uranium alloys in high temperature water. It was concluded from this work that the corrosion life of a fuel element is limited to the time for the onset of discontinuous failure. The effect of a cladding should therefore be considered from the standpoint of discontinuous failure. It has already been established that the cause of discontinuous failure is the precipitation of a network of a hydrogen-rich phase. The effectiveness of a cladding in extending corrosion life can then be measured in terms of its ability to prevent the precipitation of the hydrogen-rich phase. The corrosion data for clad specimens have already been presented in WAPD-127, Part II - "The Corrosion Testing of Zircaloy-Clad Fuel Elements."

A possible method of protection is for the Zircaloy cladding to serve as a noncorrodible barrier between the water and the fuel. Obviously this would prevent absorption of hydrogen by the specimen when no cladding defects exist. However, it was assumed throughout this development that cladding defects exist and that fuel elements must exhibit full corrosion life even though the fuel is exposed to the corrodent. If defects do exist, the alloy is exposed to the water and subject to discontinuous failure resulting from precipitation of the

DECLASSIFIED

hydrogen-rich phase. Corrosion testing of defected Zircaloy-clad rods has revealed that no precipitation of the hydrogen-rich phase has ever been observed in a specimen prior to failure, including specimens that have withstood 359 days of testing. The protective effect of the cladding appears to be greater than the ratio of the exposed to the unexposed areas of fuel to water and indicates that the Zircaloy has a role other than that of a barrier.

Two possible mechanisms have been proposed to explain the effect of the Zircaloy cladding in inhibiting the precipitation of the hydrogen-rich phase. In one the cladding is believed to exercise a constraint upon the expansion of the metal during transformation to the lower density hydrogen-rich phase. In the other the hydrogen-gettering properties of the zirconium, which is assumed to behave as a sink for hydrogen, prevent a hydrogen buildup in the alloy thereby making precipitation impossible.

In order to test the first hypothesis, thermodynamic calculations were made of the effect of internal pressure upon the formation of UH_3, in a gamma uranium matrix. The results of these calculations are shown in Fig. 61. From these results it can be seen that increasing the internal pressure, or decreasing the hydrogen pressure, has the effect of making the free energy of formation of UH_3 more positive. The data indicate that large pressures of the order of 200,000 psi are required to prevent hydride formation at the corrosion testing temperature. These pressures are, of course, unobtainable with the cladding dimensions used. Such cladding would fail at internal pressures of about 5000 psi. No thermodynamic data are available to make a similar calculation for the metas able hydrogen-rich phase in gamma-phase alloys. In Section C-6 it was shown that a compressive stress of 95,000 psi inhibited precipitation during corrosion and a stress of 25,000 psi retarded precipitation during cathodic hydriding. Therefore, the cladding may offer some restraint to expansion which might inhibit precipitation, but this effect is seen to be very small.

The ability of the cladding to getter hydrogen from the uranium has been demonstrated both analytically and experimentally. Thermodynamic calculations were made for the reaction between zirconium and uranium hydride to form zirconium hydride and uranium. It was found that the formation of zirconium hydride was favored. The free energy for the reaction

$$2Zr_{(c,\alpha)} + UH_{3(c,\gamma)} \rightarrow ZrH_{1.5(c)} + U_{(c,\gamma)} \text{ is}$$

$$\Delta F^\circ = -32{,}469 - 5.33_T \log T + 4.01 \times 10^{-3} T^2 + \frac{0.34 \times 10^5}{T} + 18.89T.$$

The free energy of this reaction at 650°F is -28,500 cal and is thus highly favored. The hydrogen-gettering effect may also be seen in Fig. 14 which shows the decomposition pressures of UH_3 and the hydrogen-rich precipitate, along with the partial pressure of hydrogen dissolved in zirconium. From these curves it can be seen that for a given concentration the partial pressure of hydrogen in zirconium at the corrosion testing temperature is much less than that of hydrogen in uranium, either as UH_3 or the plate-like precipitate. It would then be expected that if uranium and zirconium were bonded together, hydrogen would diffuse from uranium to zirconium or be gettered by the zirconium.

There is some experimental evidence for the gettering property of the cladding as shown in Figs. 62 and 63 which illustrate the microstructure of a U-10 w/o Mo plate clad with Zircaloy and electrolytically hydrided so that the

cladding and the uranium alloy both had equal access to the available hydrogen. Figs. 62 and 63 are micrographs of the exposed face and a cross-sectional view, respectively. Although there is no extensive pickup of hydrogen, the region adjacent to the cladding shows less of the precipitated phase. In this experiment the cladding can exert no mechanical constraint upon the formation of the precipitate, and its effect is limited to the gettering of hydrogen.

It is concluded that the function of the cladding, apart from its role as a barrier, is to getter the hydrogen diffusing into the uranium thereby preventing precipitation of the hydrogen-rich phase within the fuel. Eventually, of course, the cladding will become saturated with hydrogen, and precipitation will be free to take place. The element is then subject to failure at any time.

From the observations reported in Part II of WAPD-127, failure occurs by a rupture of the cladding which exposes more of the fuel to the water and leads to rapid disintegration of the alloy. The most likely cause of the cladding rupture appears to be the volume expansion in the fuel element resulting from oxidation of the hydrogen-rich precipitate to the lower density UO_2. Whether the process is abetted by hydrogen embrittlement of the cladding has not been established, but the oxidation and possible splitting of the fuel element are sufficient to rupture the cladding. The mechanism of failure which has been proposed received additional support from the results of a calculation of the theoretical fuel life described in the following section.

IV. CALCULATED LIFE OF A ZIRCALOY-CLAD URANIUM ALLOY FUEL ELEMENT

It is now apparent from the material already discussed in this report that the corrosion life of gamma-phase uranium alloys in high temperature water is intimately associated with the precipitation of a hydrogen-rich phase as a result of corrosion. It then seems reasonable that uranium alloys to be considered for a reactor fuel should also be considered from the viewpoint of hydrogen solubility and hydrogen diffusivity rather than just from the corrosion behavior of bare metal in high temperature water. In other words, since discontinuous failure results from the presence of hydrogen, its behavior in the metal is worthy of consideration. With this in mind, an attempt has been made to calculate the theoretical life of a fuel element only as a function of the hydrogen generated at the fuel-water interface. The results of these calculations illustrate the effects of different variables upon hydrogen in the metal and their magnitude. This information can then be utilized in the design of a fuel element and as another experimental avenue for extending the life of the fuel.

For the purpose of calculation the theoretical life of a fuel element is defined as the exposure time until the solubility of hydrogen is reached at the surface of the uranium alloy; that is, the time for the start of precipitation of the hydrogen-rich phase. The fuel element was simulated by means of a two-dimensional analog from which the hydrogen distribution within the element could be determined along with the amount of hydrogen diffusing through the metal to the cladding.

An electrical analog was constructed of a clad, longitudinal slab cut from a fuel rod containing defects of various sizes as illustrated in Fig. 64. The slab considered corresponds in dimensions to the clad fuel specimens tested at Bettis Plant, i.e., 2.5 in. long and 0.37 in. high. The slab width is taken as 1 cm with the defect extending all the way across it. The diffusion of

hydrogen is assumed to be in accord with Fick's first law so that the current flowing through the network is proportional to the amount of hydrogen diffusing, the potential difference is proportional to the concentration difference, and the diffusion coefficient of the hydrogen is proportional to the reciprocal of the resistance.

The network of resistors was assembled with all of the resistors at the surface of the fuel element connected together at ground potential corresponding to a hydrogen content of zero at the fuel-clad interface. Saturation of sections of the cladding could then be simulated by breaking the ground connection at the surface. A voltage was applied to the defect corresponding to the solubility of hydrogen in uranium. The measured current entering the defect then corresponds to the maximum flow of hydrogen that the fuel element can handle by diffusion before precipitation occurs. Similarly the voltage may be adjusted so that the current flowing is equivalent to the amount of hydrogen generated at the defect by corrosion. This will yield the concentration of hydrogen throughout the fuel and the amount being absorbed by the cladding for any corrosion rate. The rate of hydrogen gettering is obtained by measuring the flow of current from the surface of the element to ground potential.

For a given size defect, approximately one-half of the hydrogen entering the fuel was absorbed by the cladding within a distance from the defect edge equal to half of the defect width. From the work of Gulbranson and Andrews[9] it was determined that the gettering rate of the cladding is greater than the rate of hydrogen leaving the specimen by diffusion. Therefore, the hydrogen concentration at the fuel-clad interface is zero as assumed in the analog. From the analog it was found that approximately 190 days are required to saturate a 30-mil cladding within 20 mils of a 40-mil defect for a corrosion rate of 0.2 mg/cm^2-hr.

As corrosion proceeds, the area of attack increases corresponding to the chosen corrosion rate, and the rate of hydrogen generation increases correspondingly. Eventually a time will be reached when the rate of hydrogen generation exceeds that which the fuel is capable of handling by diffusion to the cladding. At this point failure of the element is assumed to occur. That is, precipitation of the hydrogen-rich phase takes place. The corrosion lives discussed below have been calculated as a function of the increased area of attack with time.

Fig. 65 illustrates the theoretical corrosion life of a fuel element as a function of defect size for a hydrogen diffusivity of 10^{-5} cm^2/sec and a hydrogen solubility of 15 ppm. Fig. 66 illustrates a similar calculation for a diffusivity of 10^{-6} cm^2/sec. It should be noted that the corrosion lives are relatively insensitive to defect size for both cases. Such insensitivity has been noted in WAPD-127, Part II. Reducing the diffusivity by a factor of ten reduces the life by a factor slightly greater than ten. In Fig. 67 the diffusivity has been further reduced by a factor of ten to 10^{-7} cm^2/sec. Here it can be seen that the life for a small defect size has been further reduced by a factor of ten, but now the life is extremely sensitive to defect size. The effect upon corrosion life is seen to be much greater than the proportional change in diffusivity. Furthermore, the life is now extremely sensitive to defect size and corrosion rate. For diffusivities of 10^{-5} and 10^{-6} cm^2/sec the corrosion lives were approximately proportional to the reciprocal of the corrosion rate squared. That is, reducing the corrosion rate by one-half increased the life four-fold. The effect at $D = 10^{-7}$ cm^2/sec is much greater.

DECLASSIFIED

The variation of corrosion life with corrosion rate is more readily seen in Fig. 68 for a defect size of 37 mils.

The effect of hydrogen solubility upon corrosion life is shown in Fig. 69. Once again it is seen that the lower the diffusivity, the greater is the effect upon ultimate life.

It is evident from these calculations that factors other than corrosion rate should be considered in the selection of a corrosion resistant fuel alloy, at least for those alloys susceptible to discontinuous failure. Probably the most important additional factors are the diffusivity and solubility of hydrogen in the alloy.

Fuel element life as calculated above is in fair agreement with that actually observed during corrosion. Assuming a residual hydrogen concentration of 3 ppm in the fuel alloy, the calculated life for a 40-mil defected clad rod is about 4 yr with a corrosion rate of 0.2 mg/cm^2-hr. This calculation is based upon a hydrogen diffusivity of 3.3×10^{-6} cm^2/sec, a value which has just recently been determined and not yet verified.[5] The observed corrosion life for Zircaloy-clad U-Mo rods is in excess of 1 yr with the rods still in test. It is believed that the agreement between theoretical and actual corrosion lives is sufficiently close to justify the validity of this approach. These results strongly indicate that the premature corrosion failures noted in Part II were the result of improper fabrication techniques.

Although no tests were performed with claddings other than Zircaloy, the relative effectiveness can be compared on the basis of the analytical results. An electrical analog was constructed for a fuel element clad in a material that was not a hydrogen getter. The analog for this case is different from that previously considered because of the transient nature of the problem. For the element whose cladding does not getter hydrogen, the calculated life was 260 days for a 40-mil defect and a hydrogen diffusivity of 3.3×10^{-6} cm^2/sec. This may be compared to the 4-yr life for a similar element clad in Zircaloy. Note that for such diffusivities, Zircaloy-clad specimen life is almost independent of defect size; however, in case of specimens clad with a nongettering metal the corrosion life will be almost inversely proportional to defect size.

In addition to illustrating the effects of different variables upon corrosion life, the calculations just described could be extremely useful in determining the optimum geometry for a corrosion-resistant fuel element. The cylindrical fuel rod is not the best from the standpoint of corrosion life. A far better geometry would be a flat plate. In a thin, clad fuel plate the average diffusion path from a defect to the cladding is much shorter than in a cylindrical specimen. This shorter path results in a steep concentration gradient permitting the fuel to handle more hydrogen by diffusion. For a given corrosion rate it should be possible to calculate the required fuel and cladding thicknesses such that hydrogen absorption by the cladding can always keep up with or remain ahead of hydrogen generation due to the increased area of exposure. A fuel element could then be designed that would not fail discontinuously and whose life would be determined by the rate of general corrosive attack.

An additional factor that may shorten the life of actual clad fuel elements is their transformation during corrosion test with a consequent increase in corrosion rate. Such changes in corrosion rate are generally not observed in

UNCLASSIFIED

the testing of bare samples because discontinuous failure occurs first. In Zircaloy-clad samples note that reactor radiation, which (as shown in WAPD-127, Part IV) inhibits transformation, would be expected to improve fuel life.

The previous calculations assume a perfectly continuous bond between the fuel and cladding. If this bond is deteriorated by corrosion or improper fabrication, not only is the Zircaloy unable to function as a hydrogen getter, but also increased areas of the fuel are exposed to the corrodent; both these effects will decrease the experimentally observed corrosion lives.

Many of the factors affecting the corrosion behavior of bare samples will have only a second order effect on properly clad alloys. Segregation during melting was shown to be very harmful to bare sample corrosion lives. For clad samples, however, such segregation should be harmless unless it increases the corrosion rate or leads to premature phase transformation. This behavior has been confirmed experimentally in Part II where it is shown that homogenization of the fuel has little effect on the corrosion life of clad fuel elements. Likewise, heat treatment to obtain optimum dispersion of the hydride, etc. will have little effect on Zircaloy-clad fuel element corrosion lives where hydrogen is absorbed by the cladding rather than by the fuel. On the other hand, such effects would be very important in fuel elements clad with nongettering metals such as aluminum. Of course, total life, even of a Zircaloy-clad gamma-phase alloy, will be increased to the extent of the increased failure lifetime of bare samples beyond the calculated time at which hydrogen saturation of the fuel occurs. Measures such as addition of hydrogen depolarizers to fuel or water should also increase life in direct proportion to the extent to which they decrease the fraction of the corrosion hydrogen absorbed by the fuel.

V. SUMMARY AND CONCLUSIONS

The factors affecting corrosion resistance both of bare and of clad uranium-base alloys have been reviewed and a mechanism proposed for their corrosion behavior.

For unclad gamma-phase uranium alloys exposed to a high temperature water corrodent, it is proposed that the corrosion rate is determined primarily by the oxidation of the alloy by water. This behavior is contrary to that of alpha uranium in which the corrosion rate is primarily determined by the formation and subsequent oxidation of a nonadherent hydride layer. In gamma-phase alloys the hydrogen released by the corrosion reaction, rather than forming the thermodynamically stable UH_3 phase, dissolves (at least in part) in the base metal where it precipitates as a metastable hydride. The amount of hydrogen absorbed by the metal and hence precipitating as the metastable hydride may be markedly reduced by the addition of hydrogen depolarizers such as nickel or platinum to the water or to the metal. Similarly the amount of absorbed hydrogen may be reduced by introducing sinks that preferentially absorb hydrogen. Both alpha uranium and zirconium were shown to be suitable sinks. Precipitated hydride hardens and embrittles the matrix and by its preferential corrosion eventually leads to discontinuous failure. The hydride may be made to precipitate in a less harmful manner by heat treatments which precipitate nucleating and hardening impurities. The mode of the precipitation is shown to be sensitive to stress; in fact, the assumption of elastic stress as contributing to hydride precipitation is considered necessary to explain the distribution of the precipitate during corrosion.

In order to apply a gamma-phase fuel alloy as a fuel element material, it is necessary primarily to reduce the amount of hydrogen absorbed by the fuel. This can be done by cladding the fuel with a zirconium-base alloy. Under such conditions it has been shown that fuel element lives in excess of 4 years should be obtainable with properly fabricated fuel elements before they are subject to corrosion failure. Optimum fuel element corrosion life can be achieved by

(1) decreasing the general corrosion rate,
(2) increasing the hydrogen solubility,
(3) increasing the hydrogen diffusion rate, and
(4) maintaining a proper clad-fuel bond.

For uranium-base alloys such as U_3Si that do not form a hydride during hot water corrosion, use of a Zircaloy clad is unnecessary. Therefore, the development of alternate cladding materials such as aluminum for corrosion resistant fuel elements is predicated upon the development of uranium-base alloys that do not corrode by a hydride mechanism. In addition to U_3Si both zirconium-uranium alloys and the strained alpha uranium-base alloys do not appear to corrode by a hydride mechanism.

DECLASSIFIED

VI. REFERENCES

1. R. E. Rundle, "The Hydrogen Positions in Uranium Hydride by Neutron Diffraction," J Am Chem Soc 73, 4172-74 (1951).

2. R. N. R. Mulford, F. H. Ellinger, and W. H. Zachariasen, "A New Form of Uranium Hydride," J Am Chem Soc 76, 297-98 (1954).

3. J. J. Katz and E. Rabinowitch, "The Chemistry of Uranium," National Nuclear Energy Series Div VIII, Vol. 5.

4. J. Markowitz, Bettis Plant, Private Communication.

5. M. Hill, Westinghouse Research Laboratory, Private Communication.

6. H. A. Saller and F. A. Rough, "Compilation of U. S. and U. K. Uranium and Thorium Constitutional Diagrams," Battelle Memorial Institute Report, BMI-1000, June 1955.

7. M. L. Perlman and S. I. Weissman, "Preparation of Compacts of High Density Uranium Hydride," U. S. 2,558,377

8. J. P. Howe and T. O. Jones, "Coatings and Corrosion," National Nuclear Energy Series Div VIII, Vol. 6a.

9. Progress Report ANL-5514

10. R. J. Van Thyne, "Research on Uranium-Base Alloys, Fingal Report," ARF-B 049, August 31, 1955.

11. E. A. Gulbransen and K. F. Andrew, "Solubility and Decomposition Pressures of Hydrogen in Alpha-Zirconium," Trans Am Inst Mining Met Engrs 203, 136-44 (1955).

UNCLASSIFIED

APPENDIX

Bibliography of Reports on the Development of a Corrosion Resistant Fuel Alloy for the PWR.

Armour Research Foundation: Task 6 of Subcontract No. 73-(14-309) - Research on Uranium-Base Alloys

Letter Reports Nos. 1-21 Feb. 22, 1953 - June 13, 1955

Final Report-Part I "Transformation Kinetics of U-Base Alloys"

Part II "Preparation of Alloys and Corrosion Data"

Battelle Memorial Institute: Subcontract No. 14-383 - Task 1 - "Compositional Variations in U-Mo Alloys"

Task 2 - "Bonding Behavior of U-Mo Alloys"

Monthly Progress Reports - Nov. 1954 - Sept. 1955 Final Report

Nuclear Metals, Inc.: Subcontract Supervised by Metallurgy Subdivision "Properties of U-Si Alloys" Monthly Reports Feb. 1955 - Dec. 1955.

U. S. Bureau of Mines: Subcontract Supervised by Metallurgy Subdivision "Development of U-Nb Alloys with Improved Hot Water Corrosion Resistance"

USBM-C-63 May 2, 1955

USBM-C-79 July 12, 1955

Sylvania: Subcontract No. 14-384 "Bond Strengths and Corrosion Resistance of Zircaloy-2 Clad U-Si Epsilon Alloy"

Monthly Progress Reports, Dec. 3, 1954 - May 3, 1955 Final Report

WAPD-36 - "Dilatometric Investigation of Zr-U, Zr-O, and Zr-N Alloys," R. K. McGeary, July 17, 1951

WAPD-MM-227 - "Corrosion Resistance of Uranium Alloys," R. K. McGeary and W. M. Justusson, June 5, 1953

WAPD-MDM-24 - "Corrosion of Zr-U Alloys," D. E. Thomas, Dec. 29, 1954

DECLASSIFIED

WAPD-T-195 - "Report of the Third Annual Project Corrosion Symposium," D. E. Thomas, August 4, 1954

WAPD-T-218 - "Characteristics of Corrosion Failure of U-Base Gamma Phase Alloys in High Temperature Water," W. A. Bostrom, R. A. Wolfe, E. K. Halteman, R. K. McGeary; April 22, 1955

WAPD-T-208 - "The Crystal Structure of U_2Mo," E. K. Halteman, Sept. 1955

WAPD-T-260 - "The Melting and Fabrication of Binary Alloys of Uranium with Molybdenum, Niobium, and Silicon," F. R. Lorenz, W. B. Haynes, E. S. Foster; June 27, 1955

WAPD-130 - "The Fabrication of Experimental PWR Fuel Rods by the Drawing of Co-Extruded Round Rods," J. G. Goodwin and R. W. Tombaugh, July 15, 1955

WAPD-133 - "The Fabrication of Fuel Rods of Various Uranium Alloys with Zircaloy-2 Cladding Having Intermediate Metallic Layers Between the Fuel and the Cladding," W. B. Haynes, October 29, 1955

UNCLASSIFIED

TABLE I

EFFECT OF ANNEALING AT 900°C ON THE CORROSION LIFE OF U-12 w/o Mo EXTRUSIONS (Unclad Samples in 650°F Water)

Extrusion	Corrosion Life (days) As Extruded	Corrosion Life (days) 900°C-24 hr-WQ
J 854	21-28	35-42
J 875	14-21	35-49
J 879	21-28	28-42
Mo2Cl-16	14-21	28-35
Mo2Cal-7	14-21	42-56
Mo3al-1	14-28	28-42
Mo3al-3	7-21	28-42
MM431	28-42	42-56
Average	21	39

DECLASSIFIED

TABLE II

EFFECT OF ANNEALING TIME AND TEMPERATURE ON THE CORROSION OF EXTRUDED U-Mo ALLOYS

Condition	Corrosion Life in 650°F Water (days)	
	Extrusion No. 1101-1-13 U-11.2 w/o Mo	Pre-Extrusion No. J959 U-12 w/o Mo
As-extruded	14-21	28-35
600°C - 24 hr	7-14	14-21
- 72	7-14	21-28
-168	7-14	14-28
-336	7-14	14-21
-504	7-14	14-21
700°C - 24	14-21	21-28
- 72	14-21	21-35
-168	14-21	14-28
-336	14-21	21-28
-504	14-21	21-28
800°C - 4	28-42	42-49
- 24	28-42	28-35
- 72	42-56	35-42
-168	28-35	28-35
-336	28-35	28-35
900°C - 1/2	>105	49-56
- 4	>105	42-49
- 24	49-56	28-35
- 72	70-77	35-42
-168	21-28	21-28
1000°C - 1/2	>105	49-56
- 4	>105	--
24	35-49	35-42
72	28-35	--
168	28-35	28-35

DECLASSIFIED

TABLE IV

EFFECT OF LOW TEMPERATURE ANNEALING ON
THE CORROSION PROPERTIES OF EXTRUDED U-12 w/o Mo

Days at 650°F:	0	3	7	14	21	28	35	42	49	56	63	70	77
Corrosion Rate (mg/cm^2-hr)													
As Extruded		0.32	0.30	0.36	0.47	0.67	1.4	Dis.					
900°C - 24 hr - WQ		0.11	0.16	0.22	0.29	0.43	1.0	Dis.					
WQ + 343°C - 5 wk - WQ		0.24	0.23	0.24	0.28	0.35	0.93	Dis.					
Extr. + 400°C - 5 wk - WQ		0.38	0.46	0.60	0.68	0.75	0.85	C					
WQ + 400°C - 5 wk - WQ		0.06	0.06	0.06	0.06	0.08	0.11	0.19	0.38	0.53	0.68	1.0	Dis.
Hydrogen Content (ppm)													
As Extruded	2.7		57	154		676							
900°C - 24 hr - WQ	3.2		38	102		410							
WQ + 343°C - 5 wk - WQ	4.4		48	94		282							
Extr. + 400°C - 5 wk - WQ	2.9		235	581		61							
WQ + 400°C - 5 wk - WQ	2.3			41		114		659					
Hardness (DPH)													
As Extruded	318		353	384		419							
900°C - 24 hr - WQ	318		336	371		396							
WQ + 343°C - 5 wk - WQ	321		370	377		428							
Extr. + 400°C - 5 wk - WQ	461		478	525		541							
WQ + 400°C - 5 wk - WQ	458			476	483	491		509					

TABLE V

THE EFFECTS OF VARIOUS ANNEALING ATMOSPHERES AND CORROSION TEST TIME UPON THE CORROSION PROPERTIES OF A U-12 w/o Mo ALLOY

Days in 650°F Water		As Ext. H_1	Vacuum H_2	Tank He H_3	Tank H_2 H_4	UH_3-H_2 H_5	O_2 H_9
0	H_2 Conc.	1.1	1.6	0.8	12.6	6.4	0.21
	DPH 31 kg	309	296	302	316	302	288
3	H_2 Conc.	65.1	26.5	17.7	16.6	29.0	29.5
	Corr. Rate	0.87	0.26	0.14	0.11	0.25	0.22
	Total Corr.	62.7	18.7	10.0	7.8	17.9	15.9
	DPH 30 kg	331	315	312	315	318	314
7	H_2 Conc.	386	93	41	46	63	65
	Corr. Rate	1.15	0.40	0.19	0.15	0.31	0.26
	Total Corr.	193	68	31	26	52	44
	DPH 30 kg	355	331	326	333	334	330
14	H_2 Conc.	1210	420	115	105	144	208
	Corr. Rate	3.25	0.64	0.26	0.23	0.41	0.36
	Total Corr.	1092	215	87	77	137	121
	DPH 31 kg	425	352	350	354	357	350
21	H_2 Conc.	Disint.	886	338	280	474	467
	Corr. Rate		0.98	0.38	0.36	0.53	0.47
	Total Corr.		494	191	181	267	238
	DPH 30 kg		379	371	366	381	371
28	H_2 Conc.,		Disint.	634	708	1486	1333
	Corr. Rate			0.59	0.57	0.88	0.71
	Total Corr.			396	383	596	477
	DPH 30 kg			386	387	416	408
35	H_2 Conc.			1441	1296	Disint.	Disint.
	Corr. Rate			0.97	1.09		
	Total Corr.			815	916		
	DPH 30 kg			421	429		
42				Disint.	Disint.		

TABLE VI

CORROSSION RATE OF U-12 w/o Mo ANNEALED IN VACUUM

	mg/cm^2-hr after			
Sample	3 days	7 days	14 days	21 days
A	-0.15	-0.17	-0.76	disintegrated
B	-0.10	-0.18	-0.40	disintegrated
C	-0.16	-0.18	-1.80	disintegrated
D	-0.15	-0.17	-0.42	disintegrated

UNCLASSIFIED

TABLE VII

CORROSION PROPERTIES IN 650°F WATER OF SOME GAMMA-QUENCHED U-Mo-Cr AND U-Mo-Ti ALLOYS

Composition, w/o	Corrosion Rate (mg/cm^2-hr) 7 days	56 days	112 days	Failure Period (days)
U-7 Mo	22*	-	-	1 - 7
	7.5*	-	-	1 - 7
U-7 Mo-0.3 Cr	0.29	-	-	7 - 14
	0.71	-	-	7 - 14
U-7 Mo-0.6 Cr	12*	-	-	1 - 7
	6*	-	-	1 - 7
U-7 Mo-1.0 Cr	0.02	-	-	28 - 42
	0.03	0.03	0.03	154**
U-7 Mo-0.3 Ti	2.3*			1 - 7
	8.5	-	-	7 - 14
U-7 Mo-0.6 Ti	0.40	-	-	7 - 14
	0.35	0.15	0.10	154**
U-7 Mo-1.0 Ti	0.25	-	-	42 - 56
	0.28	0.06	0.06	154**
U-9 Mo	0.16	-	-	14 - 28
	0.19	-	-	14 - 28
U-9 Mo-0.3 Cr	0.07	-	-	14 - 28
	0.09	-	-	14 - 28
U-9 Mo-0.6 Cr	0.04	0.33	0.39	126 - 140
	0.06	0.03	0.05	154**
U-9 Mo-1.0 Cr	0.09	-	-	28 - 42
	0.07	-	-	14 - 28
U-9 Mo-0.3 Ti	0.25	0.06	0.08	140 - 154
	0.25	-	-	14 - 28
U-9 Mo-0.6 Ti	0.32	0.08	0.41	112 - 124
	0.36	0.16	-	56 - 70
U-0 Mo-1.0 Ti	0.28	-	-	42 - 56
	0.29	0.19	-	70 - 84

* One day rate
** Discontinued

DECLASSIFIED

TABLE VIII

OBSERVATIONS ON MISCELLANEOUS U-Mo-Cr AND U-Mo-Ti TERNARY ALLOYS THAT HAVE BEEN CORROSION TESTED FOR 154 DAYS IN 650°F WATER.

Composition w/o	Weight Loss mg/cm^2	Hydrogen ppm	% Absorbed	Hardness DPH
U-7 Mo-0.6 Ti	308	196	7.5	590
U-7 Mo-1.0 Ti	242	205	9.9	625
U-7 Mo-1.0 Cr	144	93	7.3	625
U-9 Mo-0.6 Cr	209	151	8.7	536

TABLE IX

CORROSION BEHAVIOR OF ARC MELTED U-Mo AND U-Mo-Pt ALLOYS IN 650°F WATER
(X = weight loss in mg/cm^2-hr; Y = failure time in days)

	9 w/o Mo		9 w/o Mo 0.3 w/o Pt		9 w/o Mo 0.6 w/o Pt		9 w/o Mo 1.2 w/o Pt		12 w/o Mo		12 w/o Mo 0.3 w/o Pt		12 w/o Mo 0.6 w/o Pt	
	X	Y	X	Y	X	Y	X	Y	X	Y	X	Y	X	Y
As Cast	0.58	14	0.12	84	0.10	168*	0.08	168*	0.22	28	0.15	112	0.11	154
	0.51	14	0.11	70	0.10	168*	0.08	224*	0.30	28	0.15	112	0.11	154
γQ	0.13	14	0.02	84	0.014	70	0.006	112	0.16	42	0.16	112	0.13	154*
	0.15	14	0.02	42	0.014	84	0.008	112	0.26	42	0.16	154*	0.13	210*
γQ + 400°C 7 days	0.52	7	0.32	14	0.015	56	0.003	98	0.06	28	0.063	98	0.031	154*
	0.93	7	0.24	14	0.015	28	0.003	84	0.24	1	0.063	154*	0.031	182
γQ + 400°C 35 days	--	0	--	0	--	0	12	1	0.05	28	+0.012	1	+0.014	1
	--	0	--	0	--	0	25	1	0.08	28	+0.008	7	+0.014	1
γQ + 500°C 2 days	--	0	--	0	--	0	0.03	14	0.46	28	0.07	140	0.04	14
	--	0	--	0	--	0	0.03	14	0.13	56	0.08	154	0.07	140
γQ + 500°C 7 days	--	0	--	0	--	0	--	0	4.2	7	0.06	14	0.03	70
	--	0	--	0	--	0	--	0	3.4	7	0.18	14	0.08	84
γQ + 500°C 21 days	--	0	--	0	--	0	--	0	1.6	1	0.26	1	0.25	7
	--	0	--	0	--	0	--	0	4.3	7	0.42	1	0.83	7

* Removed before failure for examination

TABLE X

POST TEST OBSERVATIONS ON SOME U-Mo AND U-Mo-Pt SPECIMENS

TESTED IN 650°F DEGASSED WATER

Composition w/o	Condition	Test Time days	Wt. Loss mg/cm^2	H_2 ppm	H_2 %	DPH	Metallographic Observations
9 Mo-0.6 Pt	As Melted	168	440	140	3.6	541	Needles Clearly Seen. Concentration follows the coring
9 Mo-0.6 Pt	As Melted	168	300	170	6.7	543	Ditto
9 Mo-1.2 Pt	As Melted	168	224	39	1.9	517	Ditto
9 Mo-1.2 Pt	As Melted	224	255	87	4.1	---	Ditto
12 Mo-0.3 Pt	γQ	154	420	13	0.3	443	No needles - Grain boundary etching
12 Mo-0.6 Pt	γQ	154	327	14	0.5	356	Ditto
12 Mo-0.6 Pt	γQ	210	389	15	0.4	---	Ditto
12 Mo	γQ	25	235	368	20	400	Dense hydride needles distributed throughout the matrix
12 Mo-0.3 Pt	γQ + 400°C - 7 days	154	226	13	0.7	472	No needles - Grain Boundary Etching
12 Mo-0.6 Pt	γQ + 400°C - 7 days	154	171	11	0.7	481	Ditto

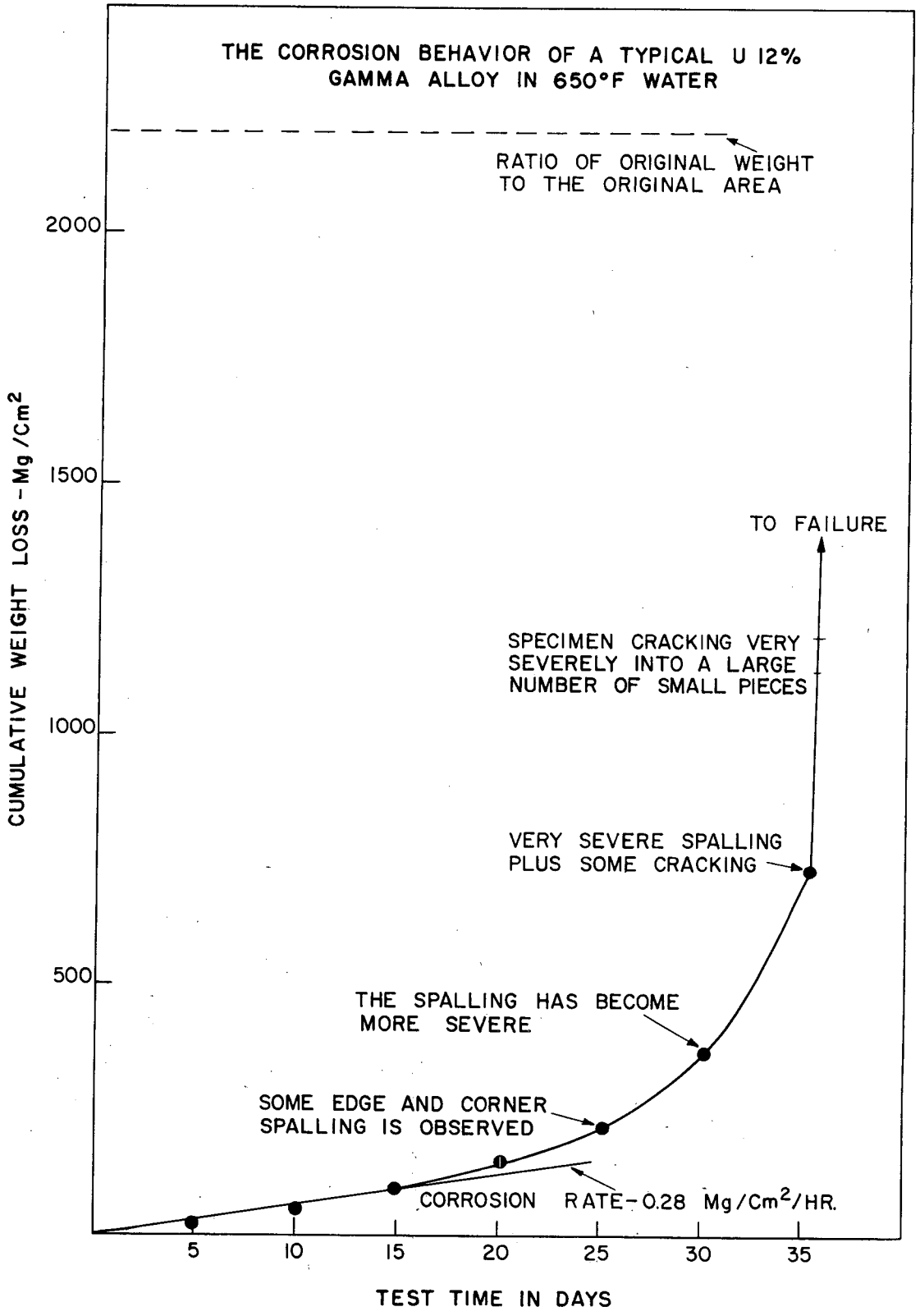

Fig. 1. Typical corrosion behavior of a U-12 w/o Mo alloy in 650°F water

Neg 17421-24

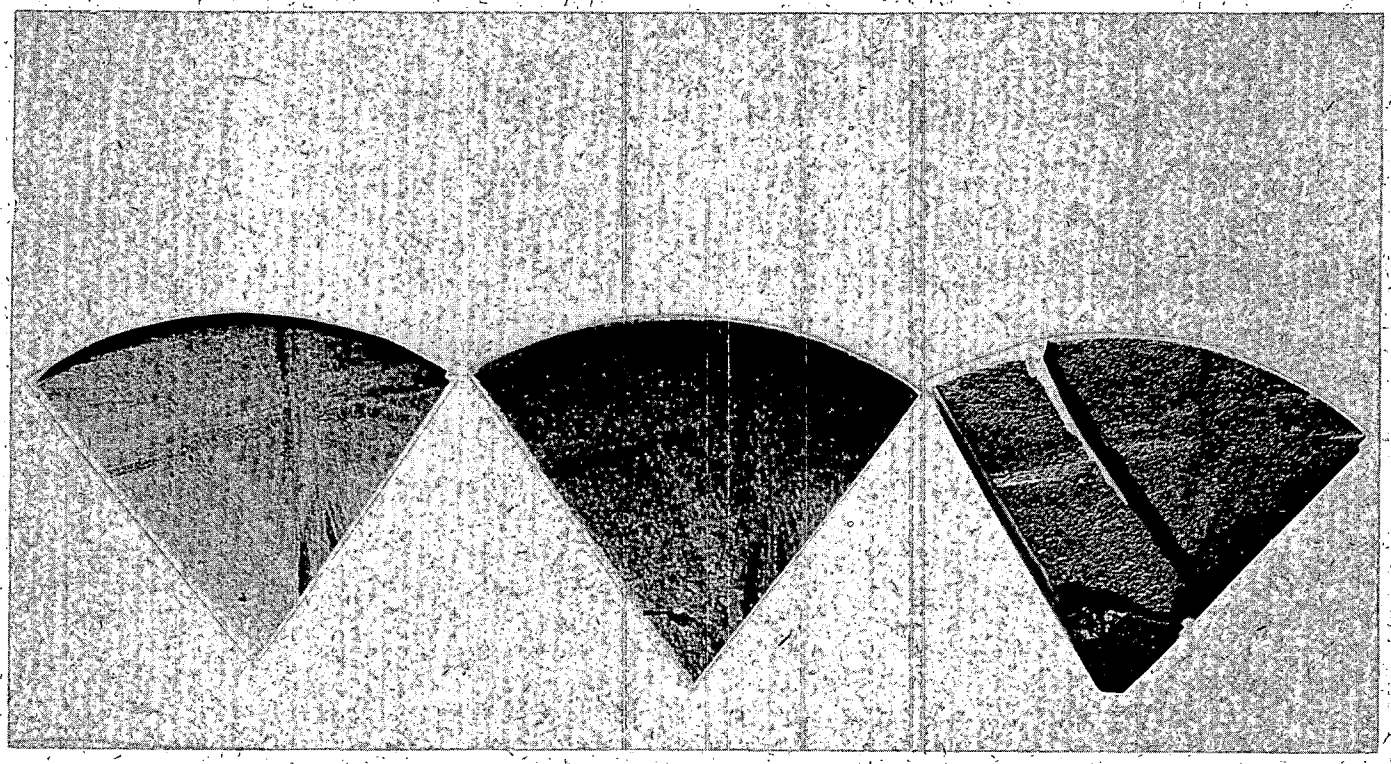

7 days 14 days 28 days

Fig. 2. Discontinuous failure of a U-9 w/o Mo alloy upon exposure to 650°F water

Neg 17420-51

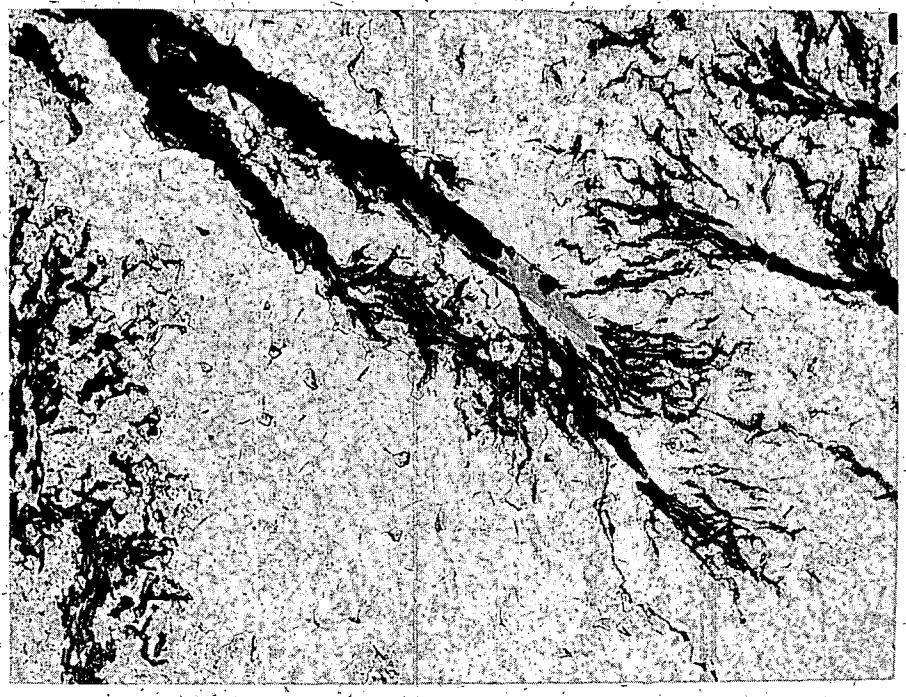

Neg 17420-9 100X

Fig. 3. Gamma phase U-9 w/o Mo alloy after 115 days exposure to 650°F water (unetched)

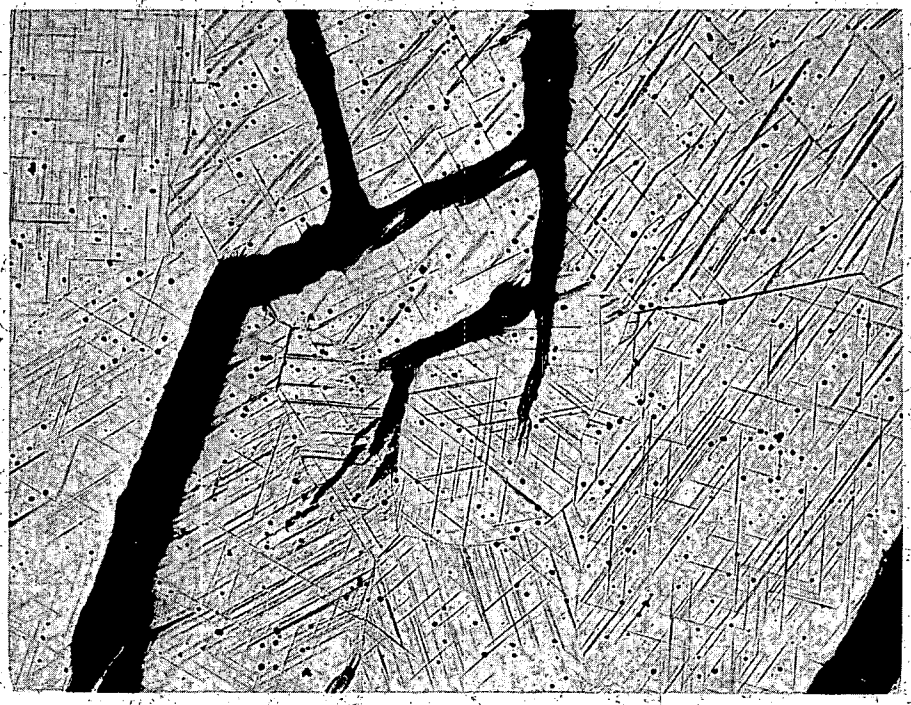

Neg. 17420-10 100X

Fig. 4. Gamma-phase U-9.8 w/o Mo alloy after 28 days exposure to 650°F water

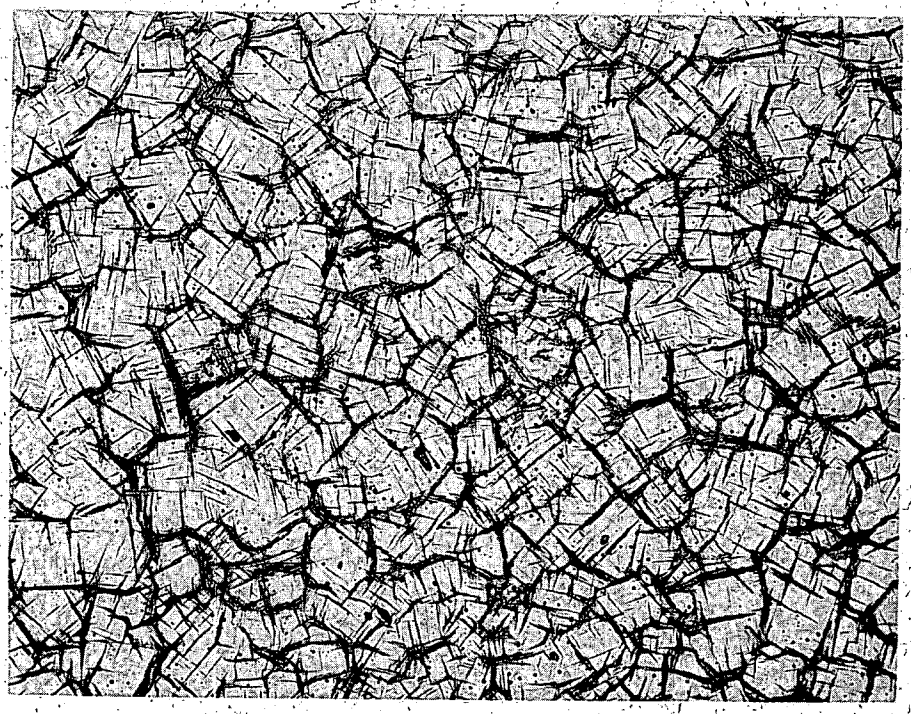

Neg 17420-11 100X

Fig. 5. U-12 w/o Mo alloy, water quenched after 24 hr at 900°C and corrosion tested 14 days in 650°F water

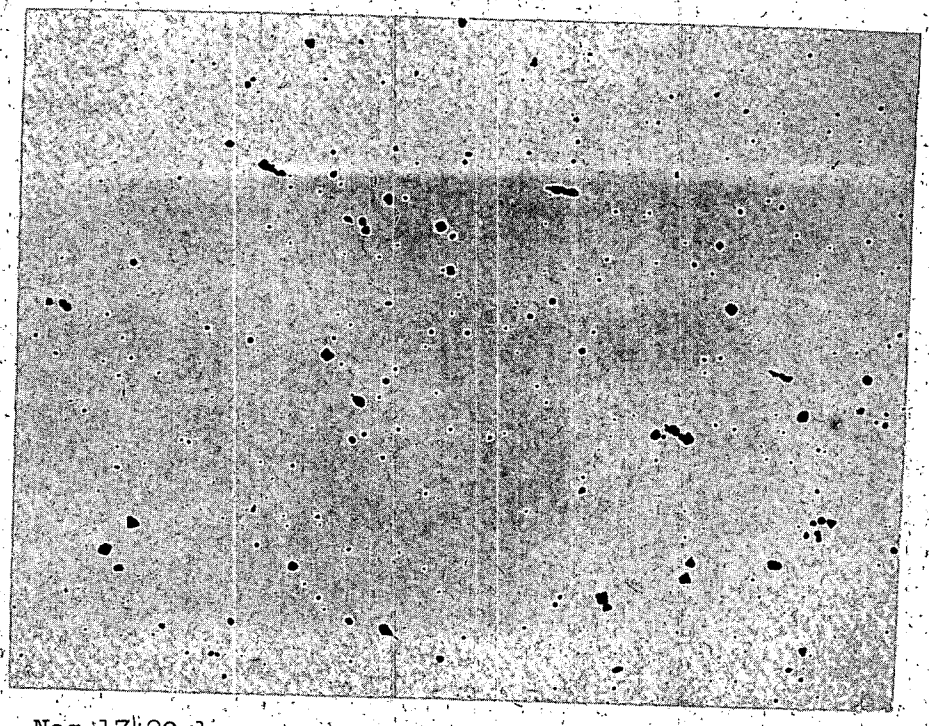

Neg 17420-1 250X

Fig. 6. U-12 w/o Mo alloy, water quenched after 24 hr at 900°C

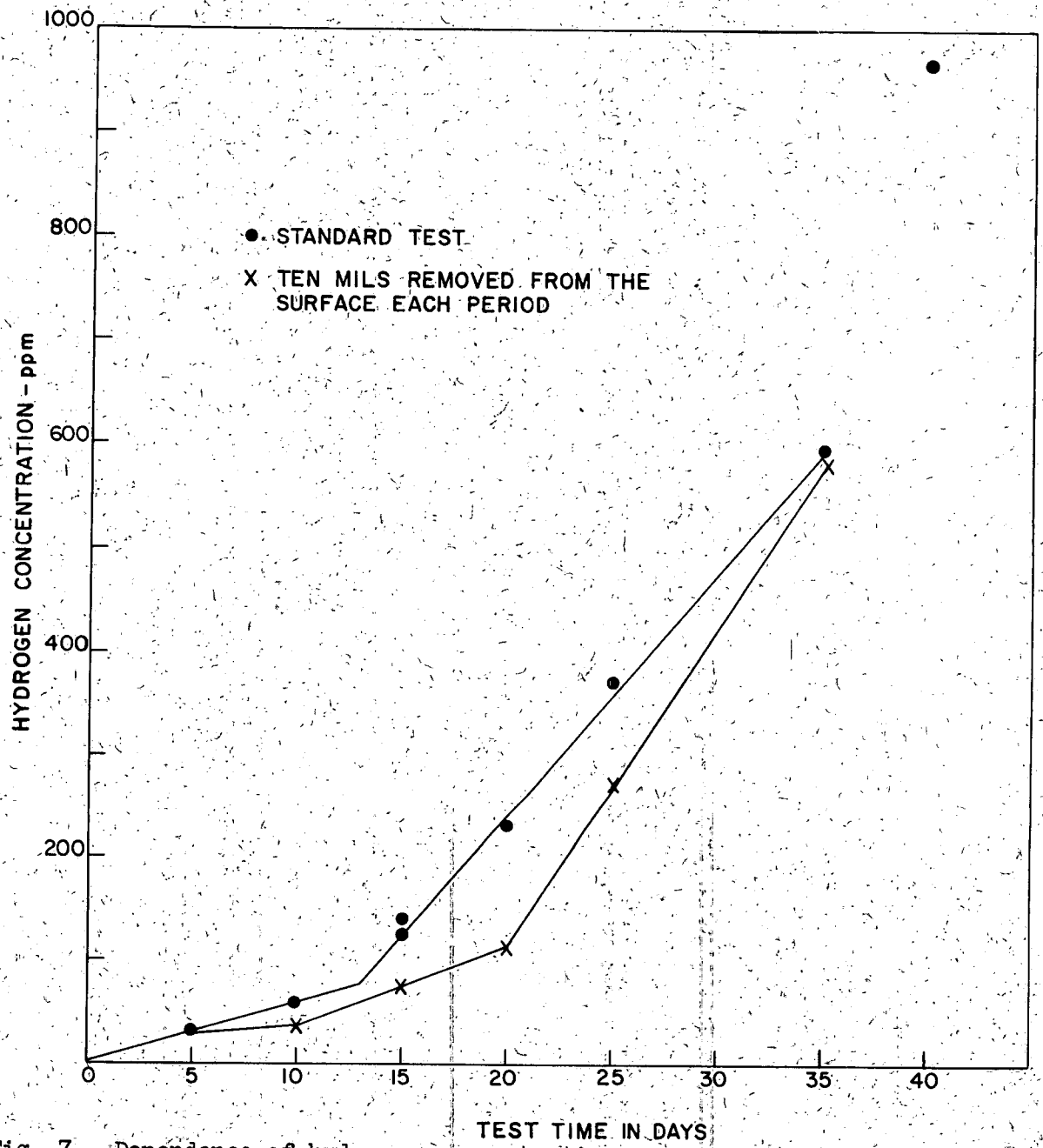

Fig. 7. Dependence of hydrogen concentration upon exposure time for a gamma-quenched U-12 w/o Mo alloy, corrosion tested in 650°F degassed water

Neg. 17421-18

DECLASSIFIED

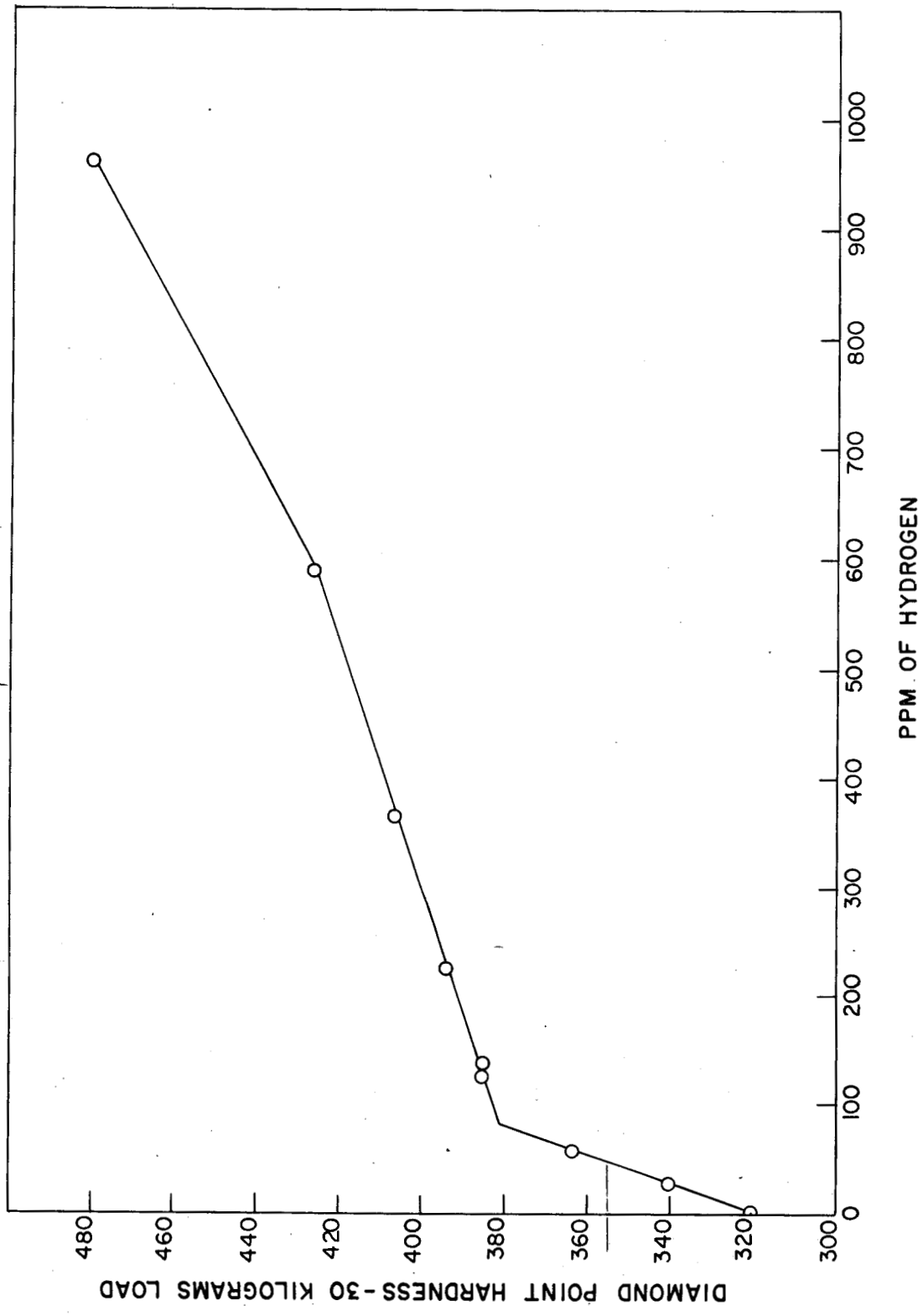

Fig. 8. Hardness of U-12 w/o Mo as a function of hydrogen concentration after corrosion testing in 650°F degassed water

Neg 17421-15

64

DECLASSIFIED

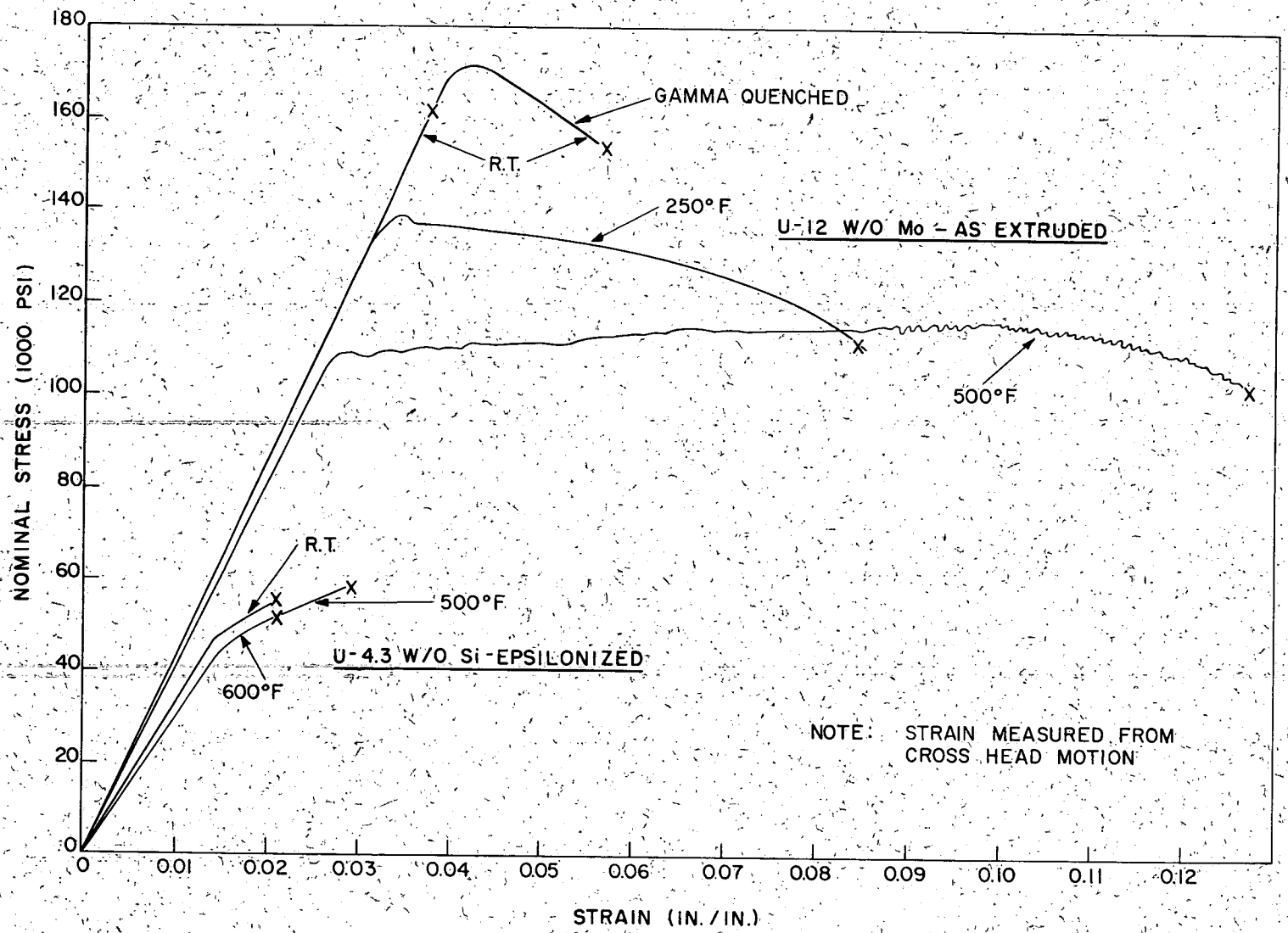

Fig. 9. Stress-strain curves for a U-12 w/o Mo alloy and a U-4.3 w/o Si alloy
Neg 17421-23

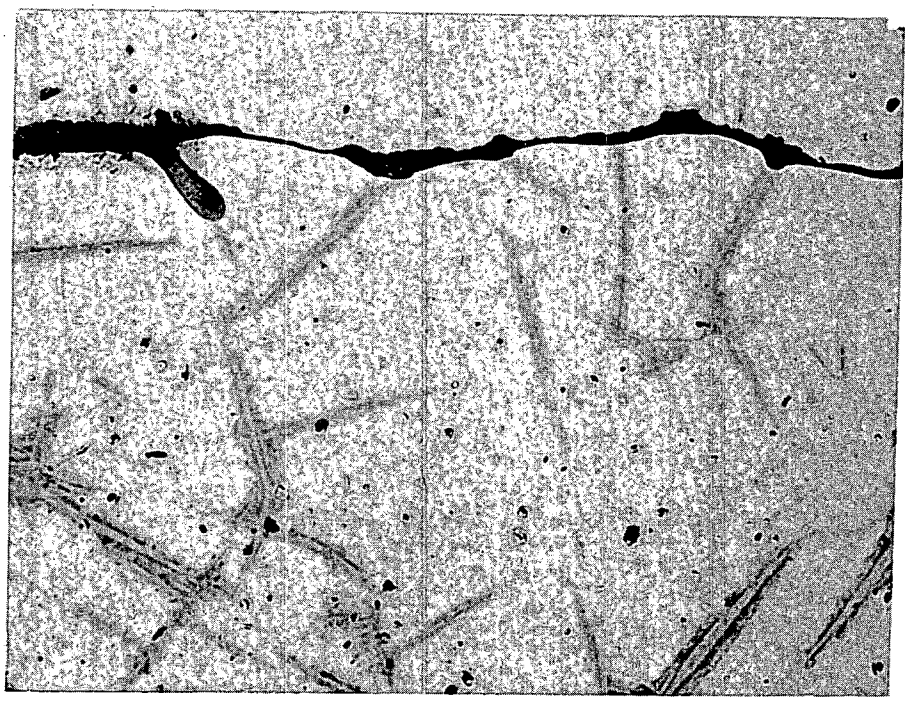

Surface supporting material

U-Mo specimen

Neg 17420-42 500X

Fig. 10. A mechanically polished section (unetched) of a corrosion tested specimen showing an oxide "finger" pentrating in from the surface

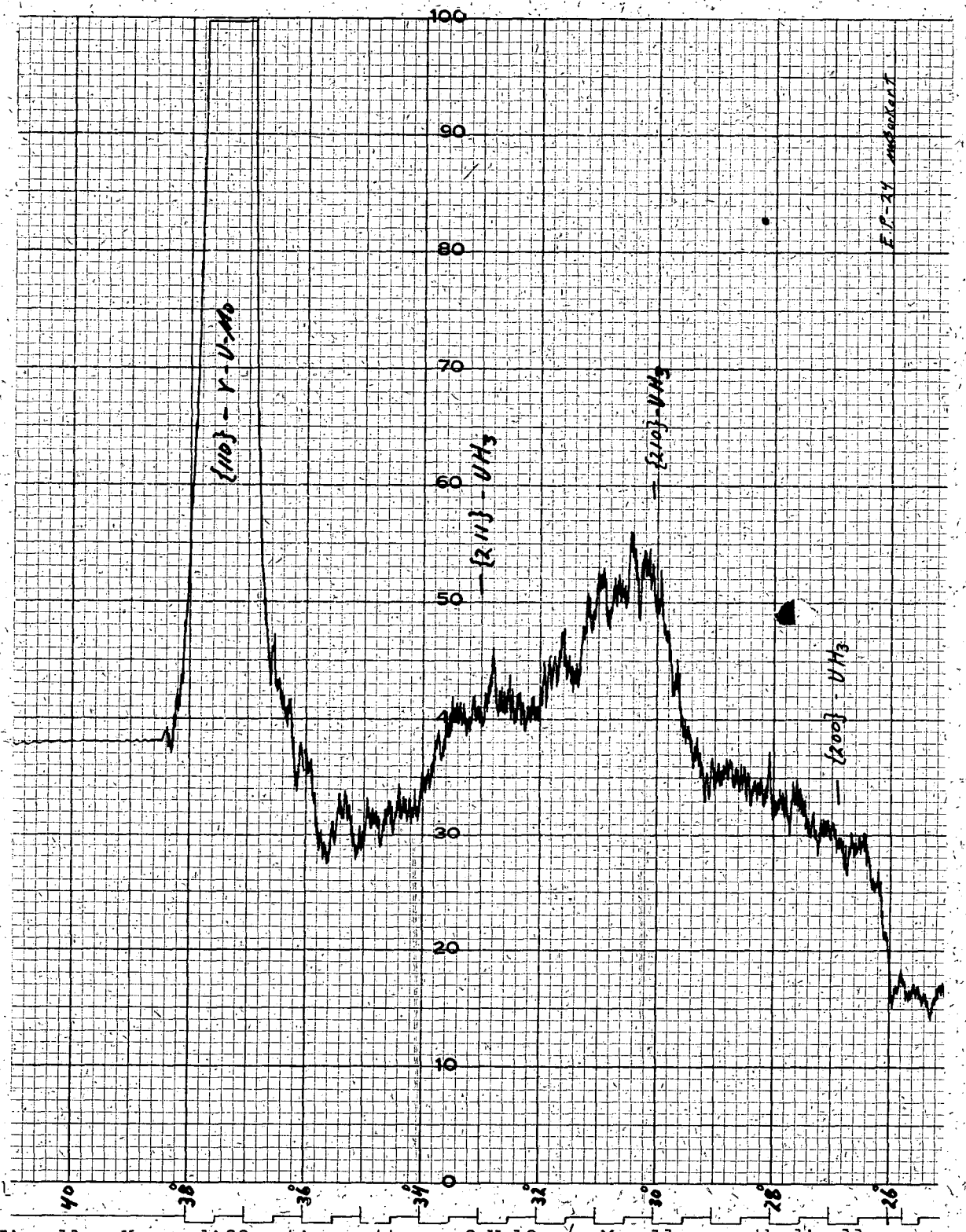

Fig. 11. X-ray diffraction pattern of U-10 w/o Mo alloy, cathodically hydrided for 1 wk, at 100°C

Neg 17421-1

UNCLASSIFIED

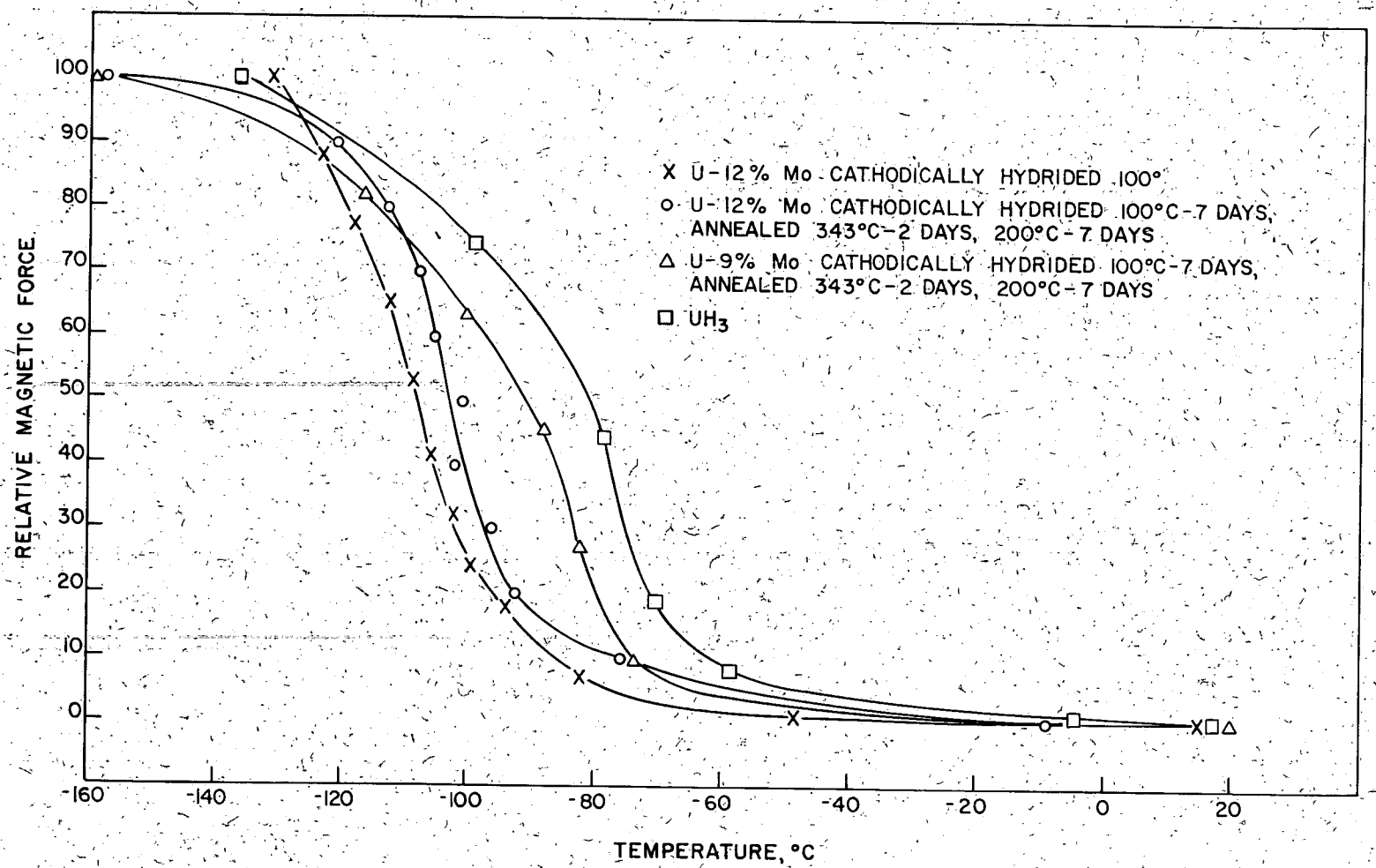

Fig. 12. Relative magnetic force as a function of temperature

Neg 17421-7

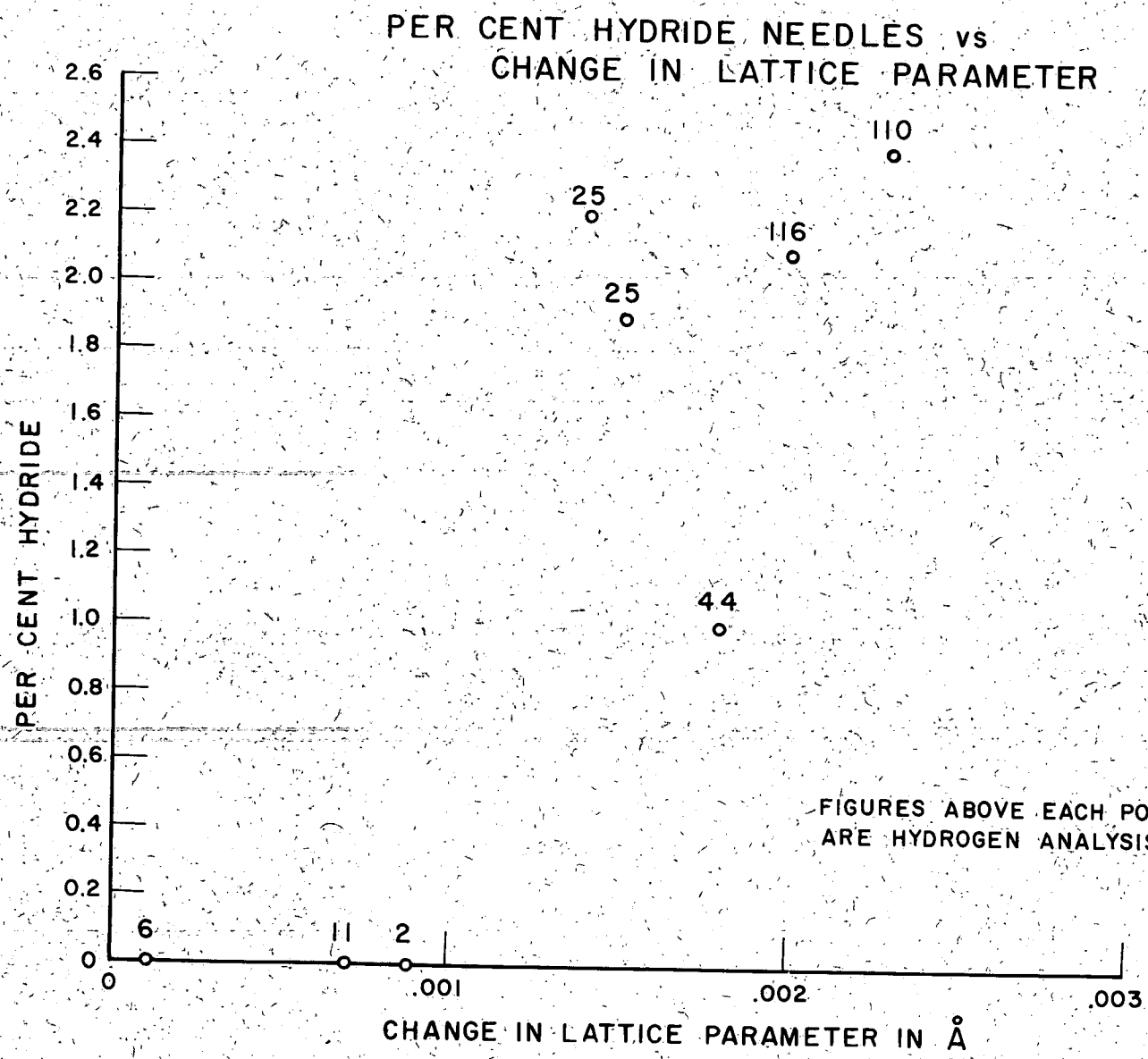

Fig. 13. Change in lattice parameter as a function of hydrogen content in a U-10 w/o Mo alloy

Neg 17421-19

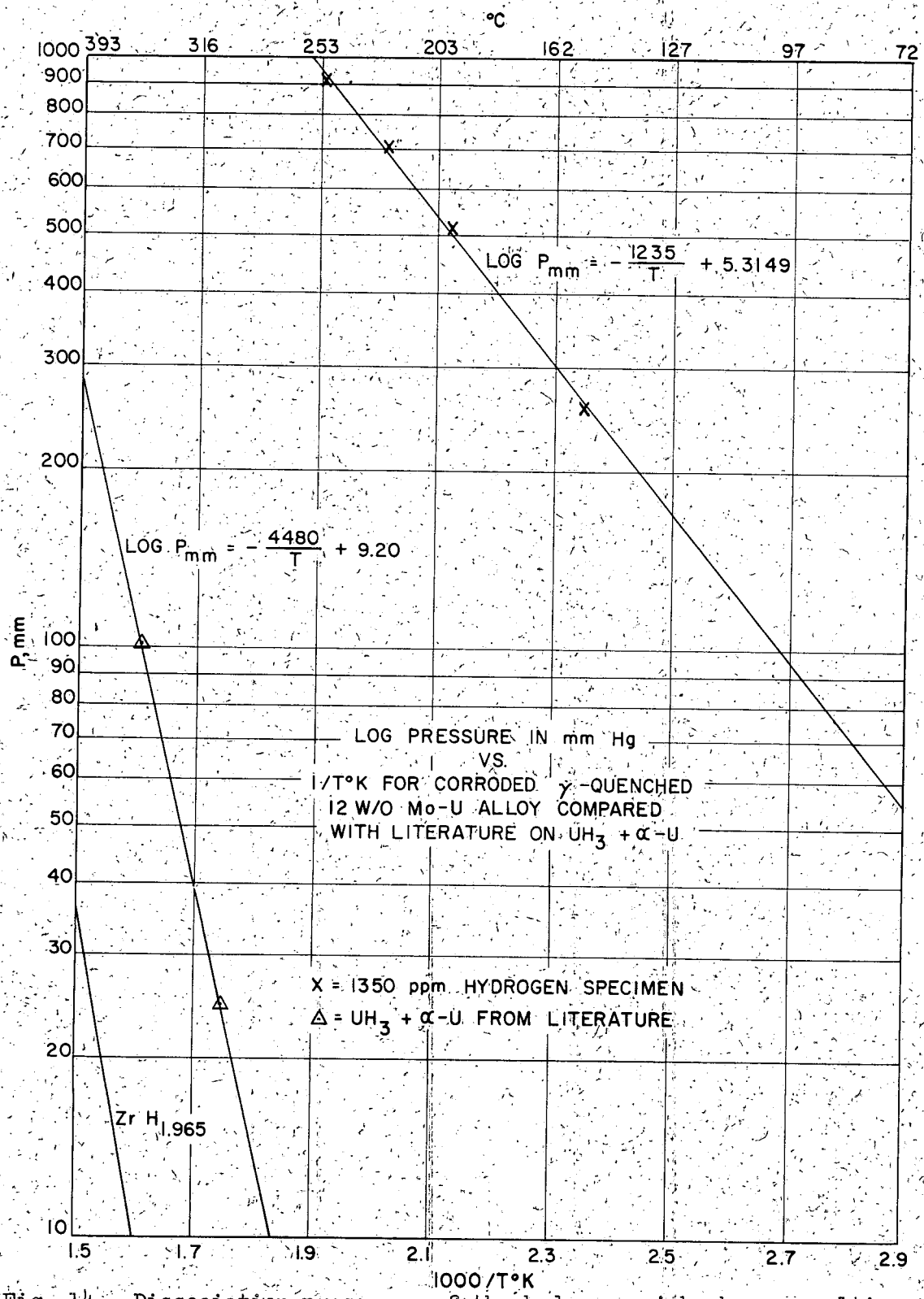

Fig. 14. Dissociation pressures of the hydrogen-rich phase resulting from corrosion, UH_3 and Zr $H_{1.965}$

Neg 17421-2

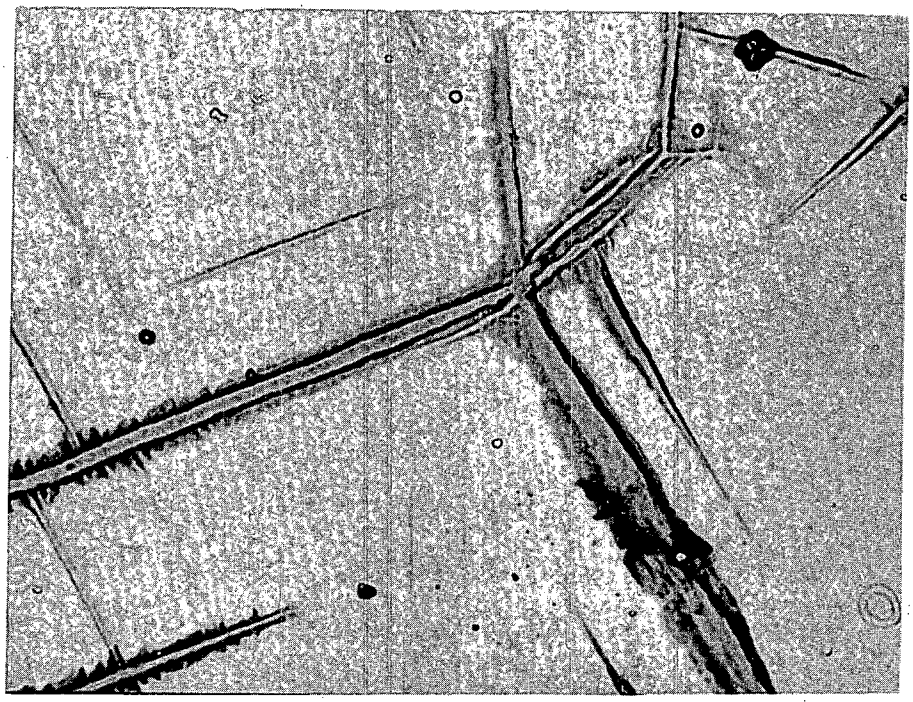

Neg 17420-45 1000X

Fig. 15. Gamma-quenched U-12 w o Mo specimen, corrosion tested 28 days in 650°F water indicating possible two-phase structure of plates

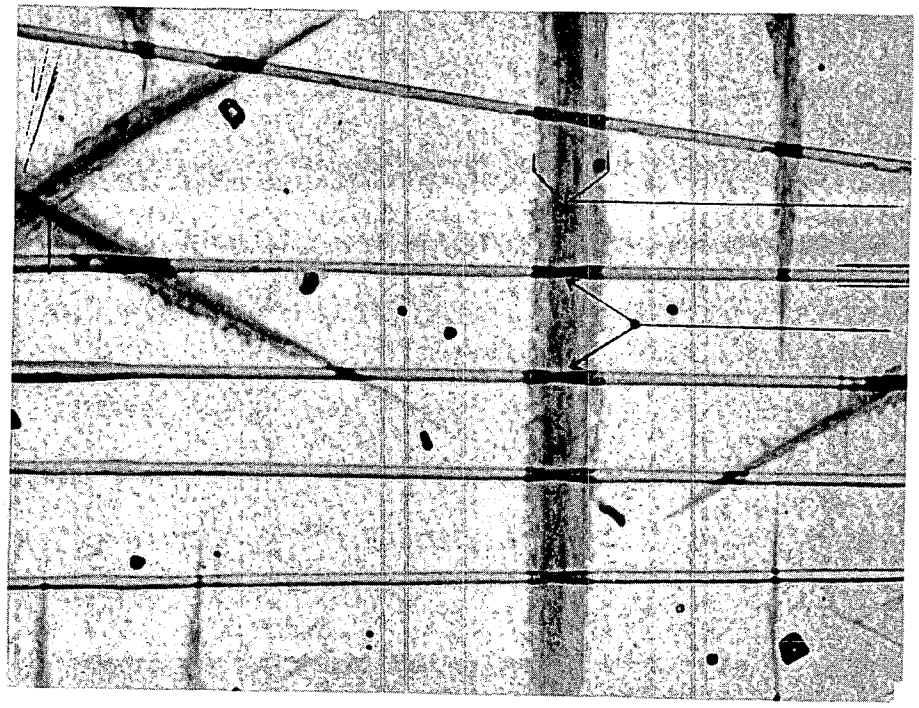

Neg 17420-33 1000X

Fig. 16. Diamond scratch widths indicating relative hardness of phases shown in Fig. 15

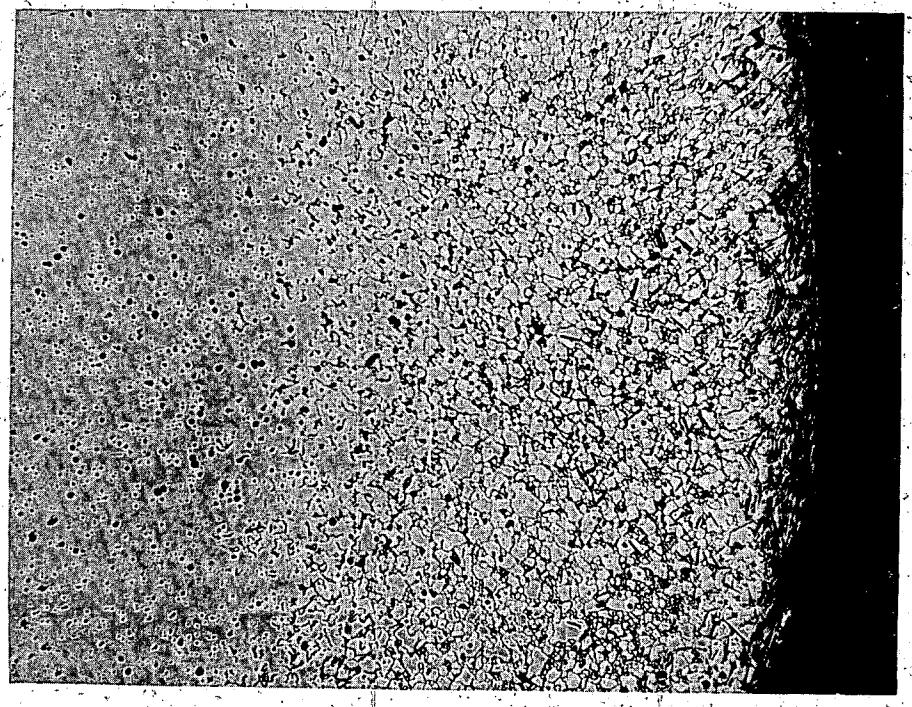

Neg 17420-16 75X

Fig. 17. U-12 w/o Mo, vacuum annealed at 900°C for 24 hr, then cathodically hydrided for 40 hr at 100°C

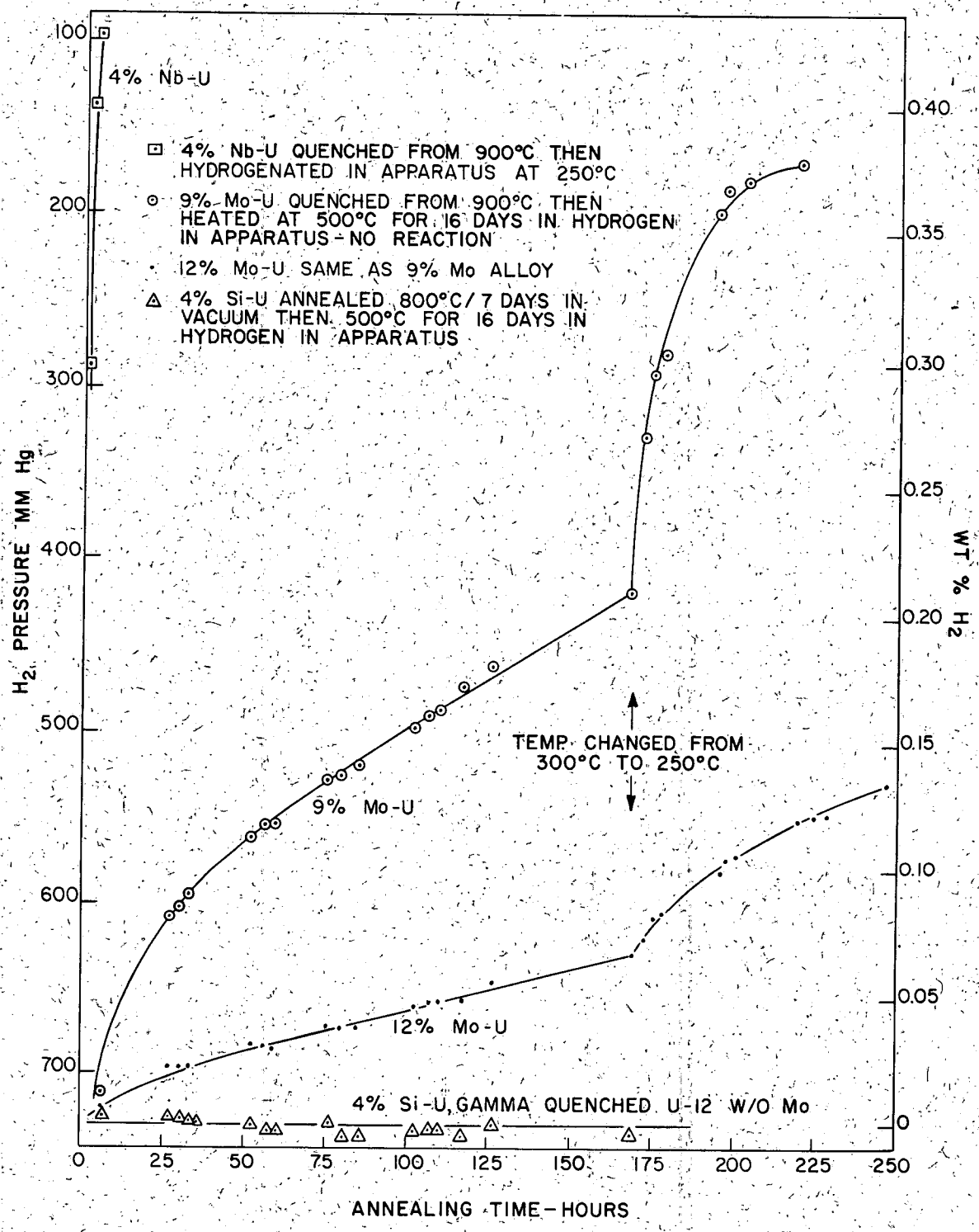

Fig. 18. The reaction of uranium alloys with molecular hydrogen

Neg 17421-12

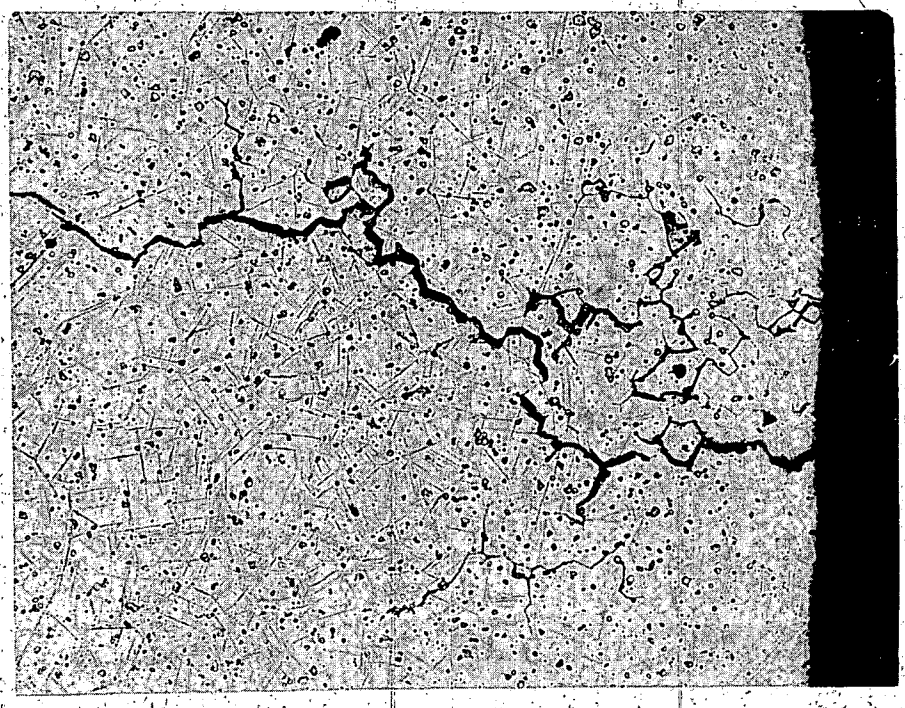

Neg 17420-23 250X

Fig. 19. U-12 w/o Mo alloy, exposed 14 days to 650°F water and then annealed in vacuum for 1 day at 406°C

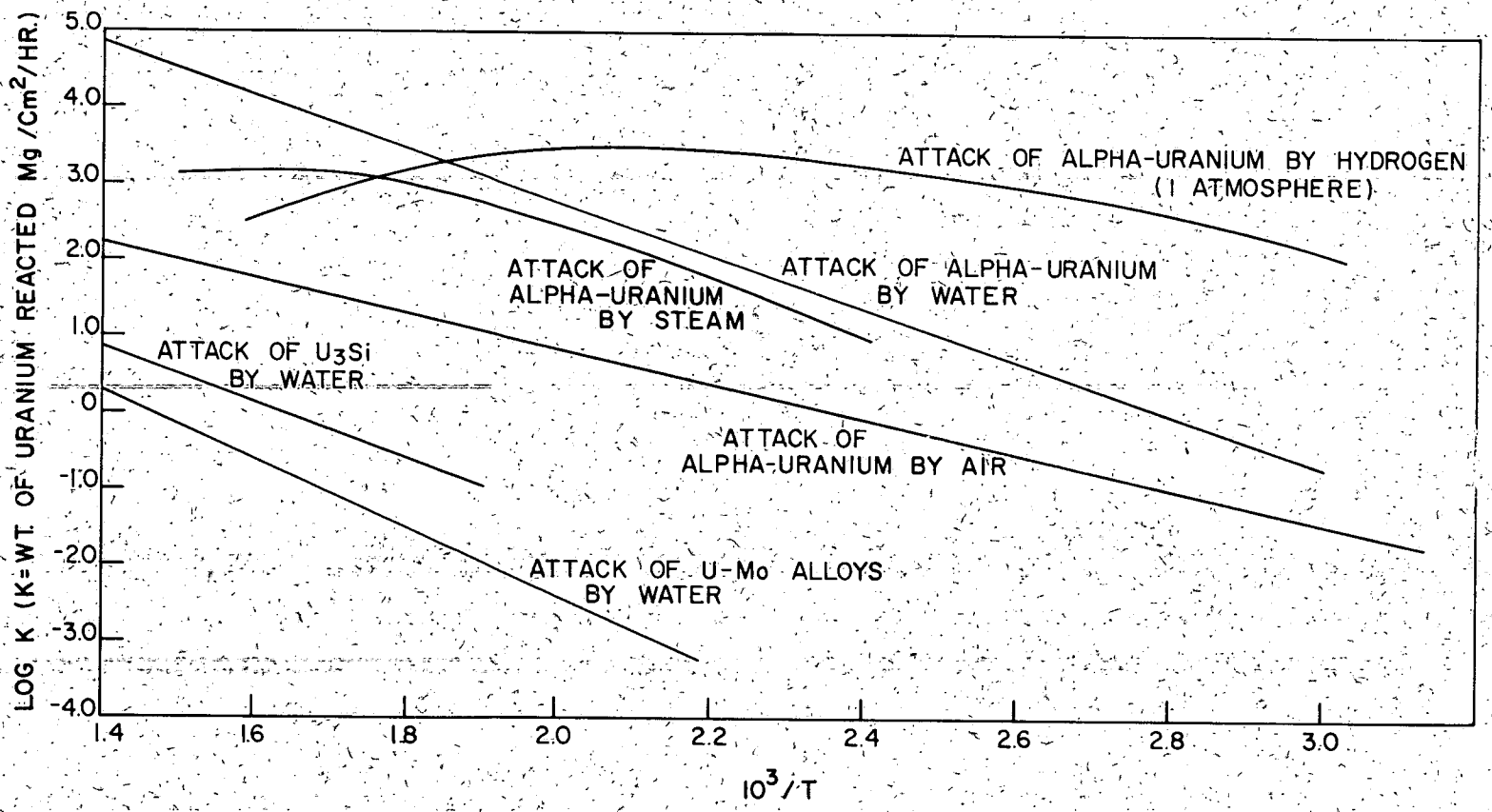

Fig. 20. The rate of attack on uranium alloys of various corrosive media

Neg 17421-29

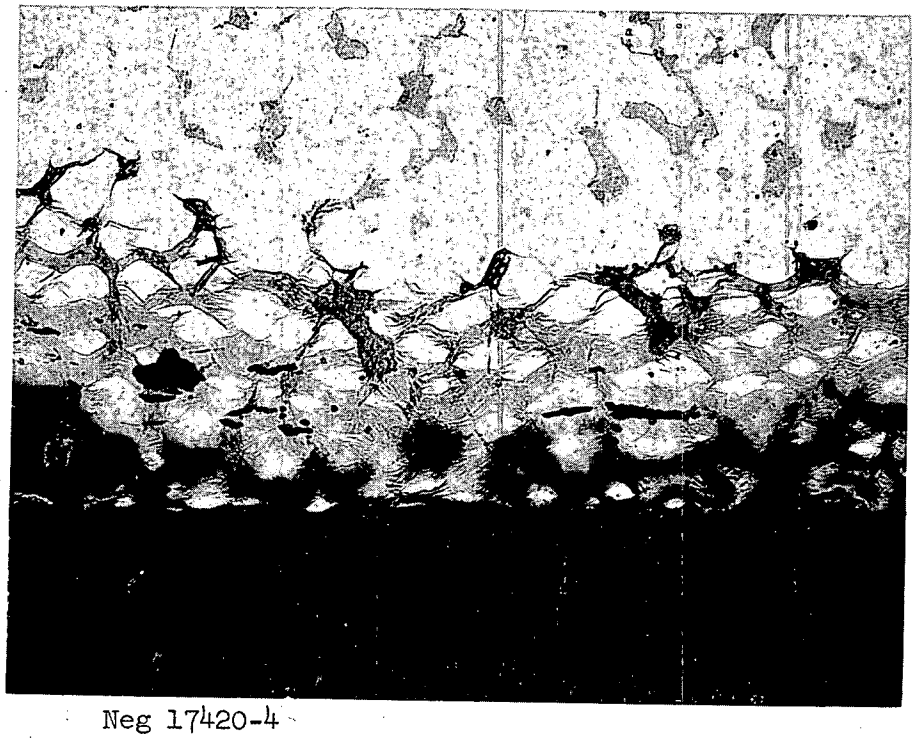

Neg 17420-4 250X

Fig. 21a. U-9 w/o Mo, gamma-quenched and then annealed 21 days at 400°C, cathodically hydrided 3 days at 100°C

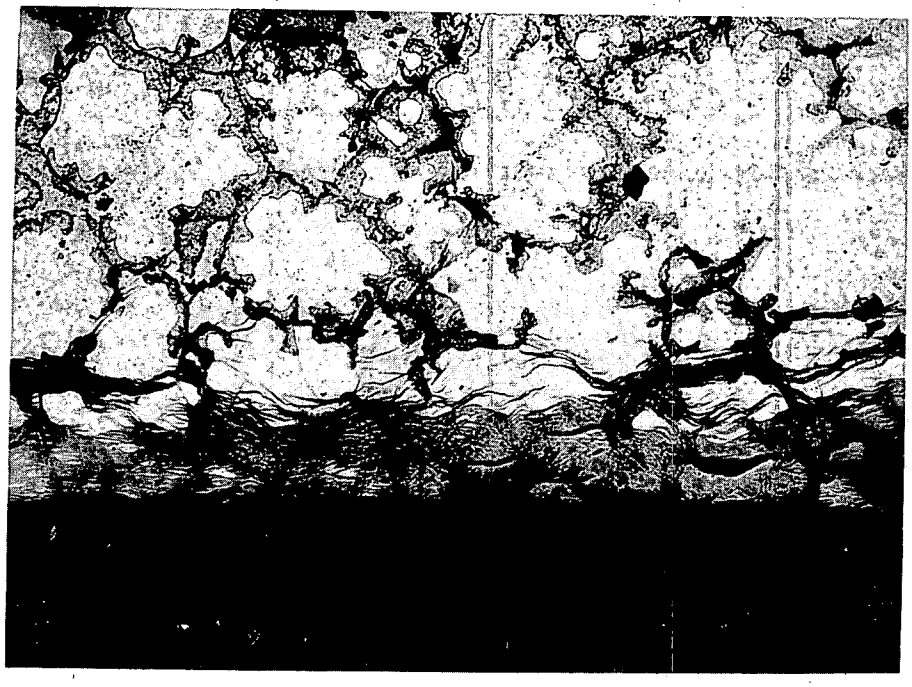

Neg 17420-6 250X

Fig. 21b. U-10 w/o Mo alloy, gamma-quenched and then annealed 21 days at 400°C, cathodically hydrided for 3 days at 100°C

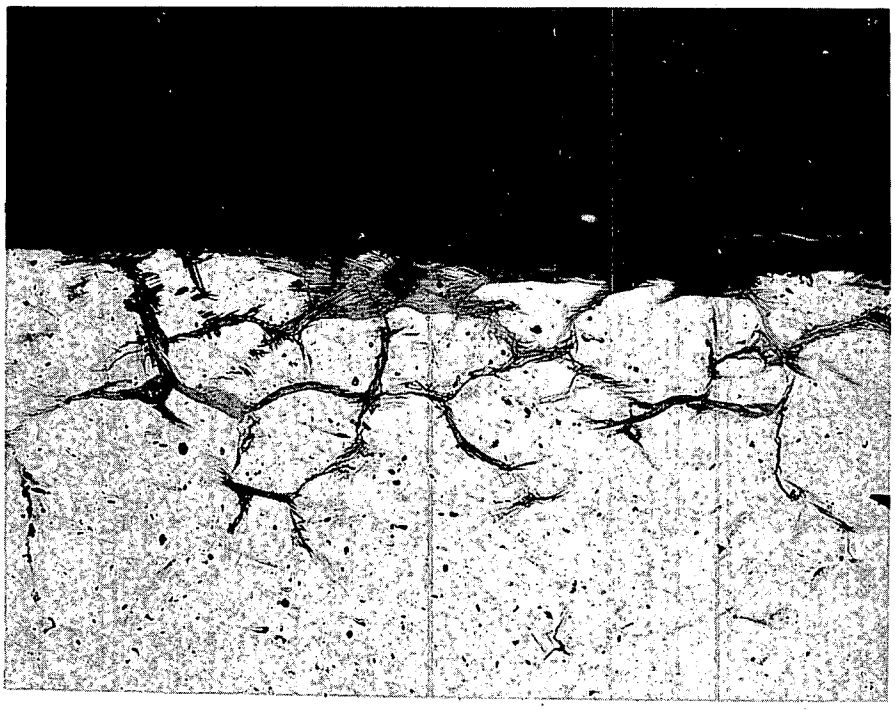

Neg 17420-3 250X

Fig. 22a. U-12 w/o Mo alloy, gamma-quenched and then annealed 21 days at 400°C, cathodically hydrided 3 days at 100°C

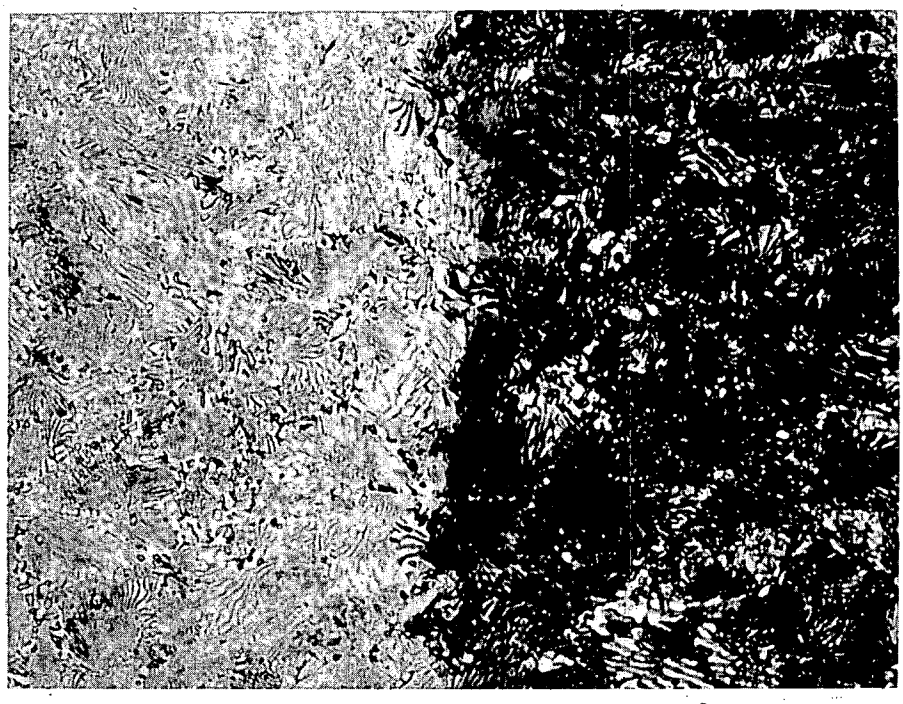

Neg 17420-29 250X

Fig. 22b. U-7 w/o Mo alloy, gamma-quenched and then annealed 7 days at 550°C, cathodically hydrided 3 days at 100°C

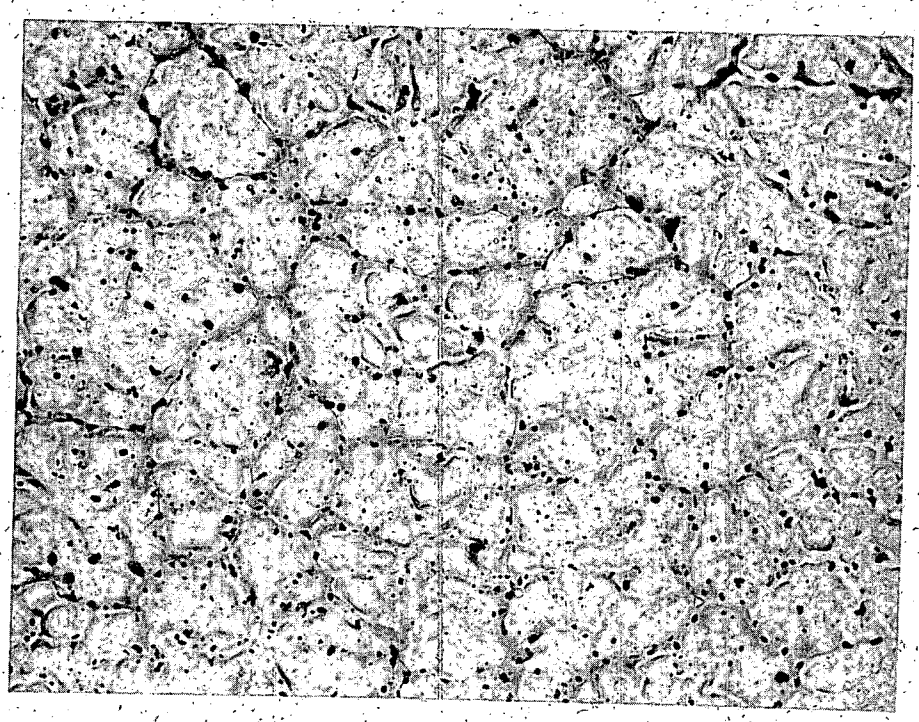

Neg 17420-31 250X

Fig. 23 a. Microsegregation in an induction melted and chill cast heat of U-12 w/o Mo

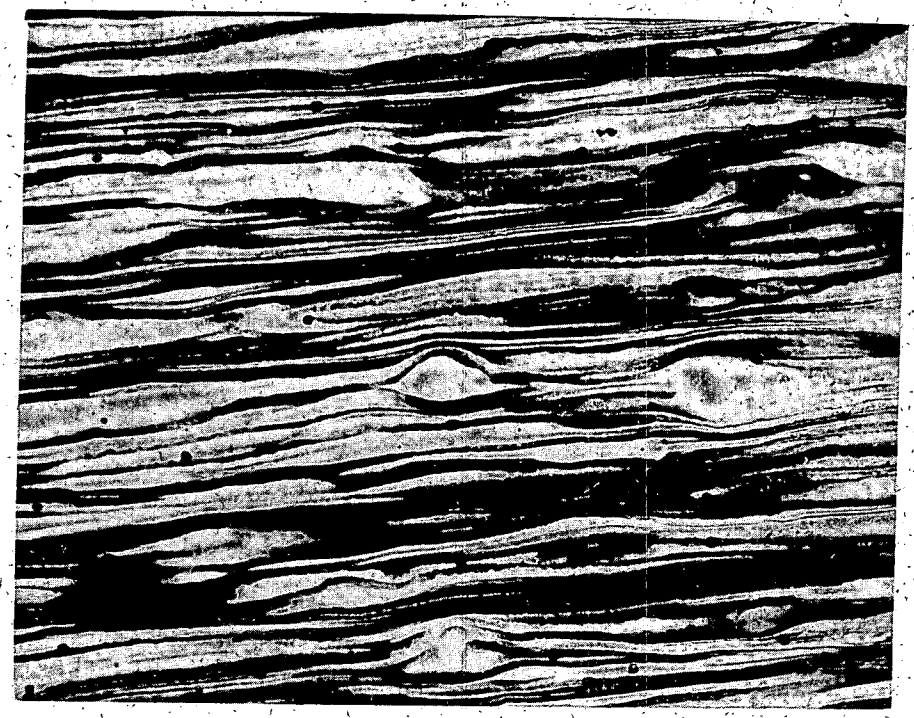

Neg 17420-37 250X

Fig. 23 b. Microsegregation in an extruded rod of duplex melted U-12 w/o Mo

DECLASSIFIED

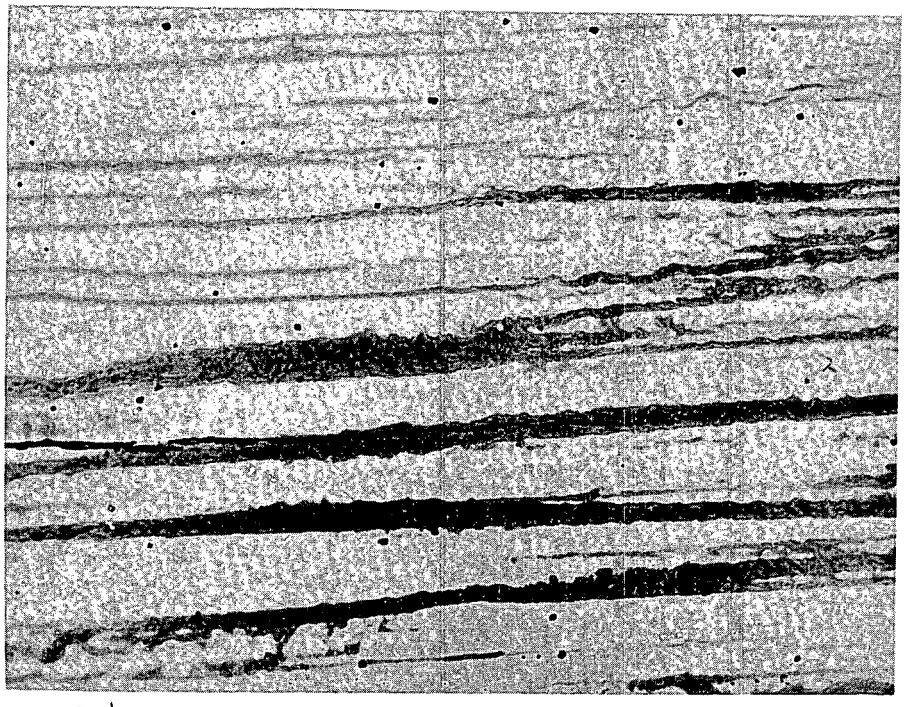

Neg 17420-15 250X

Fig. 23c. Corrosion of a segregated extrusion of U-12 w/o Mo. Longitudinal section of a sample corrosion tested 14 days in 650°F water.

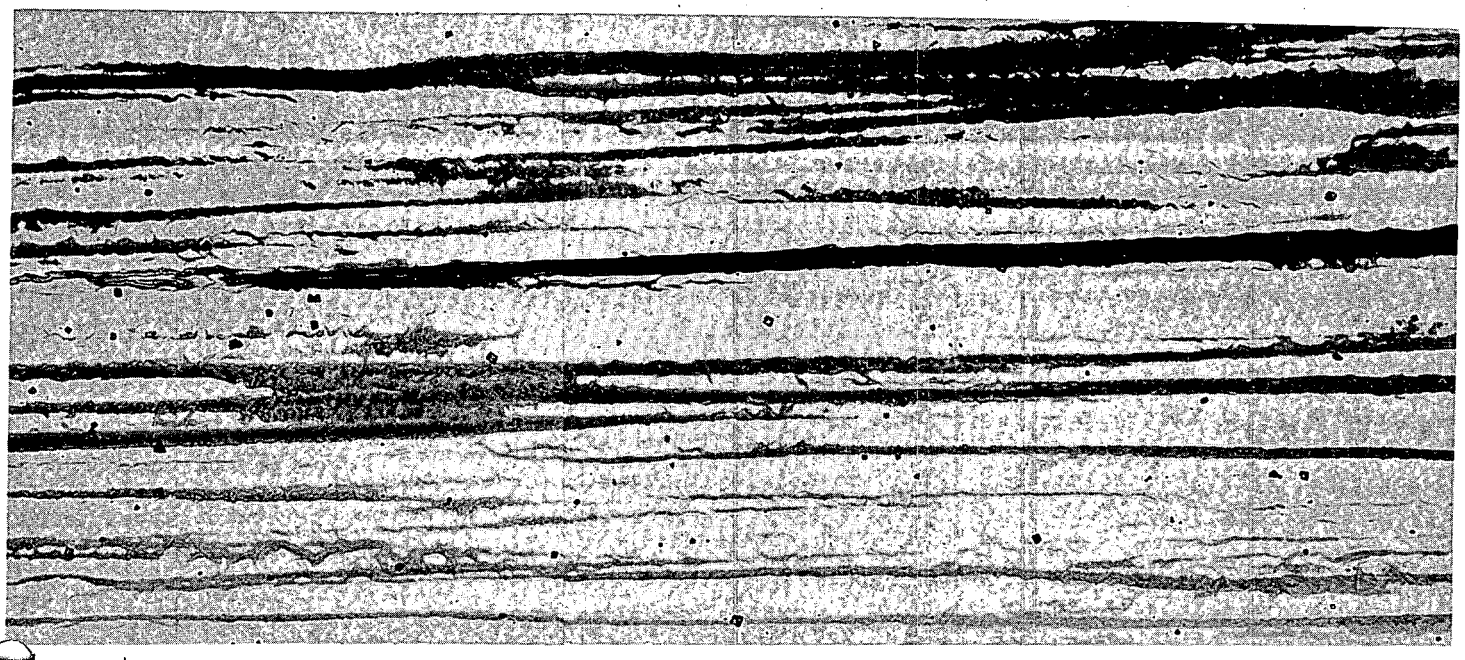

Neg 17420-50 250X

Fig. 23d. Preferential corrosive attack along a segregated stringer in the sample shown in Fig. 23c

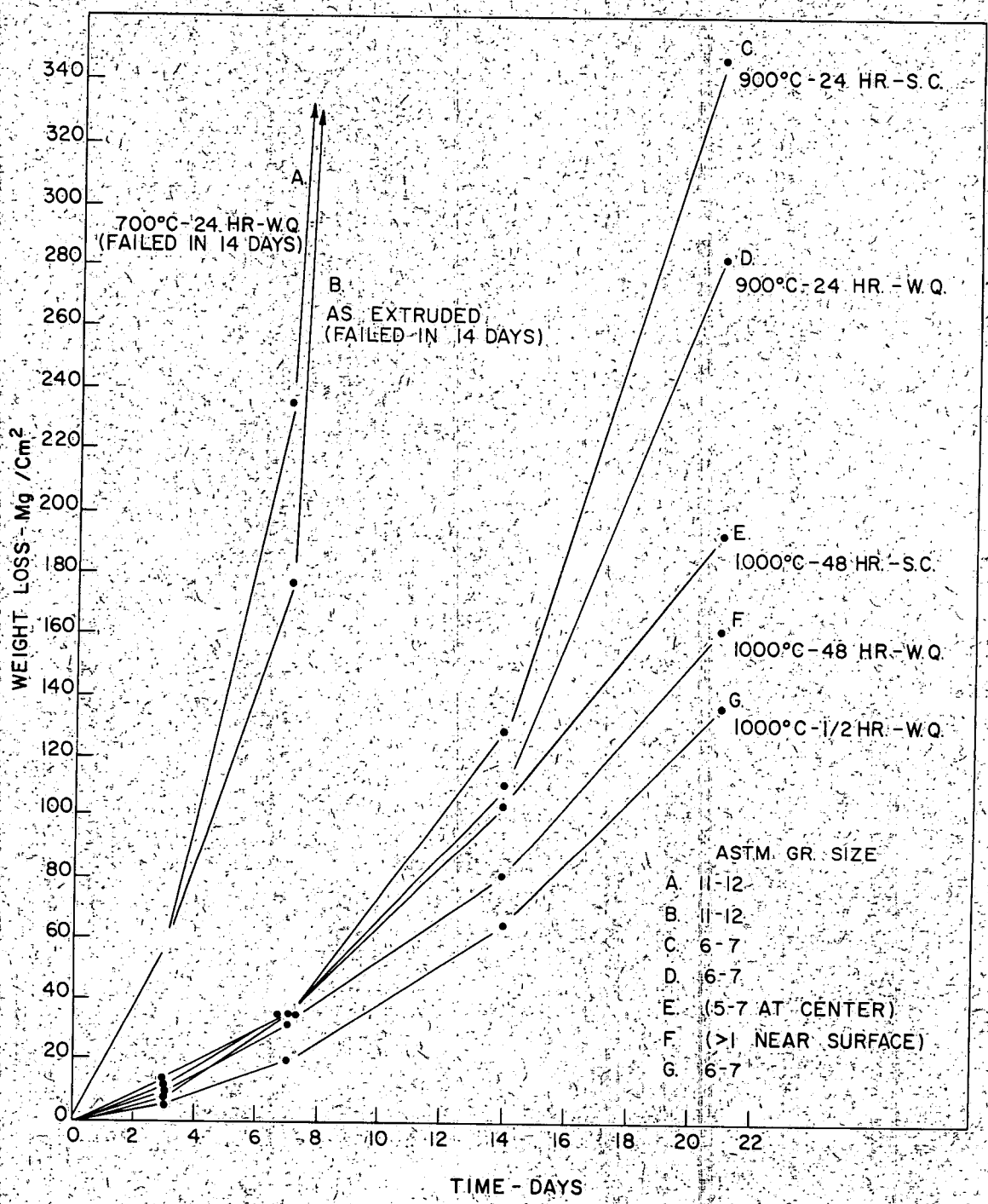

Fig. 24. Effect of homogenization temperature on the corrosion of U-12 w/o Mo Extrusion No. MOZC1-16
Neg 17421-11

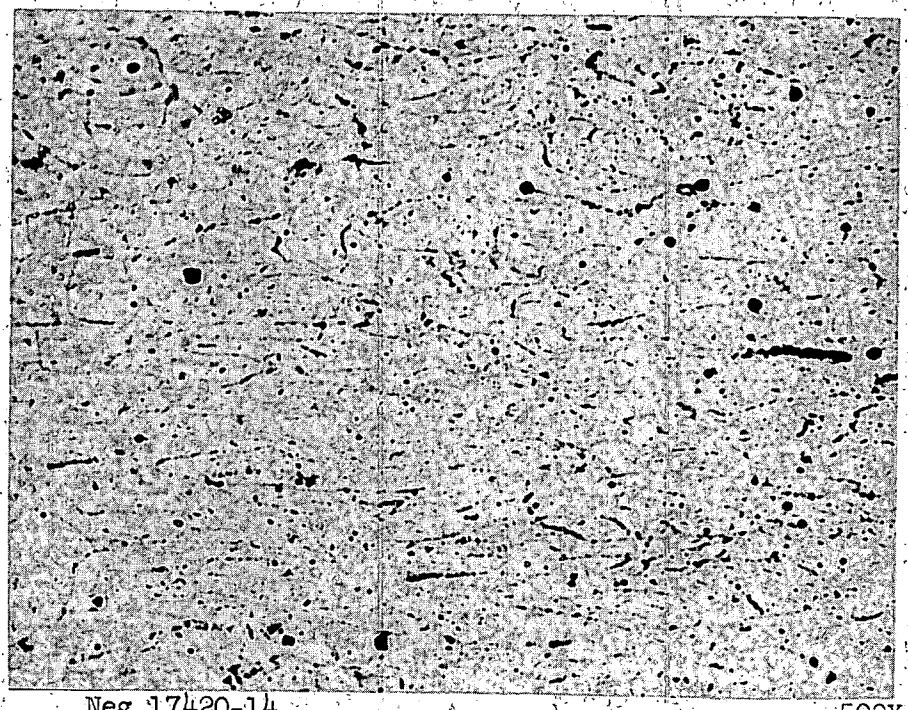

Neg 17420-14 500X

Fig. 25. Longitudinal view of an as-extruded U-12 w/o Mo alloy (Extrusion No. J959)

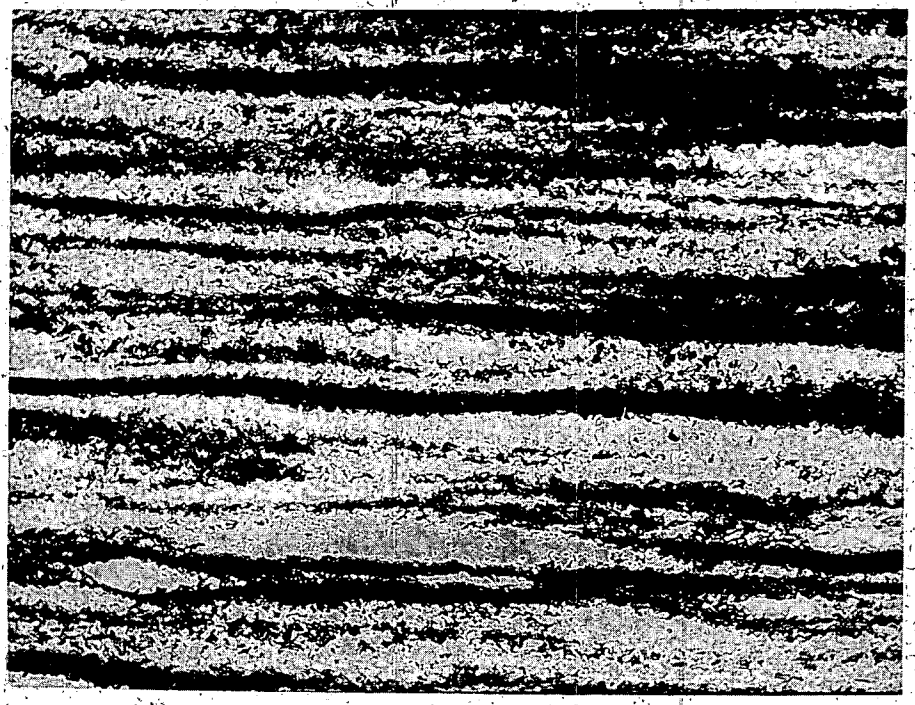

Neg 17420 250X

Fig. 26. Extrusion No. 1101-1-13 (U-11.2 w/o Mo), annealed at 600°C for 168 hr and then corrosion tested in 650°F water for 7 days

Neg.
17420-27

500X

Fig. 27a. As extruded

Neg
17420-19

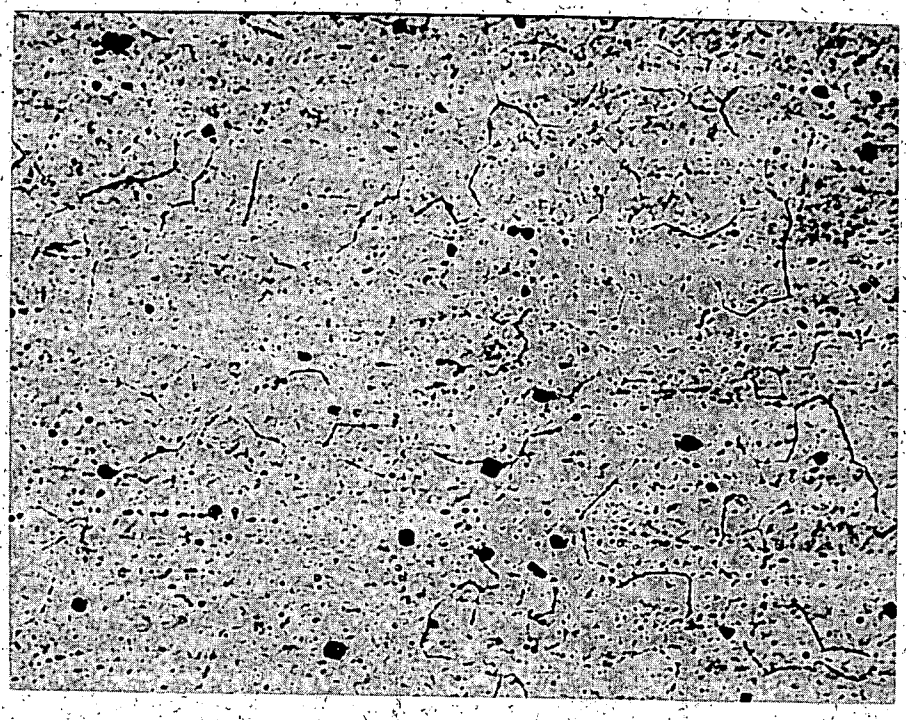

500X

Fig. 27b. Extruded and annealed 1/2 hr at 1000°C-1/2-water quenched

Fig. 27. Effect of annealing time upon impurity distribution in a U-11.2 w/o Mo alloy

Neg
17420-44

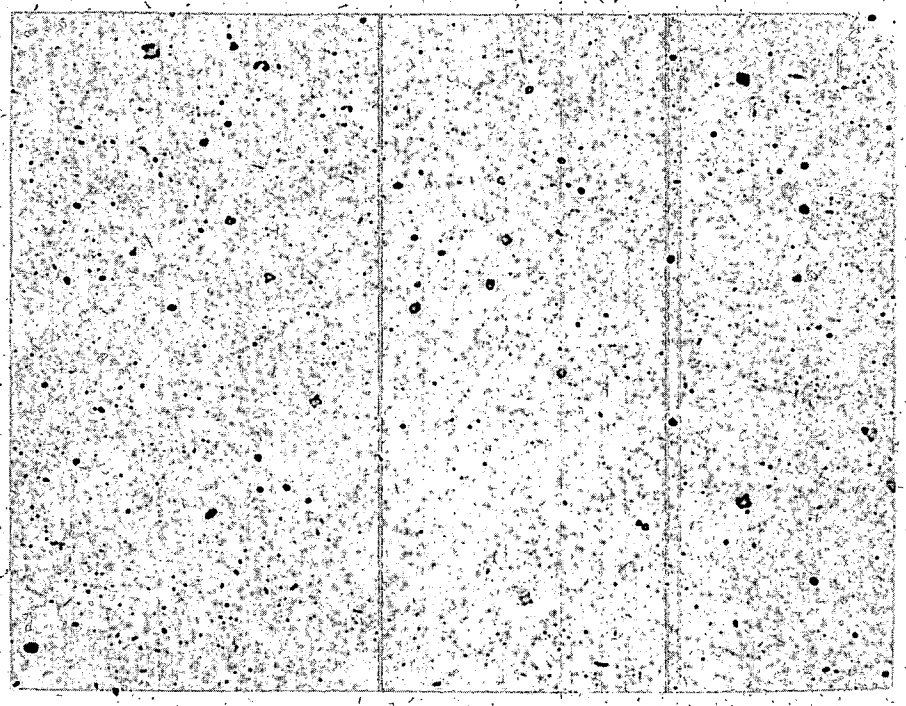

500X

Fig. 27c. Extruded and annealed 24 hr at 1000°C-water quenched

Neg
17420-48

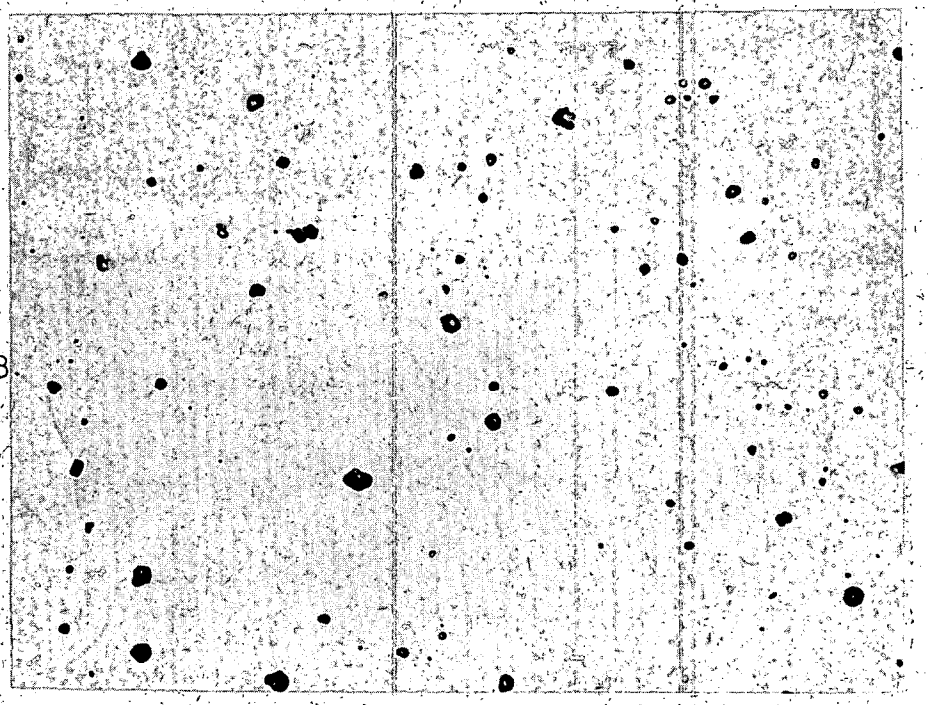

500X

Fig. 27d. Extruded and annealed 168 hr at 1000°C-water quenched

Fig. 27. Effect of annealing time upon impurity distribution in a U-11.2 w/o Mo alloy

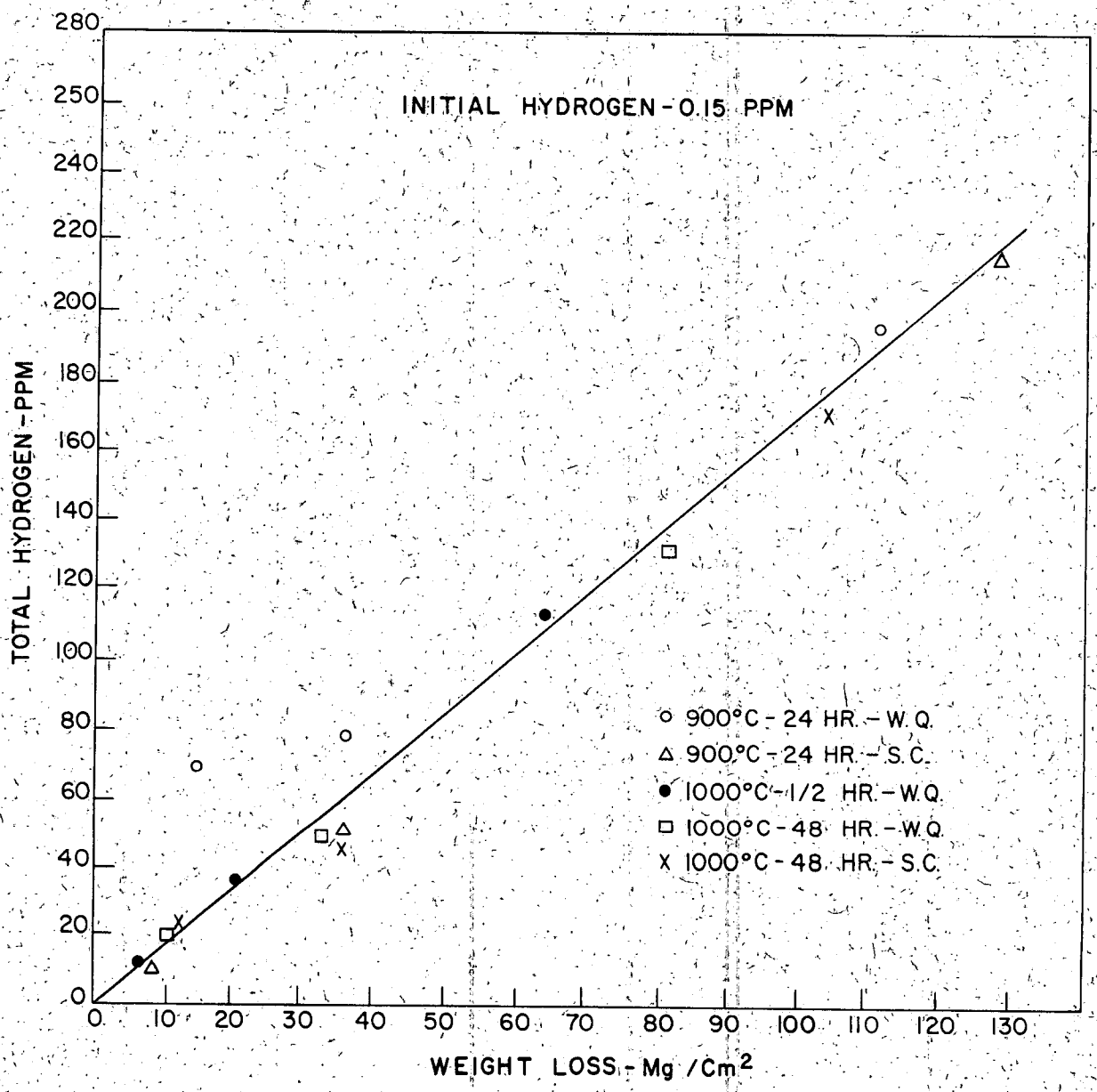

Fig. 28. Increase in hydrogen content of a U-12 w/o Mo alloy during corrosion in 650°F water

Neg 17421-10

DECLASSIFIED

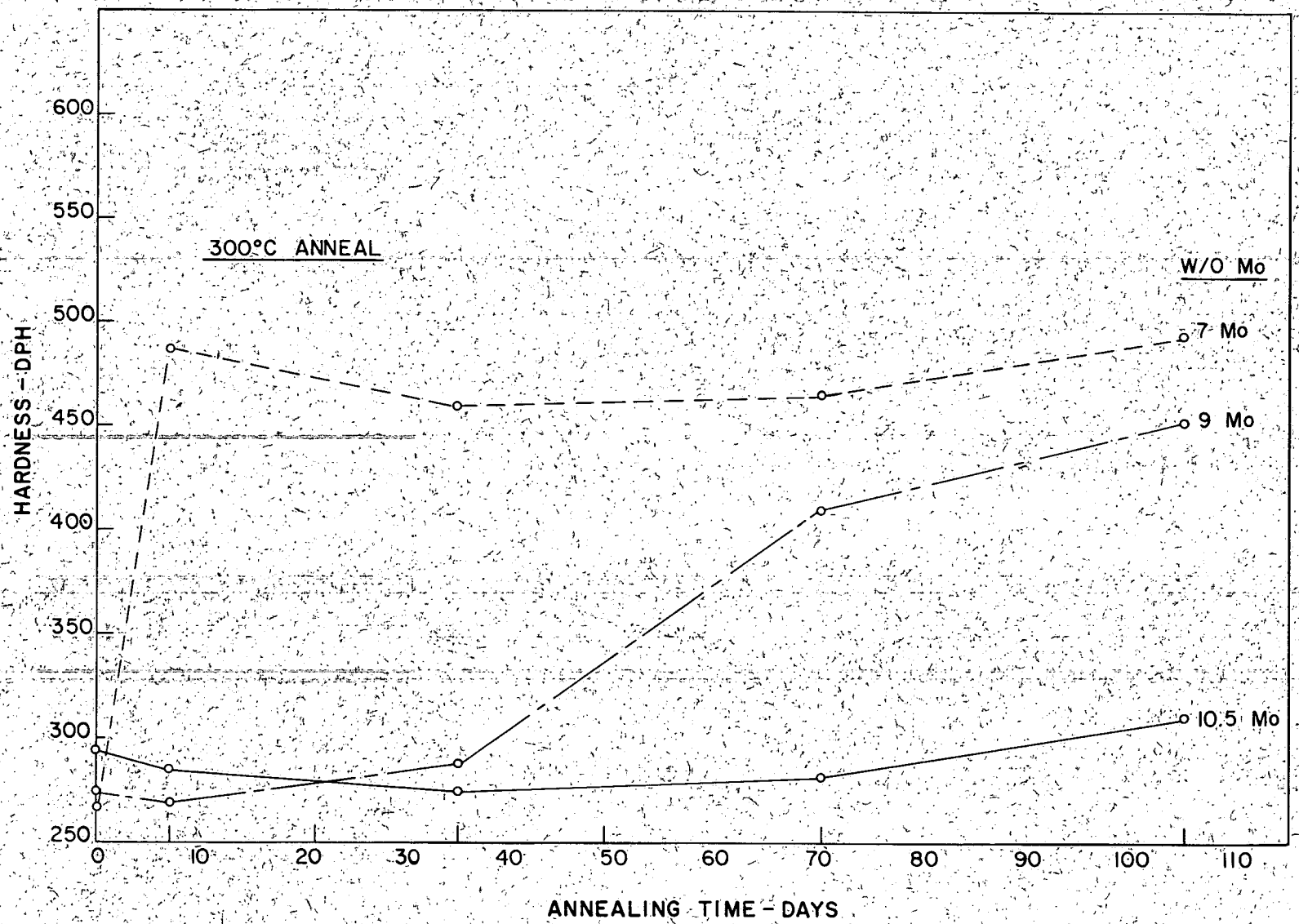

Fig. 29. Hardness of U-Mo alloys as a function of annealing time at 300°C

Neg 17421-24

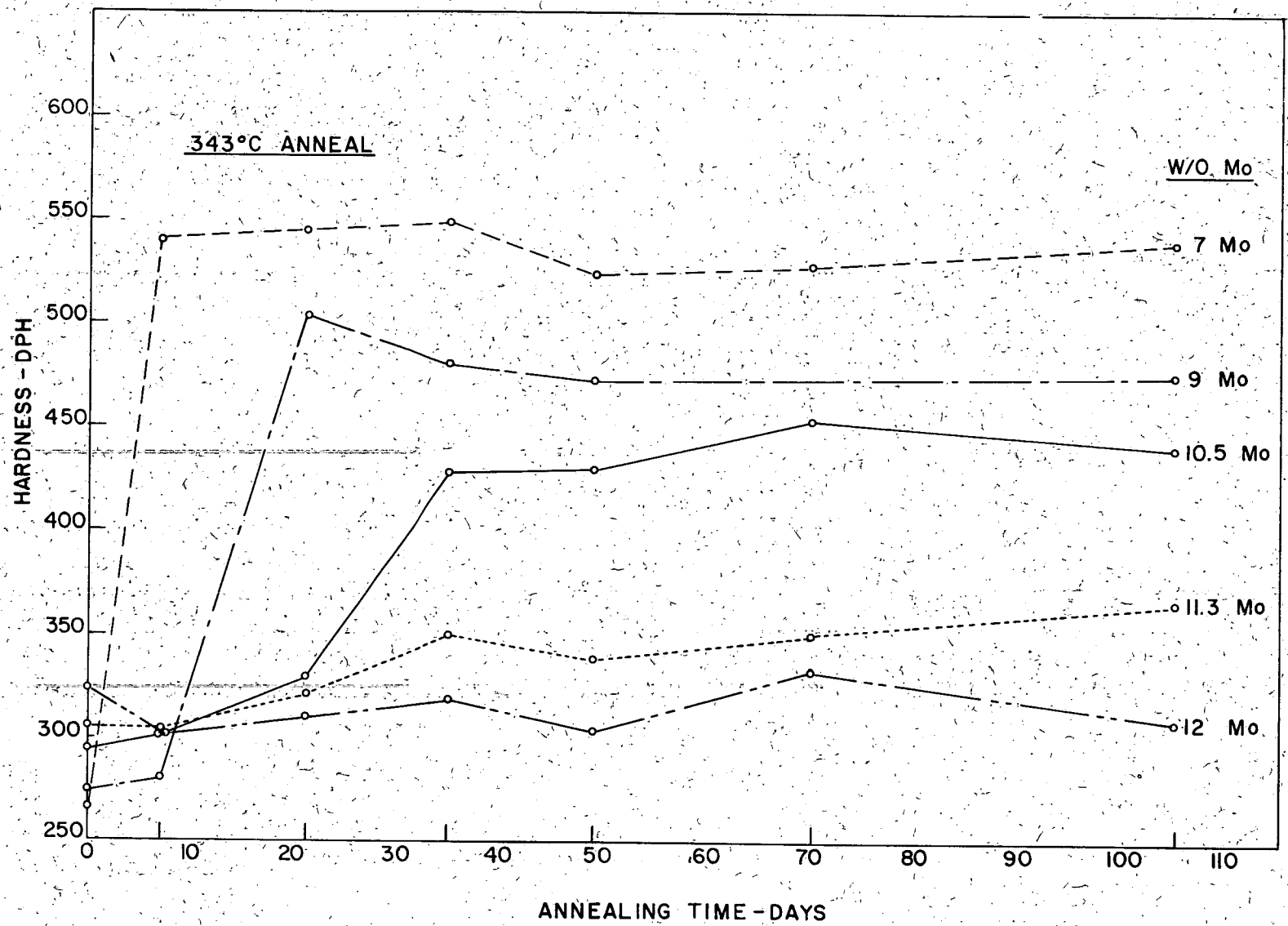

Fig. 30. Hardness of U-Mo alloys as a function of annealing time at 343°C

Neg 17421-8

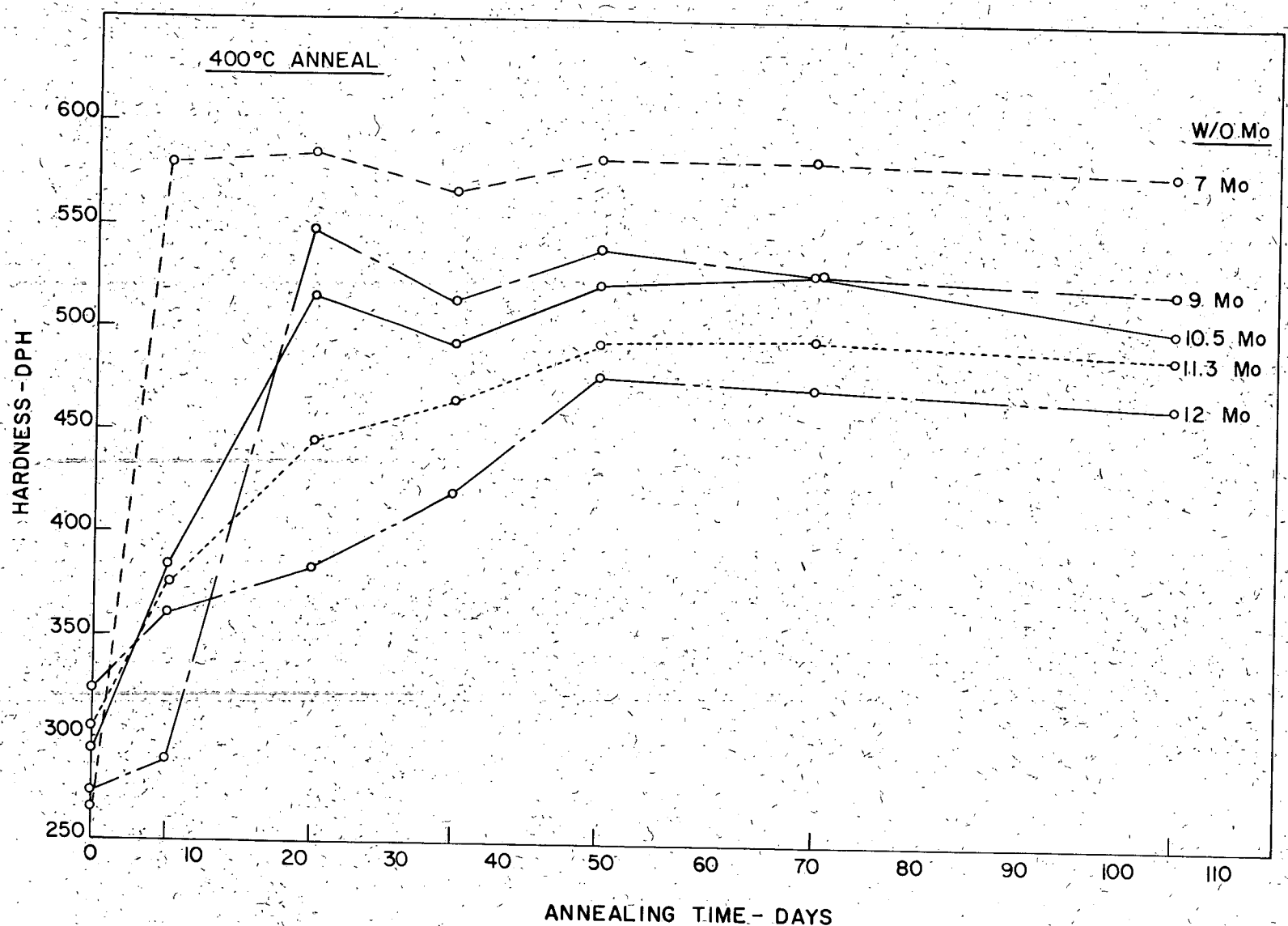

Fig. 31. Hardness of U-Mo alloys as a function of annealing time at 400°C

Neg 17421-21

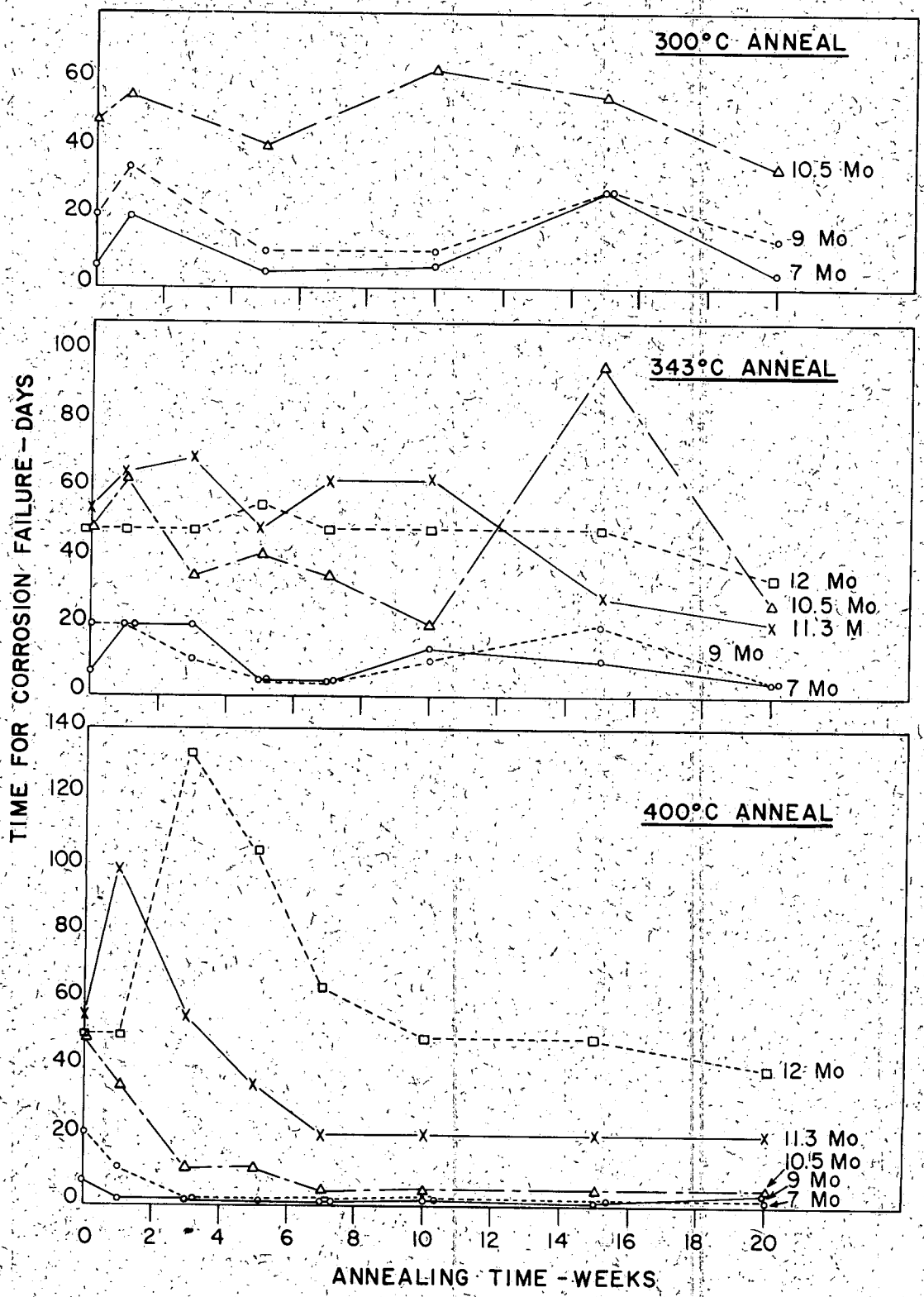

Fig. 32. Corrosion life of U-Mo alloys in 650°F water as a function of low temperature annealing time

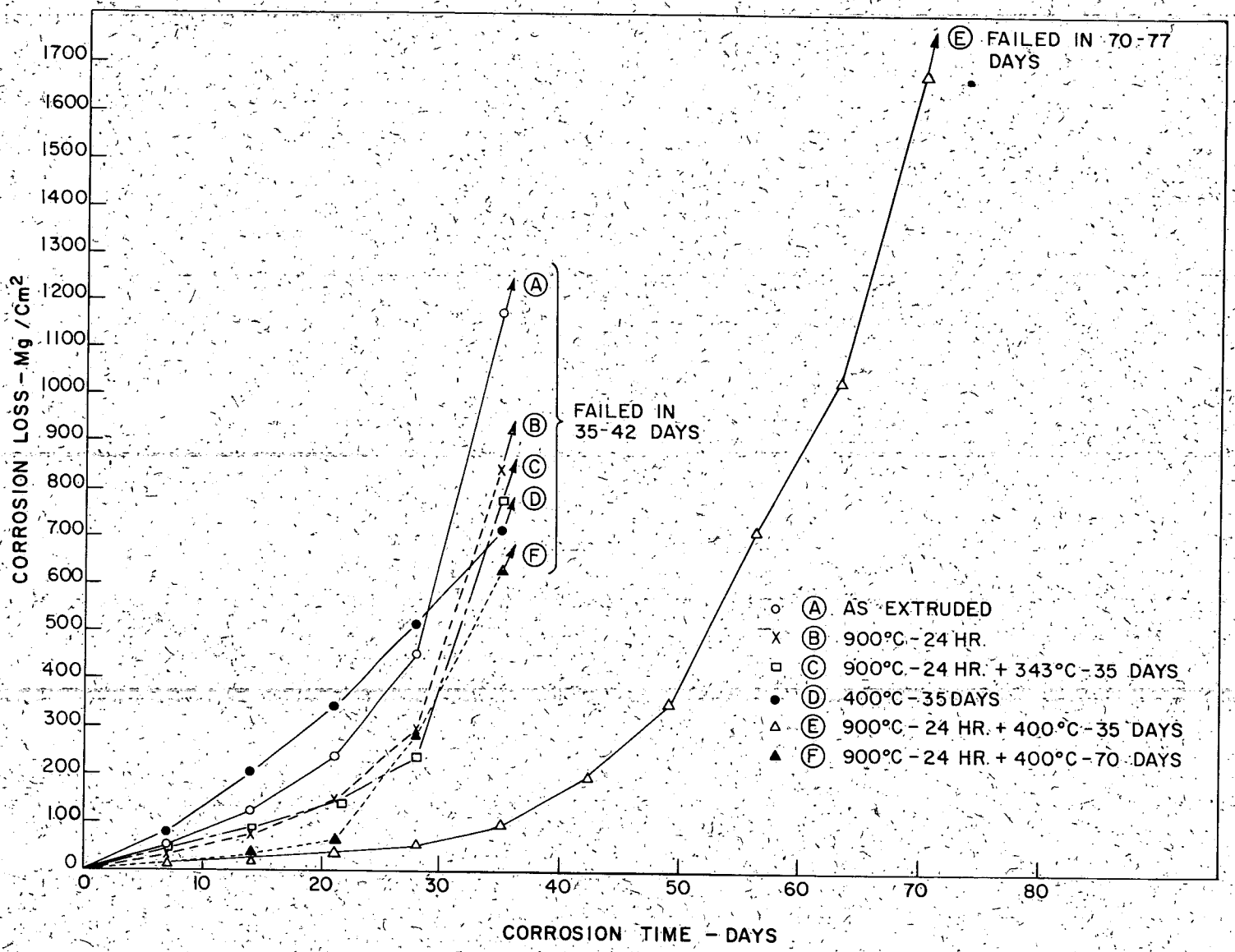

Fig. 33. The effect of low temperature annealing on the corrosion of U-12 w/o Mo alloys

Neg 17421-5

Neg
17420-21

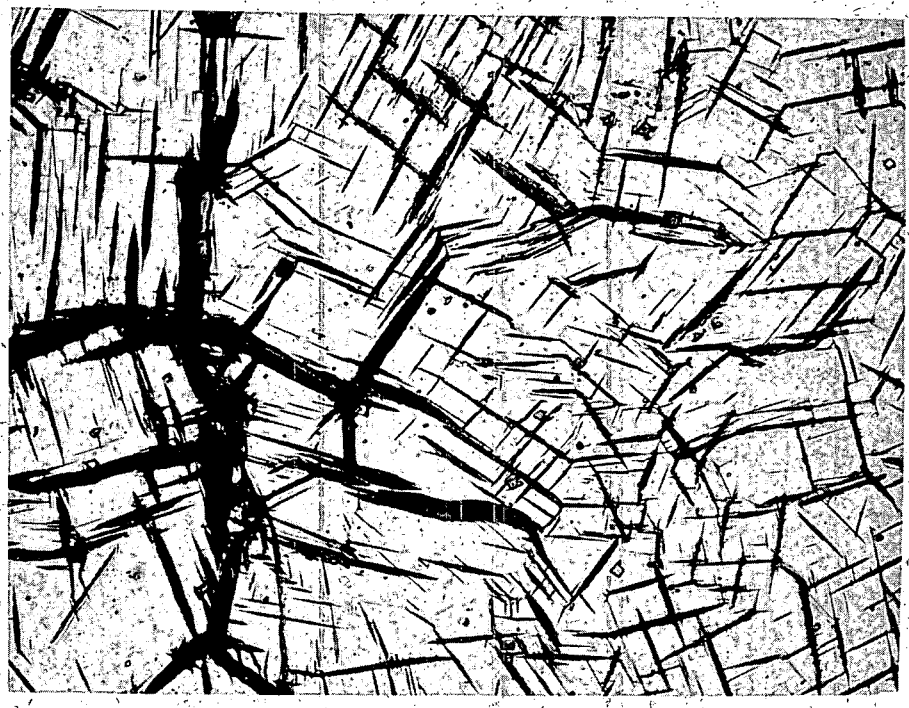

250X

Fig. 34a. Annealed 24 hr 900°C-water quenched-corrosion tested 28 days 650°F water

Neg
17420-32

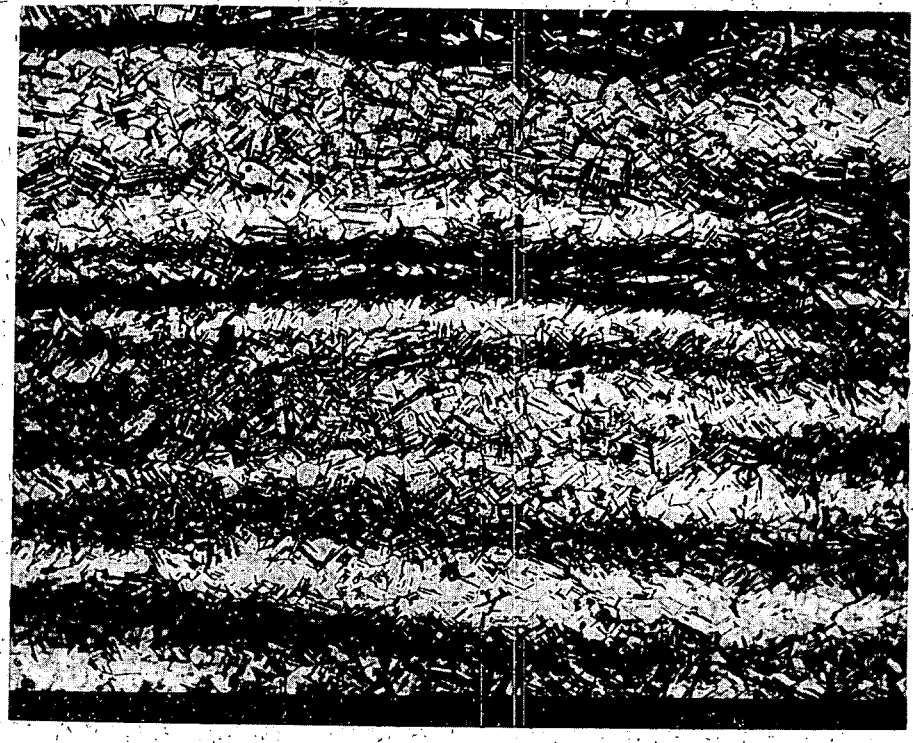

250X

Fig. 34b. Annealed 5 wk 400°C-water quenched-corrosion tested 28 days 650°F water

DECLASSIFIED

Neg
17420-24

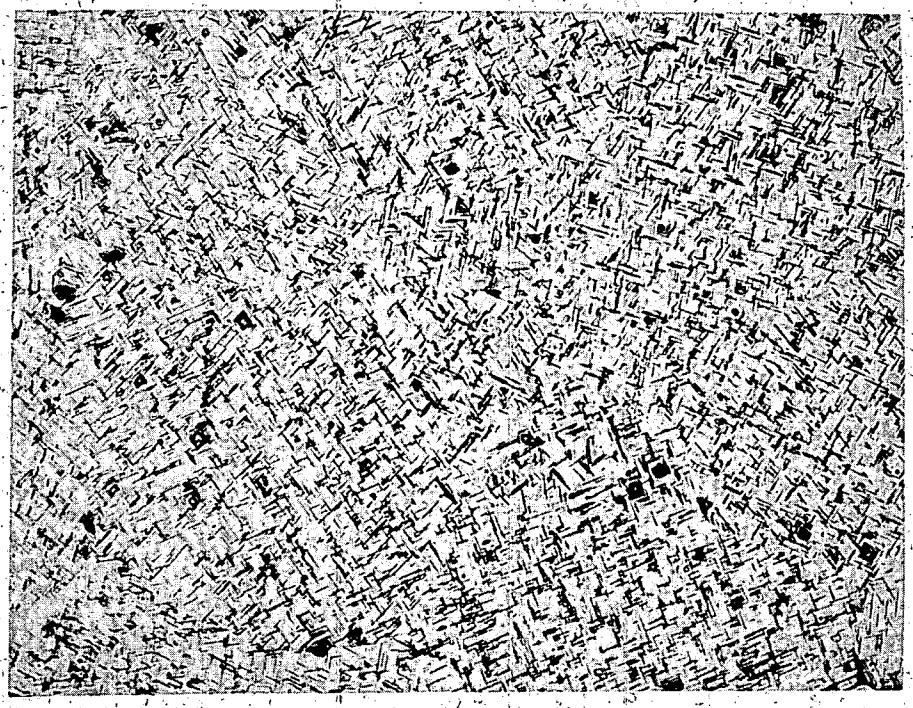

250X

Fig. 34c. Annealed 24 hr 900°C-water quenched then annealed 5 wk 400°C-corrosion tested 28 days 650°F water

Neg
17420-18

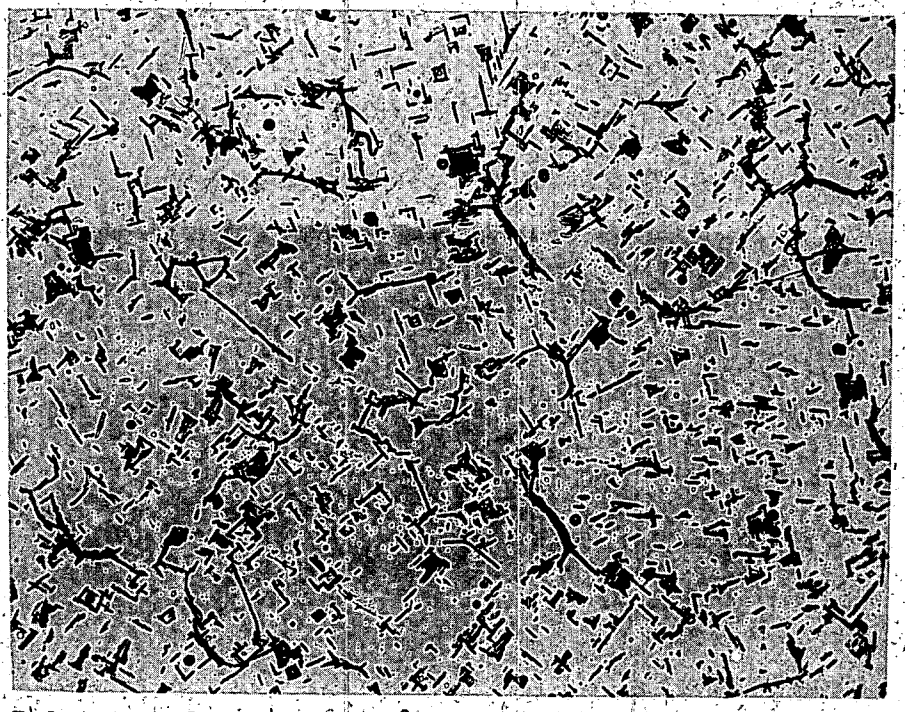

250X

Fig. 34d. Annealed 24 hr 900°C-water quenched then annealed 10 wk 400°C-corrosion tested 28 days 650°F water

Fig. 34. The effect of low temperature annealing on the corrosion of U-12 w/o Mo

DECLASSIFIED

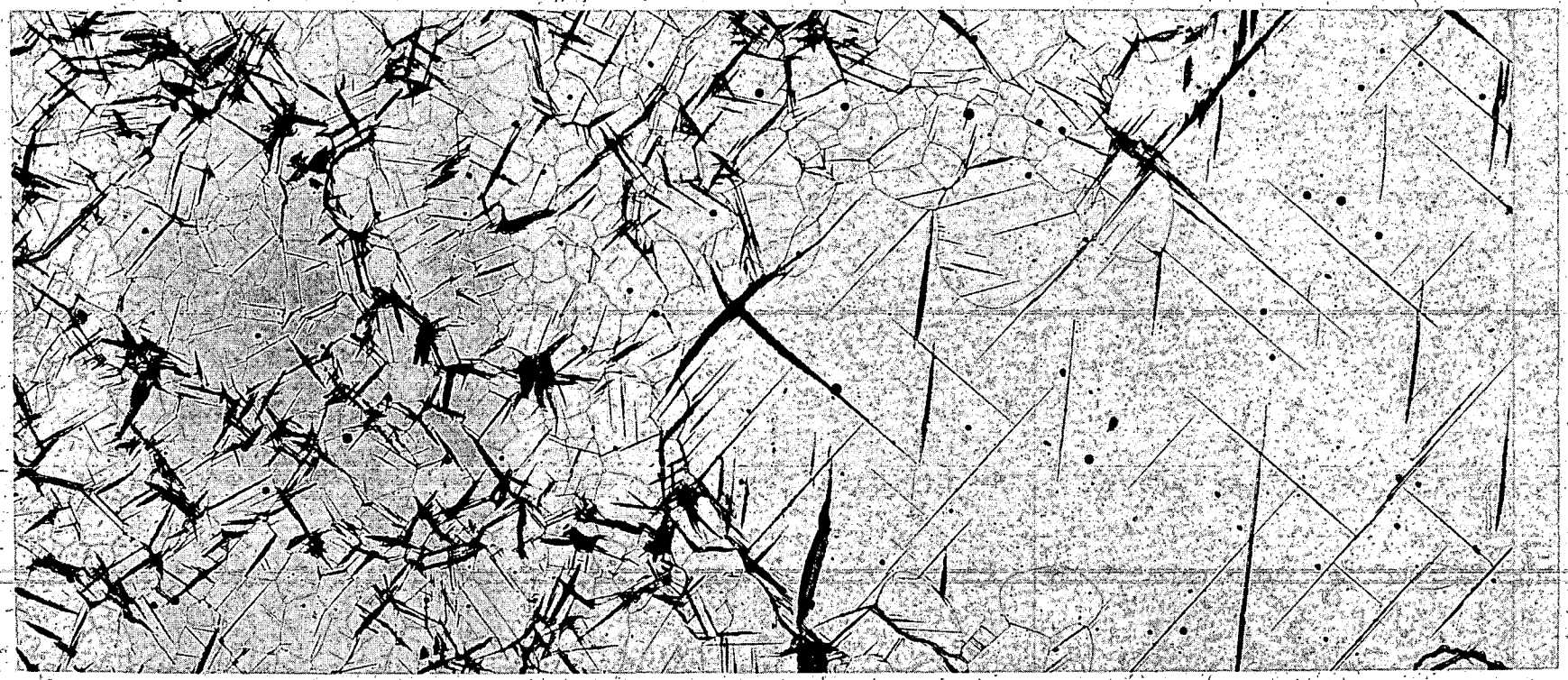

Neg 17420-49 250X

Fig. 35. U-12 w/o Mo alloy, annealed 48 hr at 1000°C, corrosion tested 14 days in 650°F water

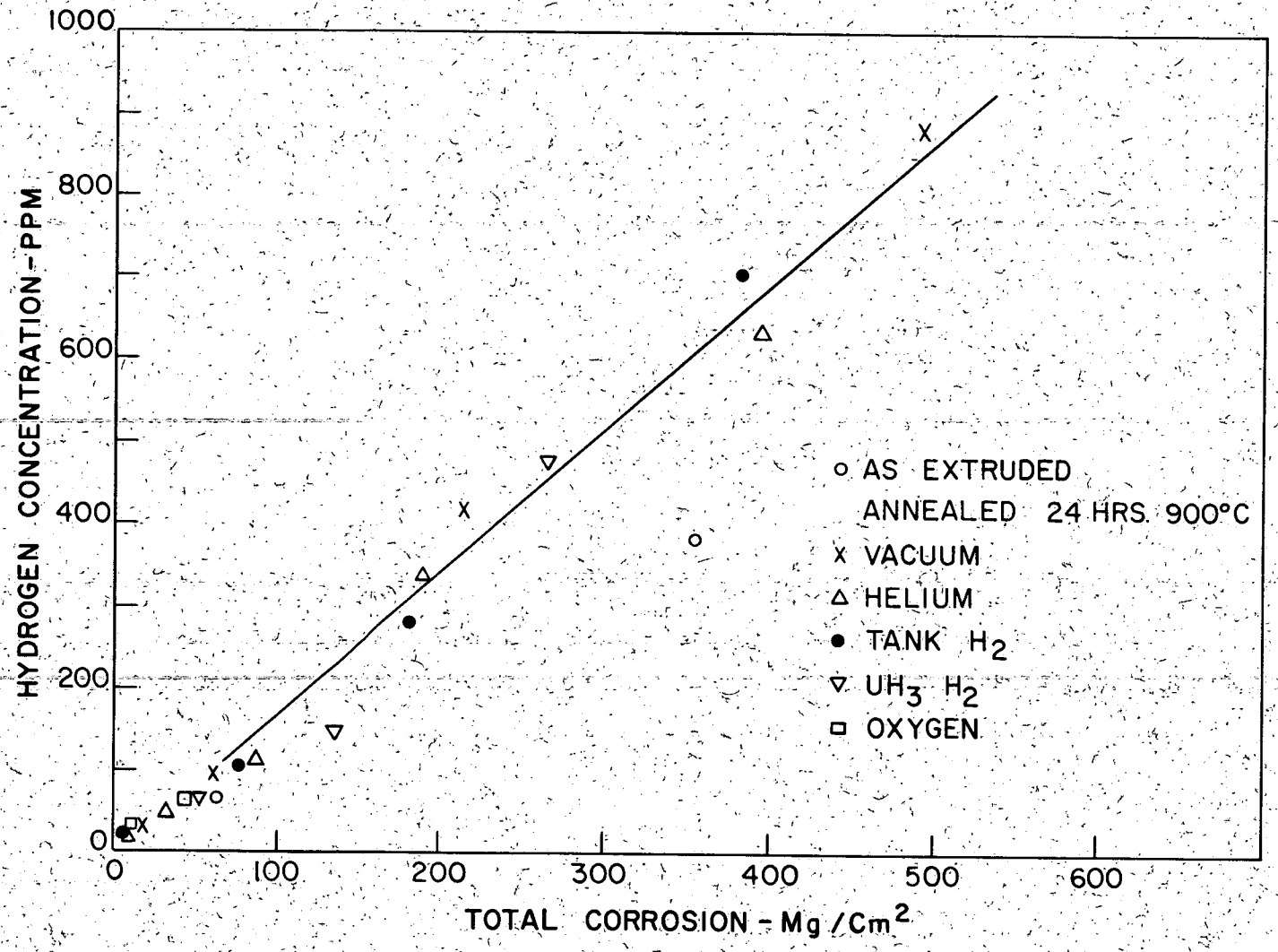

Fig. 36. Hydrogen concentration as a function of total corrosion for a U-12 w/o Mo alloy annealed in various atmospheres

Neg 17421-27

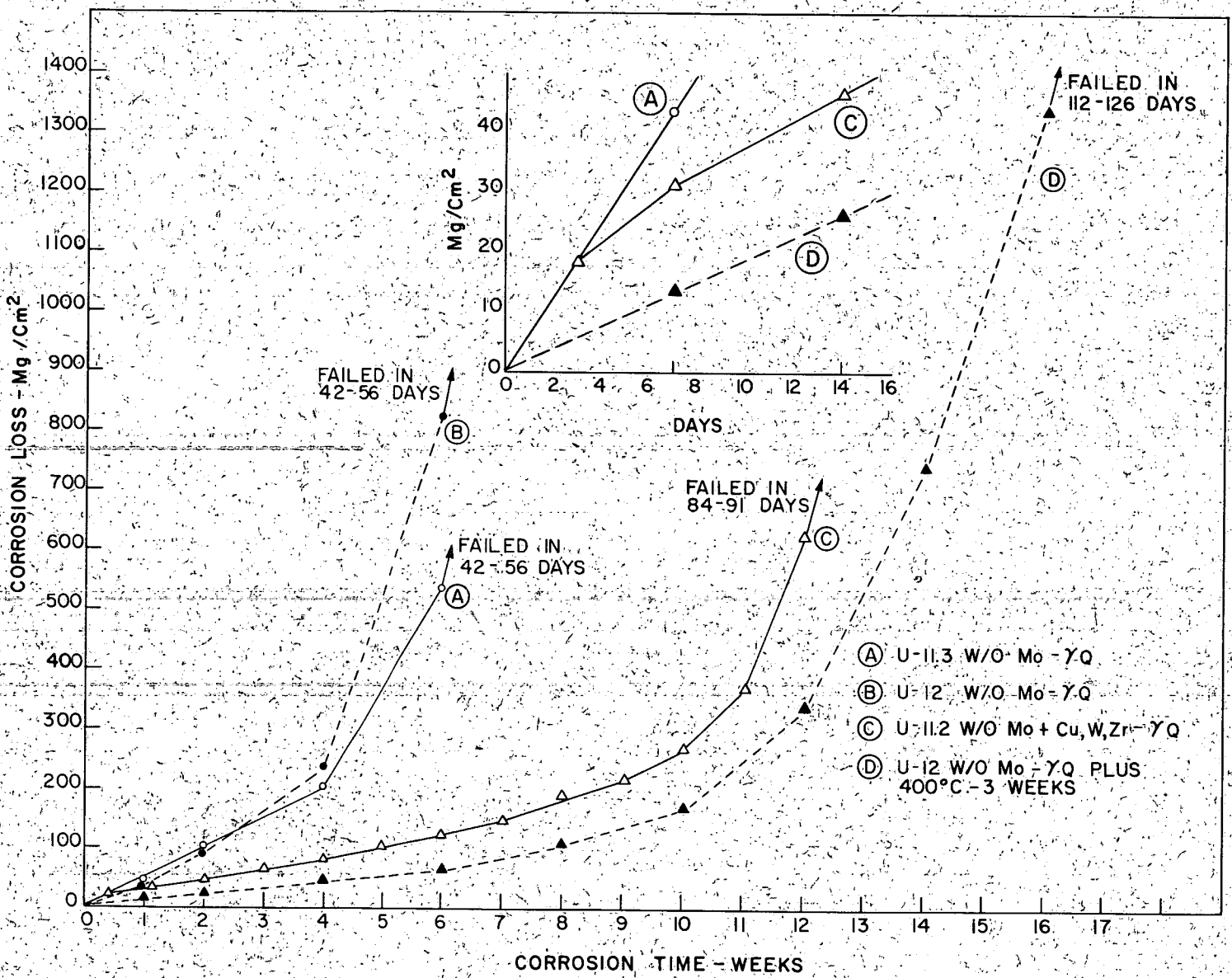

Fig. 37. Effect of impurities on the corrosion of U-11.2 w/o Mo alloy

Neg 17421-22

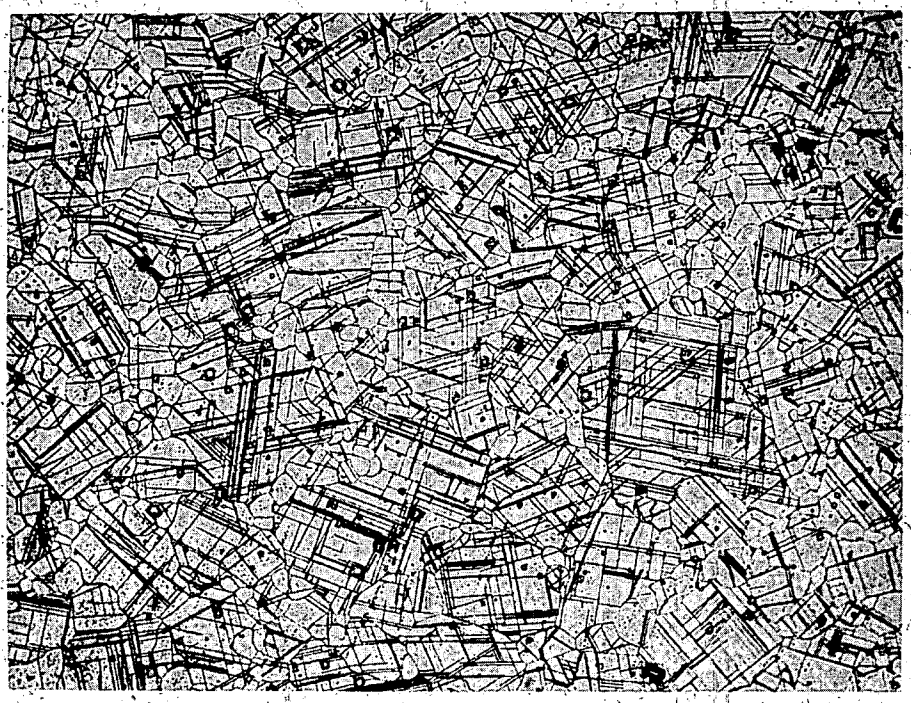

Neg 17420-5 250X

Fig. 38. U-11.2 w/o Mo alloy, gamma-quenched from 900°C and corrosion tested 28 days at 650°F

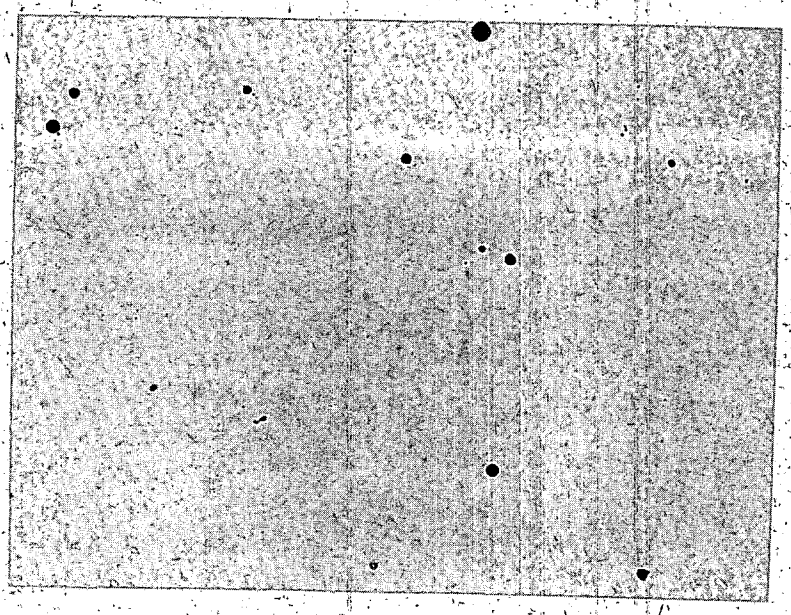

Neg 17420-38 250X

Fig. 39. Microstructure of U-7 w/o Mo-0.6 w/o Ti specimen prior to corrosion testing

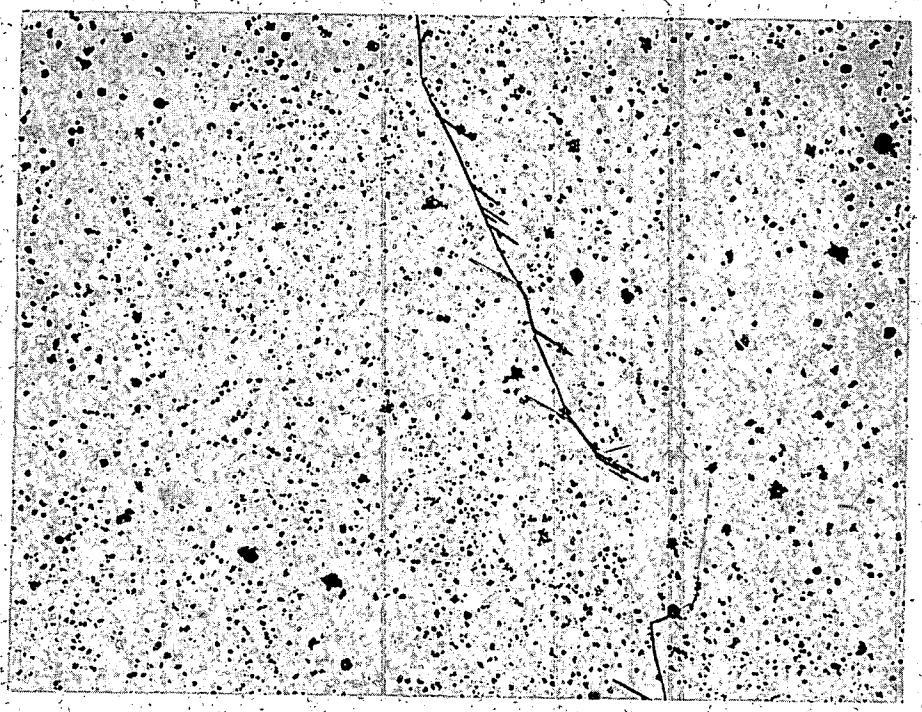

Neg 17420-39 250X

Fig. 40. U-7 w/o Mo-0.6 w/o Ti specimen after corrosion testing for 154 days in 650°F degassed water

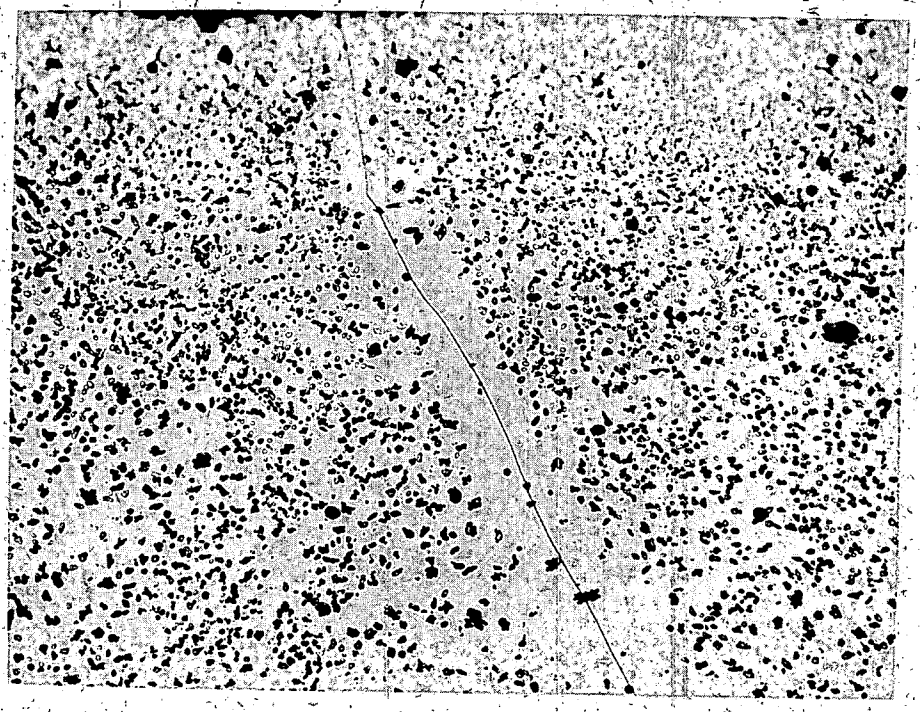

Neg 17420-35 250X

Fig. 41. Another area of the specimen shown in Fig. 40

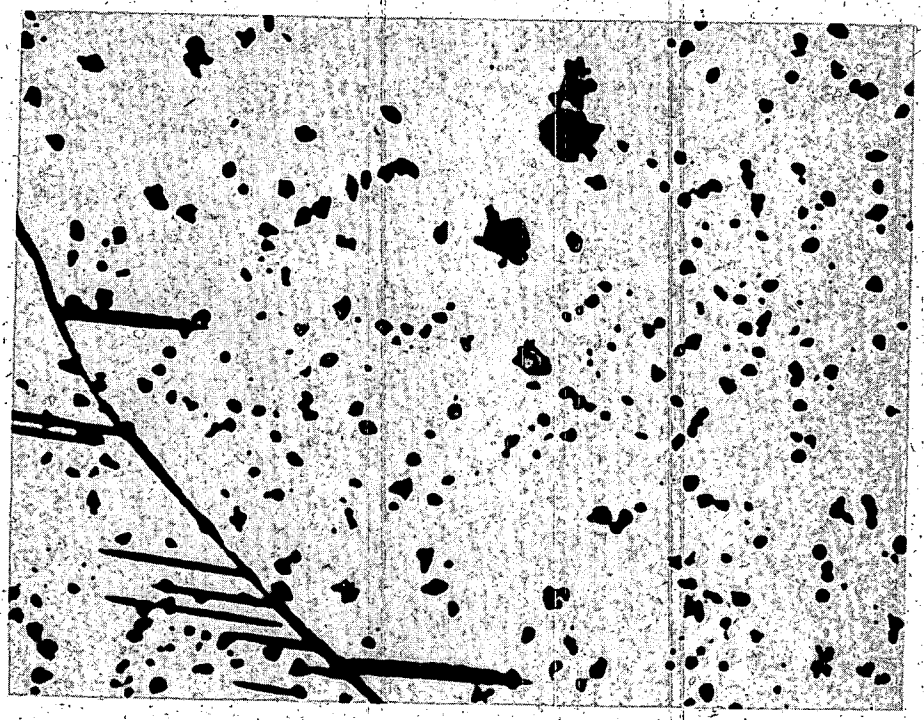

Neg 17420-34 1000X

Fig. 42. The same specimen shown in Figs. 41 and 42 at 1000X magnification

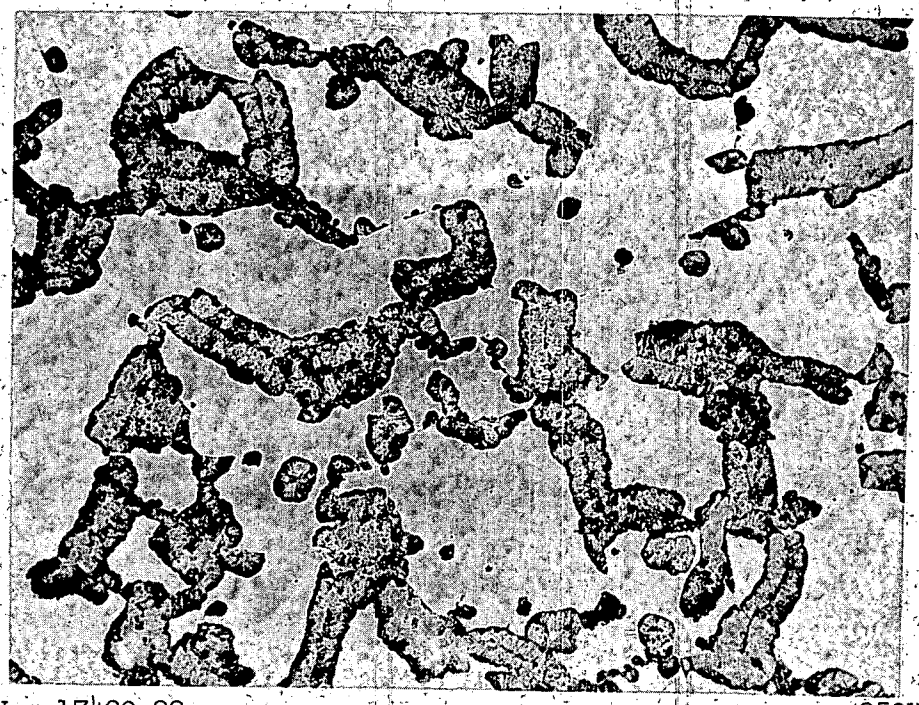

Neg 17420-22 250X

Fig. 43. U-9% Mo alloy, water quenched after 24 hr at 900°C, then annealed 35 days at 400°C

Neg 17420-25 250X

Fig. 44. U-9 w/o Mo-0.3 w/o Pt alloy, water quenched after 24 hr at 900°C, then annealed 35 days at 400°C

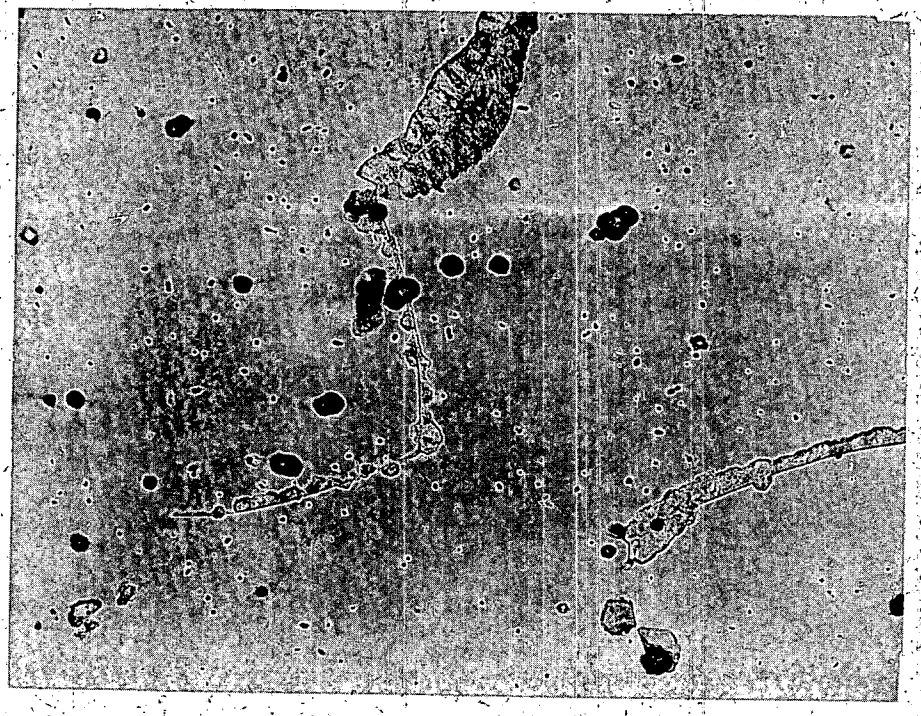

Neg 17420-43 250X

Fig. 45. U-9 w/o Mo-0.6 w/o Pt alloy, water quenched after 24 hr at 900°C, then annealed 35 days at 400°C

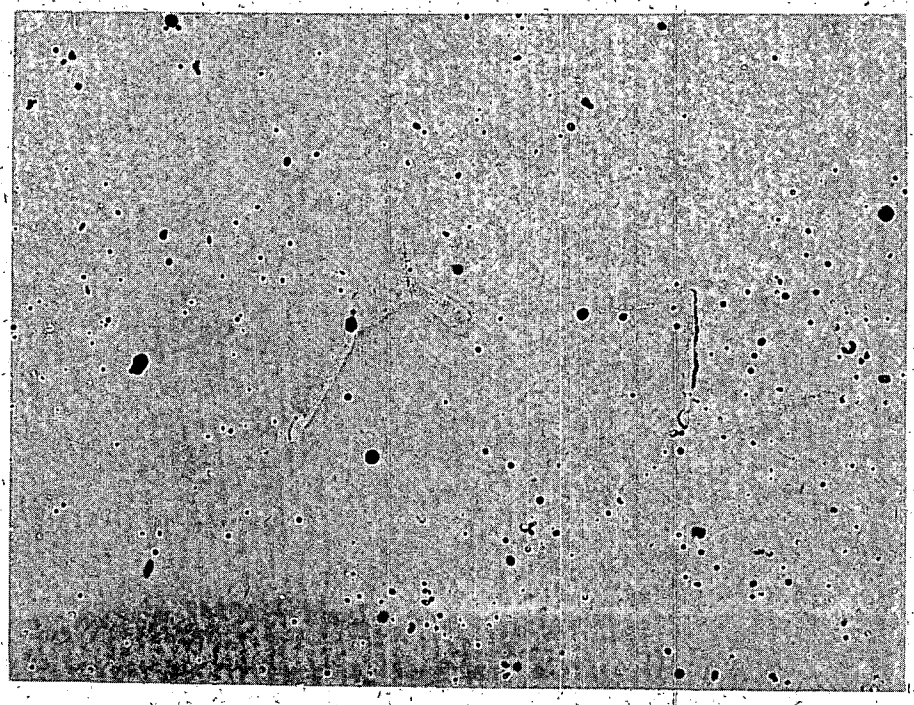

Neg 17420-40 250X

Fig. 46. U-9 w/o -1.2 w/o Pt alloy, water quenched after 24 hr at 900°C, then annealed 35 days at 400°C

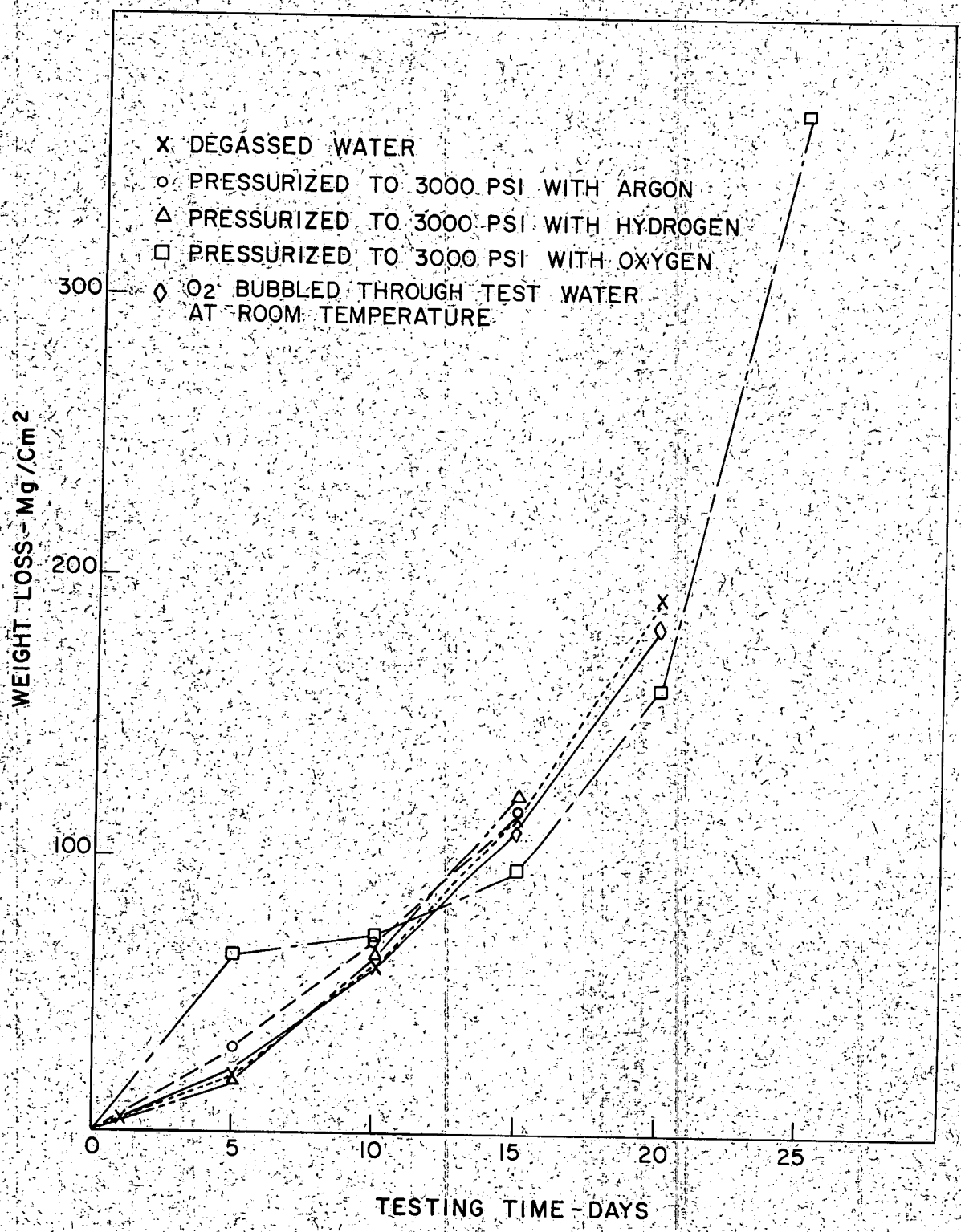

Fig. 47. The influence of gas additions to the test water on the corrosion properties of gamma-quenched U-12 w/o Mo
Neg 17421-17

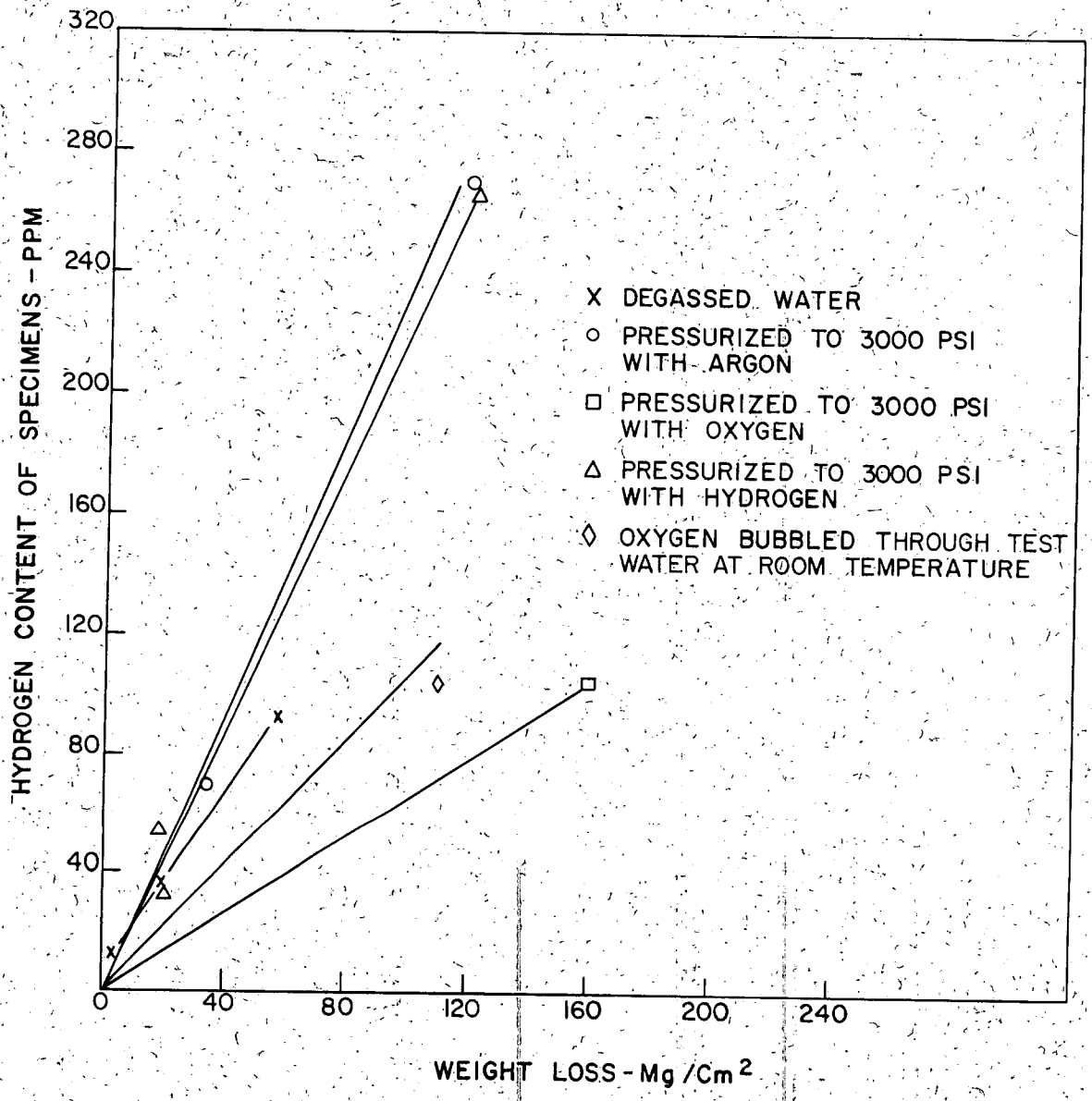

Fig. 48. The influence of gas additions to the test water on the hydrogen pickup of U-12 w/o specimens during corrosion

Neg 17421-9

UNCLASSIFIED

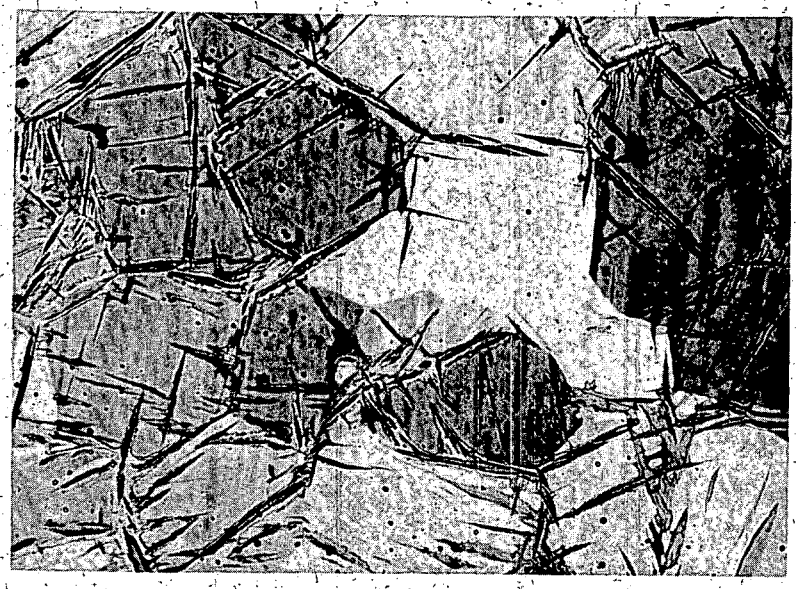

Neg 17420-7 250X

Fig. 49. U-12 w/o Mo alloy, corrosion tested 15 days in degassed water at 650°F

Neg 17420-41 250X

Fig. 50. U-12 w/o alloy, corrosion tested 15 days in 650°F water pressurized to 3000 psi with argon

UNCLASSIFIED

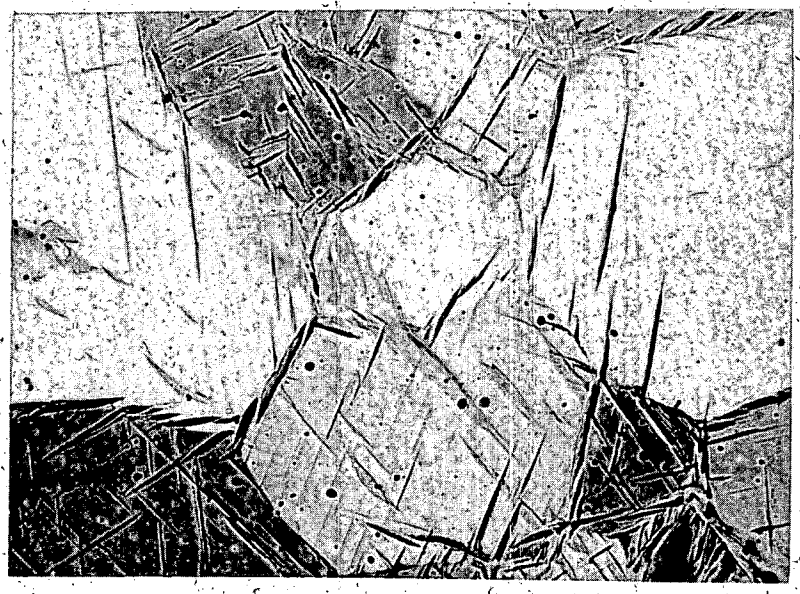

Neg 17420-8 250X

Fig. 51. U-12 w/o Mo alloy, corrosion tested 15 days in 650°F water pressurized to 3000 psi with hydrogen

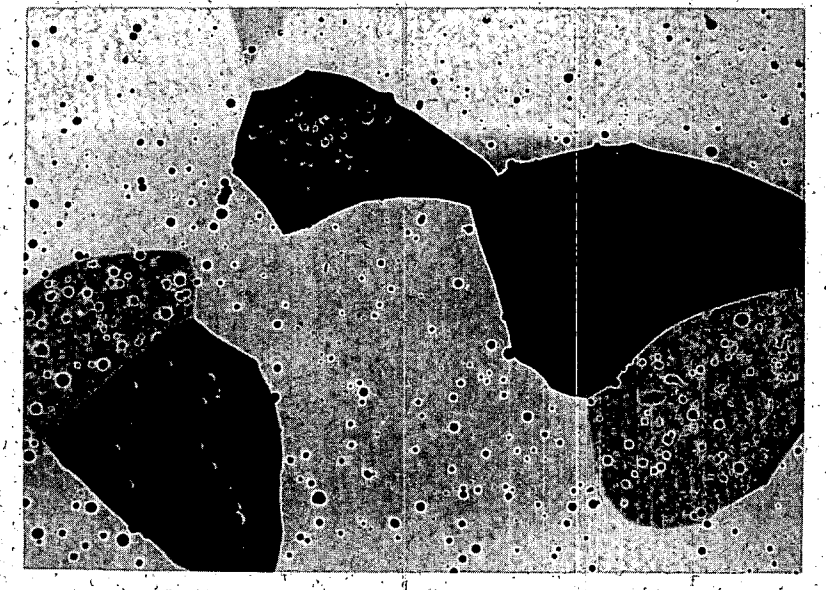

Neg 17420-20 250X

Fig. 52. U-12 w/o Mo alloy, corrosion tested 15 days in 650°F water pressurized to 3000 psi with oxygen

UNCLASSIFIED

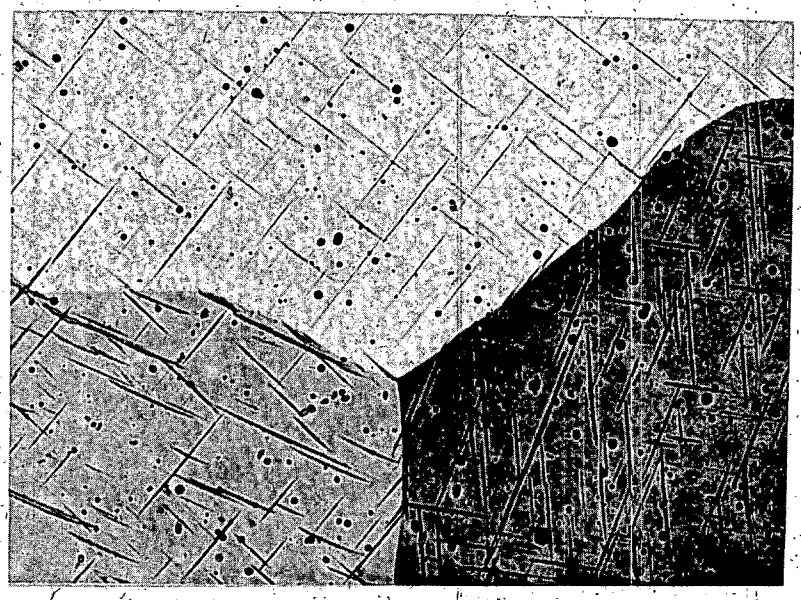

Neg 17420-30 250X

Fig. 53. U-12 w/o Mo alloy, corrosion tested 15 days in 650°F water through which oxygen was continually bubbled

DECLASSIFIED

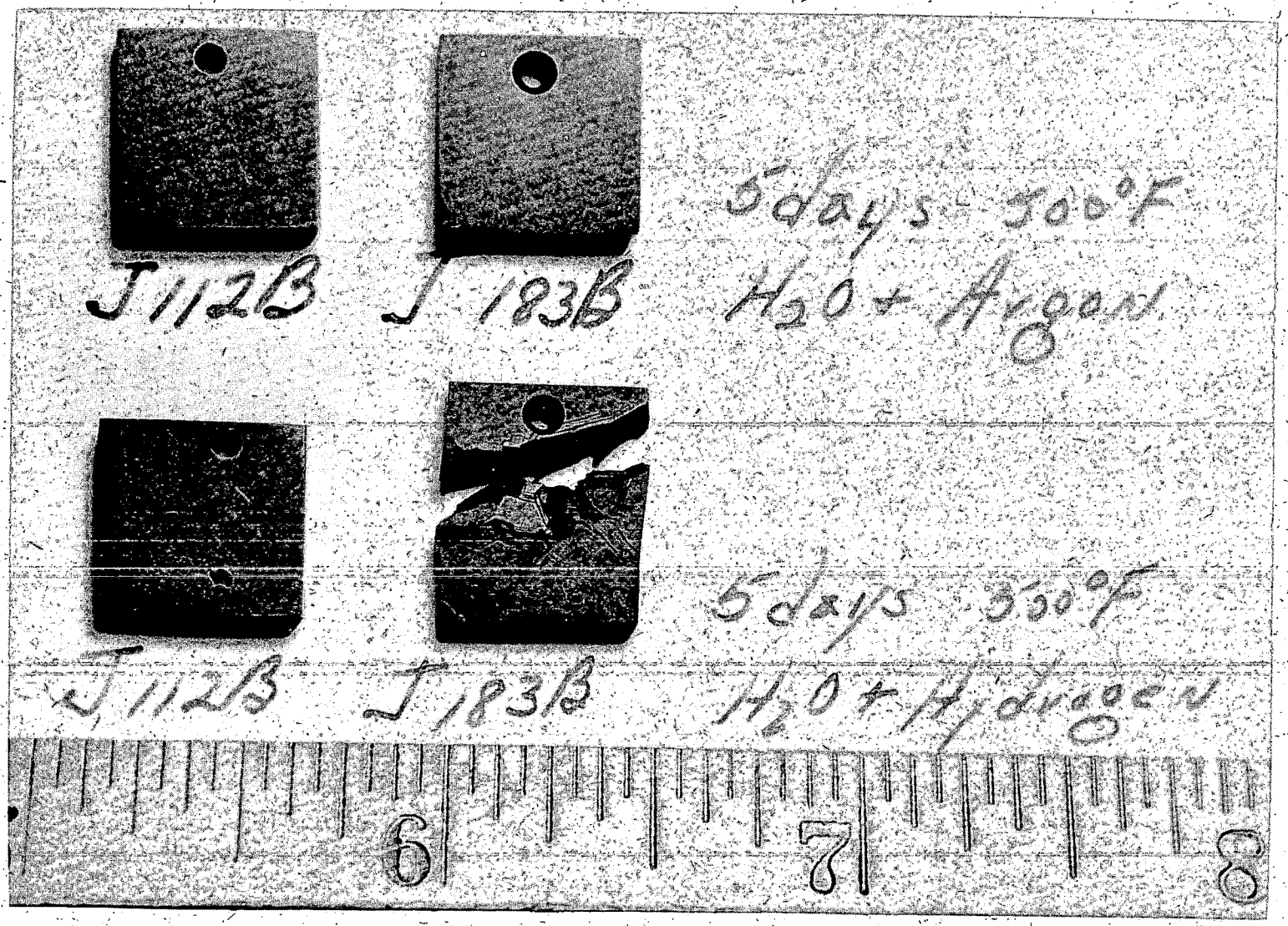

Fig. 54. The effect of hydrogen and argon additions to the test water on the corrosion of a U-4 w/o Nb alloy

Neg 17420-54

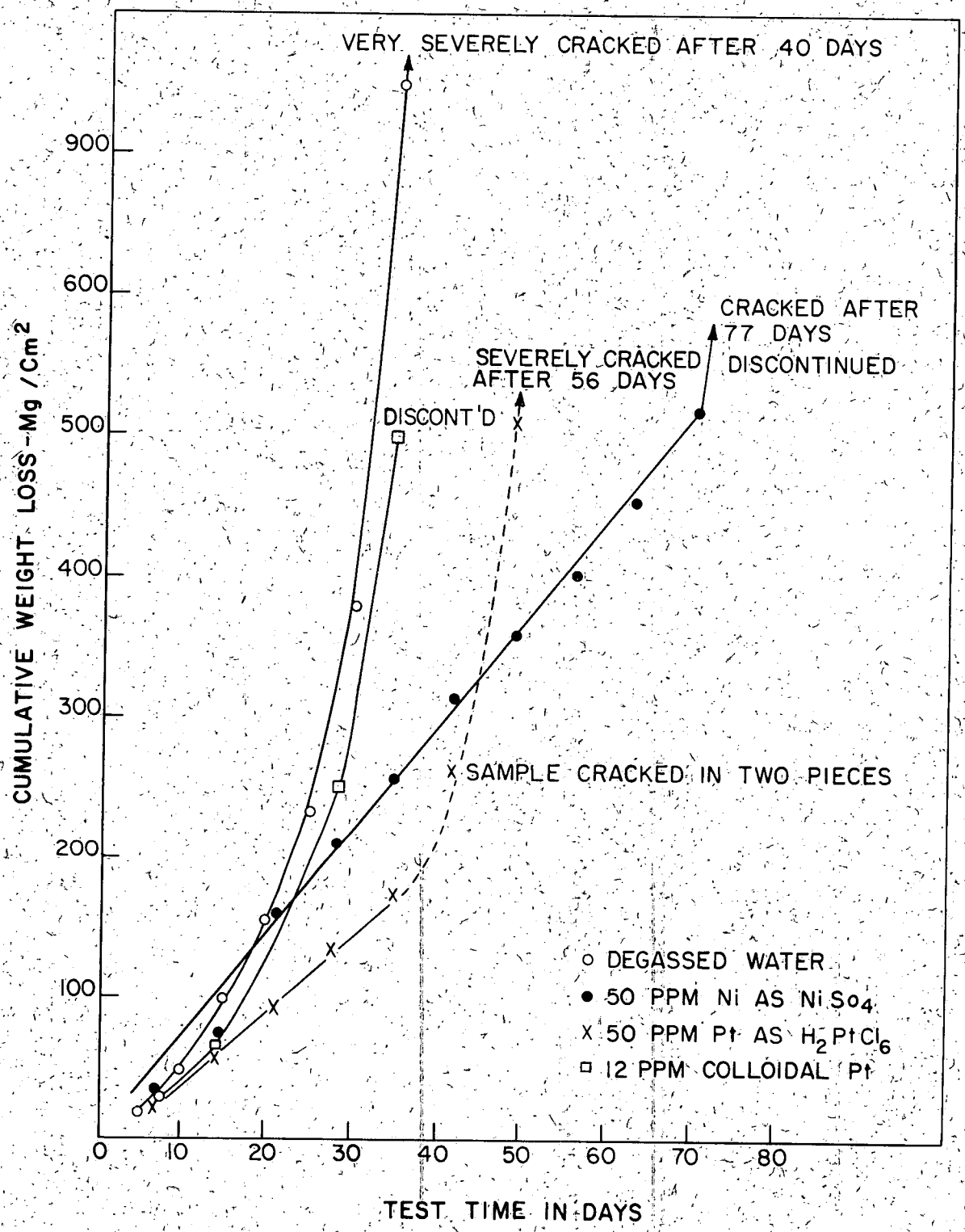

Fig. 55. The influence of water additions on the corrosion of U-12 w/o Mo at 650°F

Neg 17421-16

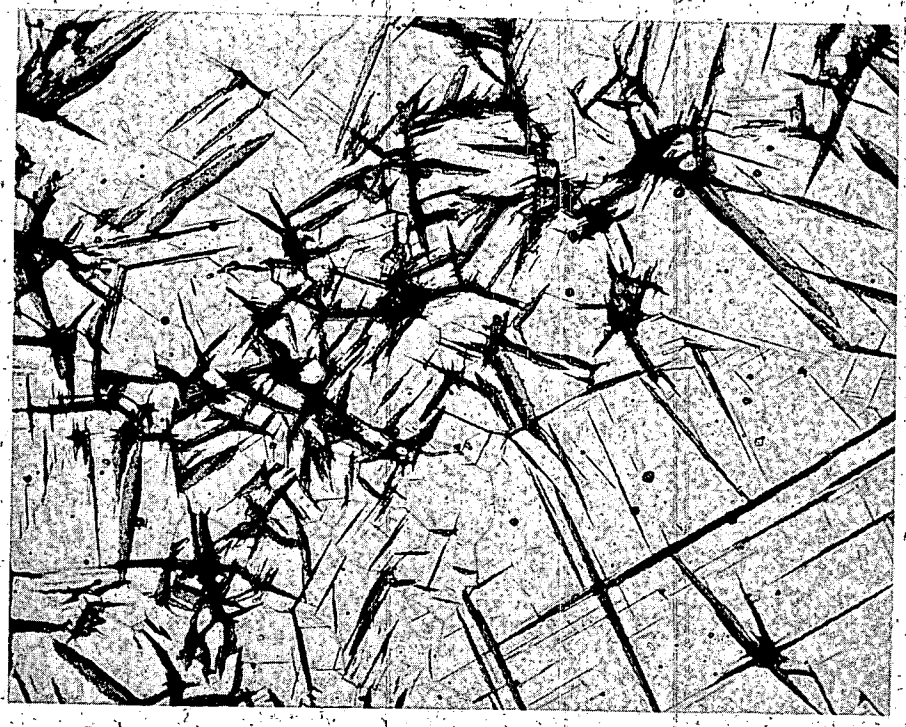

Neg 17420-2 250X

Fig. 56a. U-12 w/o Mo alloy, corrosion tested in 650°F degassed water

Neg 17420-17 250X

Fig. 56b. U-12 w/o Mo alloy, corrosion tested in 650°F water containing 10 ppm colloidal platinum

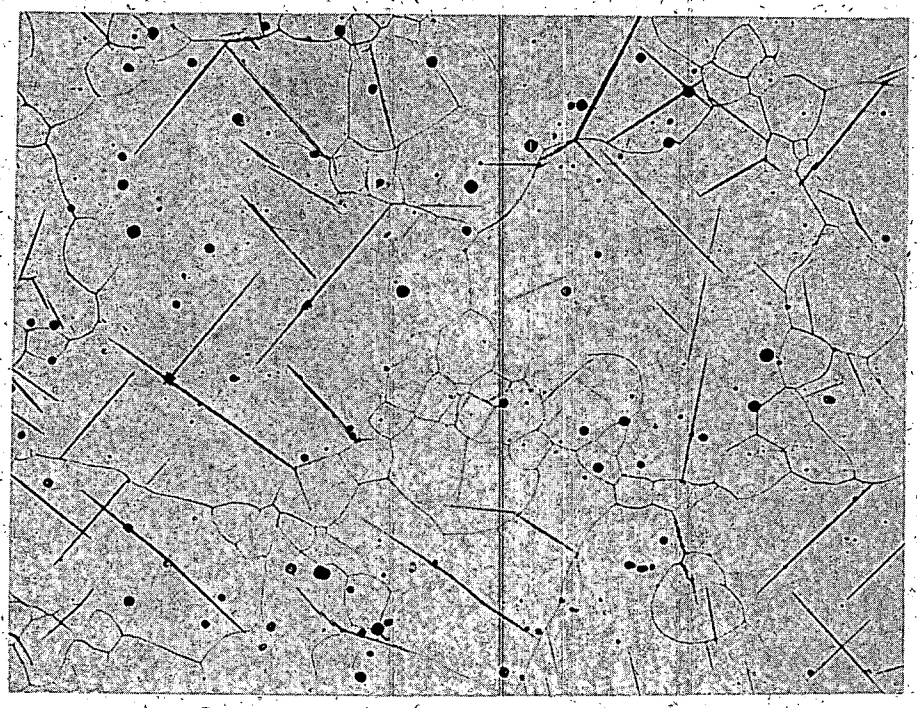

Neg 17420-46 250X

Fig. 56c. U-12 w/o Mo alloy, corrosion tested in 650°F water containing 50 ppm Ni as $NiSO_4$

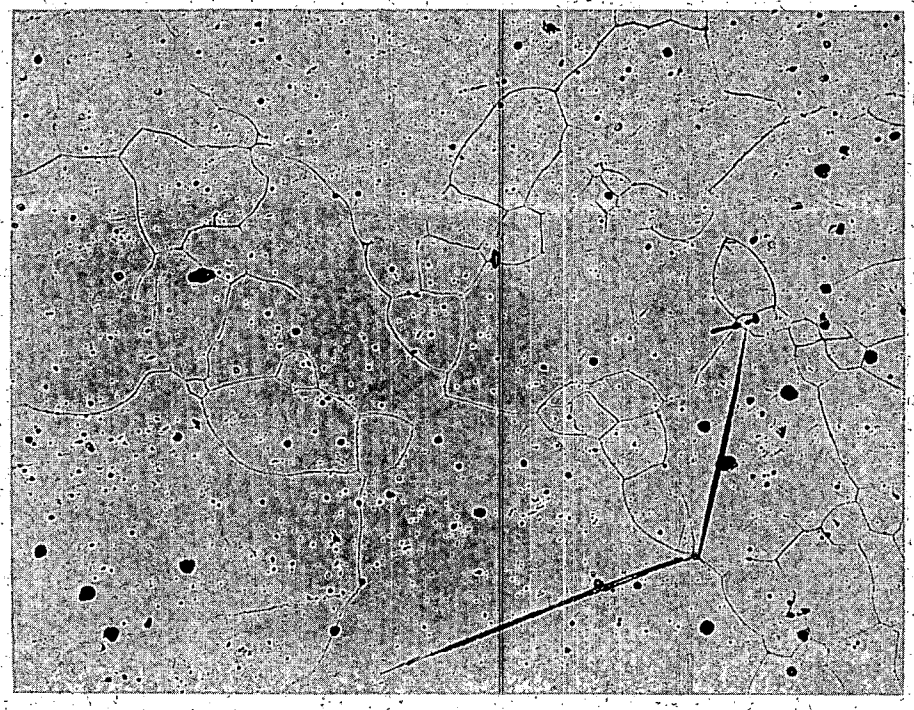

Neg 17420-36 250X

Fig. 56d. U-12 w o Mo alloy, corrosion tested in 650 F water containing 50 ppm Pt as H_2PtCl_6

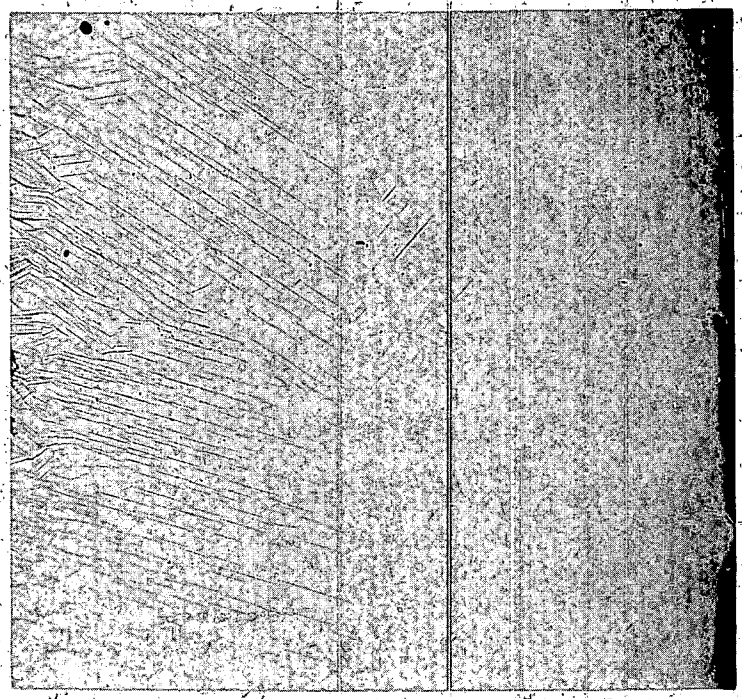

Neg 17420-28 50X

Fig. 57. Gamma-quenched U-10 w/o Mo alloy, cathodically hydrided 18 hr while stressed in bending. Note that plates form perpendicular to the direction of tensile stress.

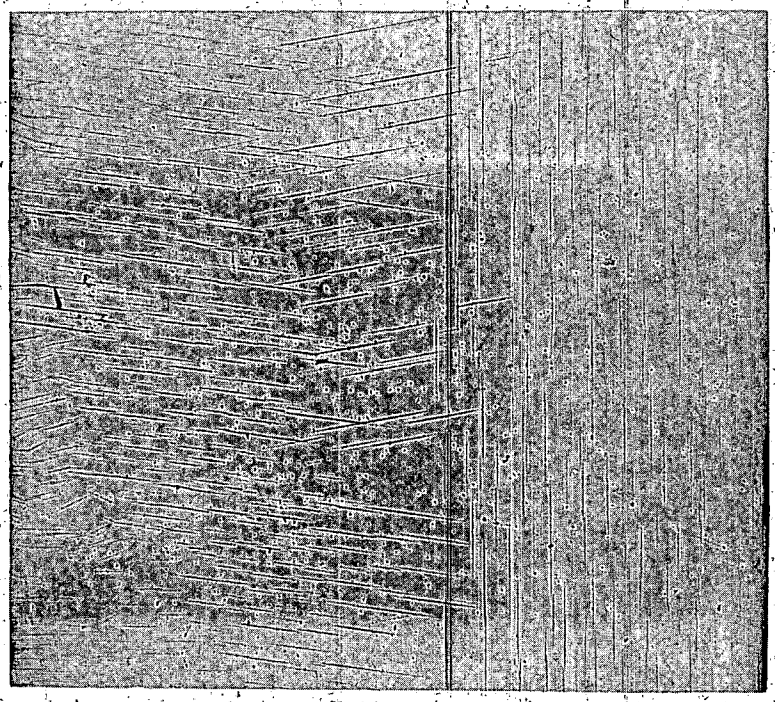

Neg 17420-12 50X

Fig. 58. Same specimen as shown in Fig. 57 after 54 hr. Note that plates have now formed on the compression side parallel to the direction of compressive stress.

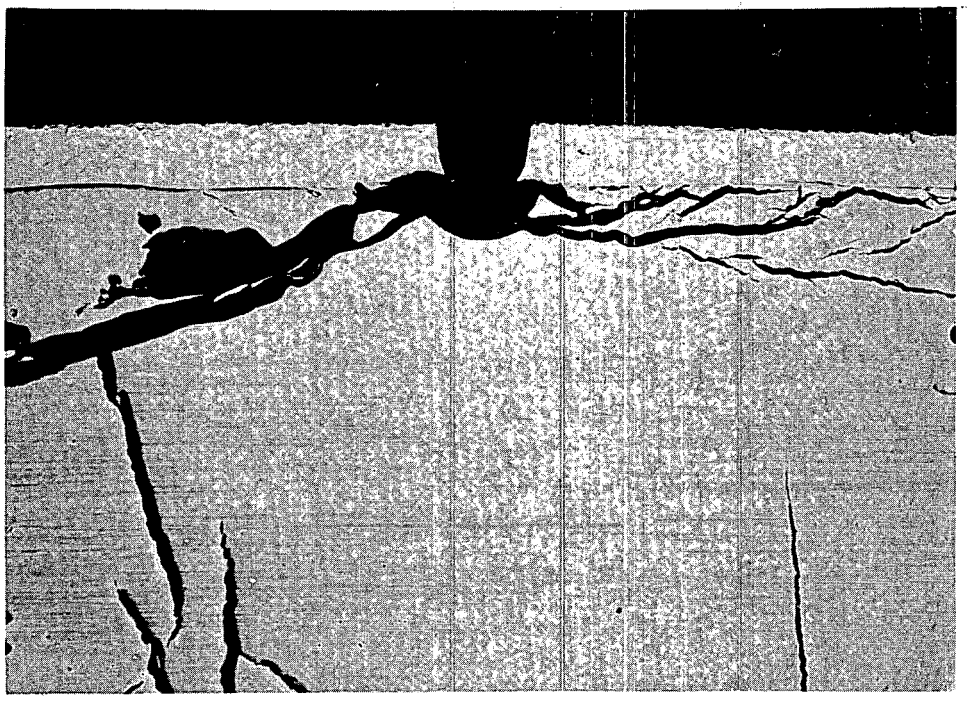

Neg 17420-26 13X

Fig. 59. Stressed Zircaloy-clad U-12 w/o Mo specimen, corrosion tested with cladding defect under tension

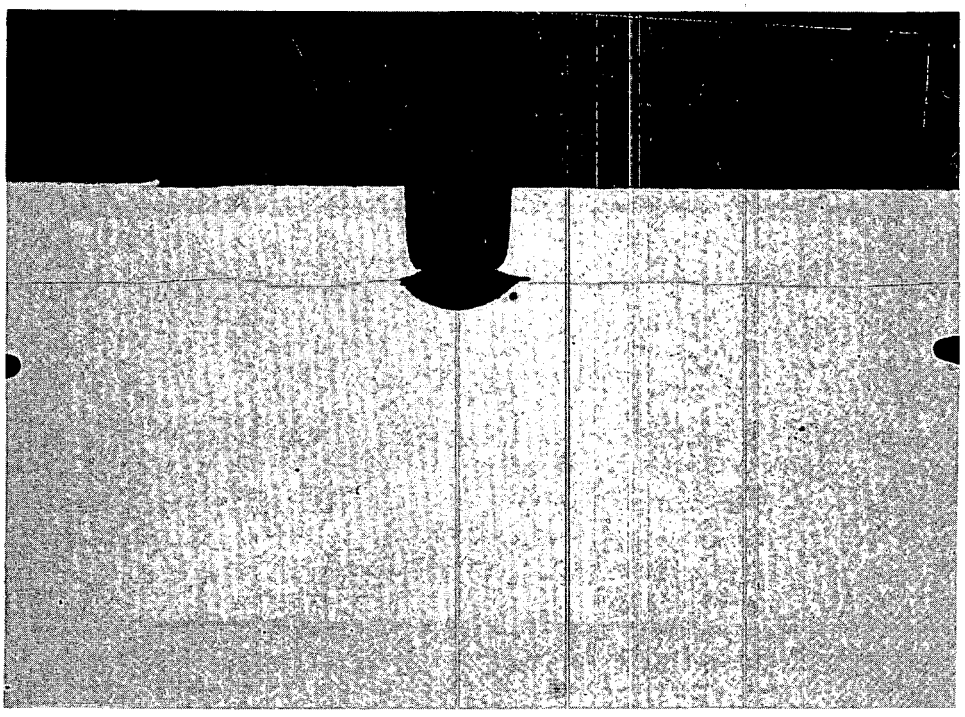

Neg 17420-47 13X

Fig. 60. Stressed Zircaloy-clad U-12 w/o Mo specimen, corrosion tested with cladding defect in compression

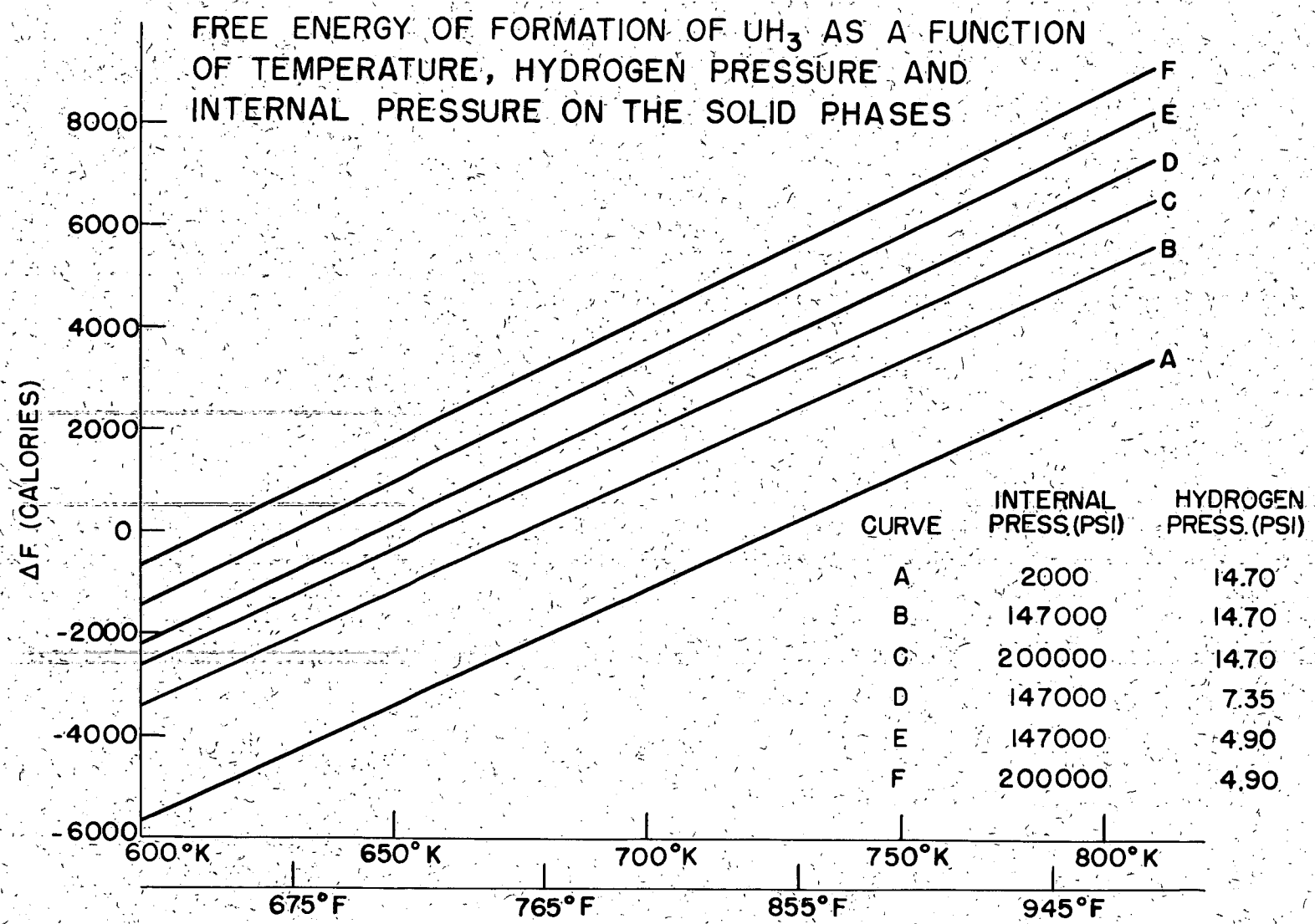

Fig. 61. Free energy of formation of UH_3 as a function of temperature, hydrogen pressure, and internal pressure on the solid phases

Neg 17421-20

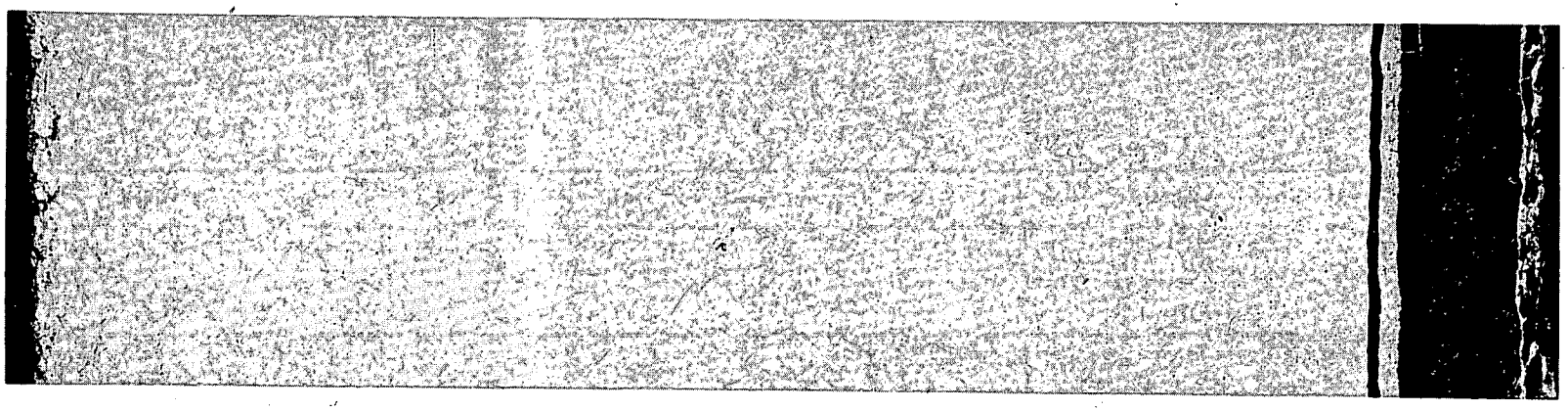

Neg 17420-52 50X

Fig. 62. Photomicrograph of a section just below the surface of a cathodically hydrided Zircaloy-clad specimen illustrating the hydrogen gettering ability of the cladding on the right

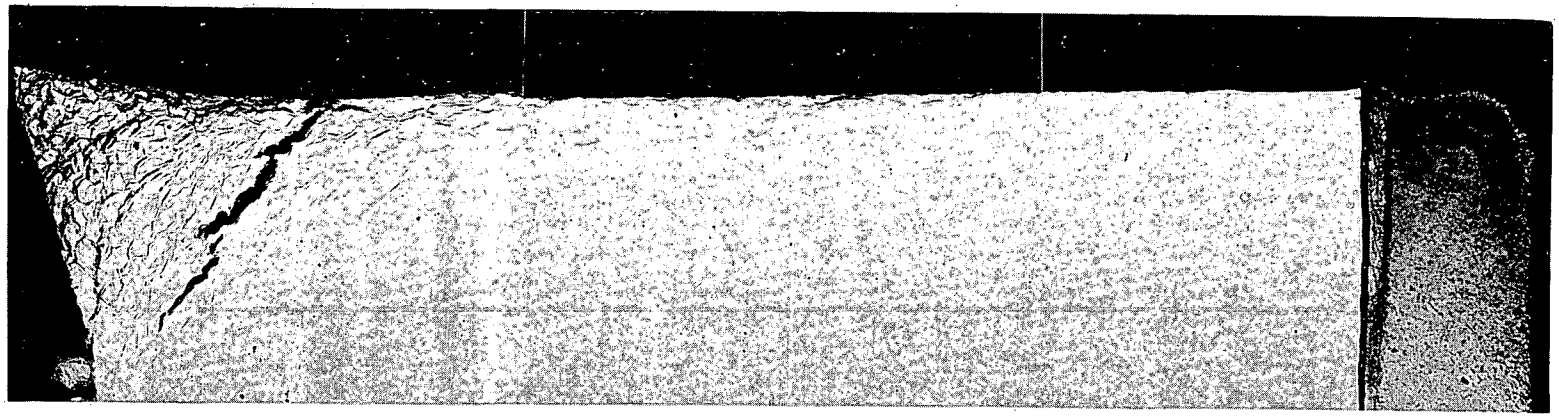

Neg 17420-53 50X

Fig. 63. Photomicrograph of the section perpendicular to that shown in Fig. 62

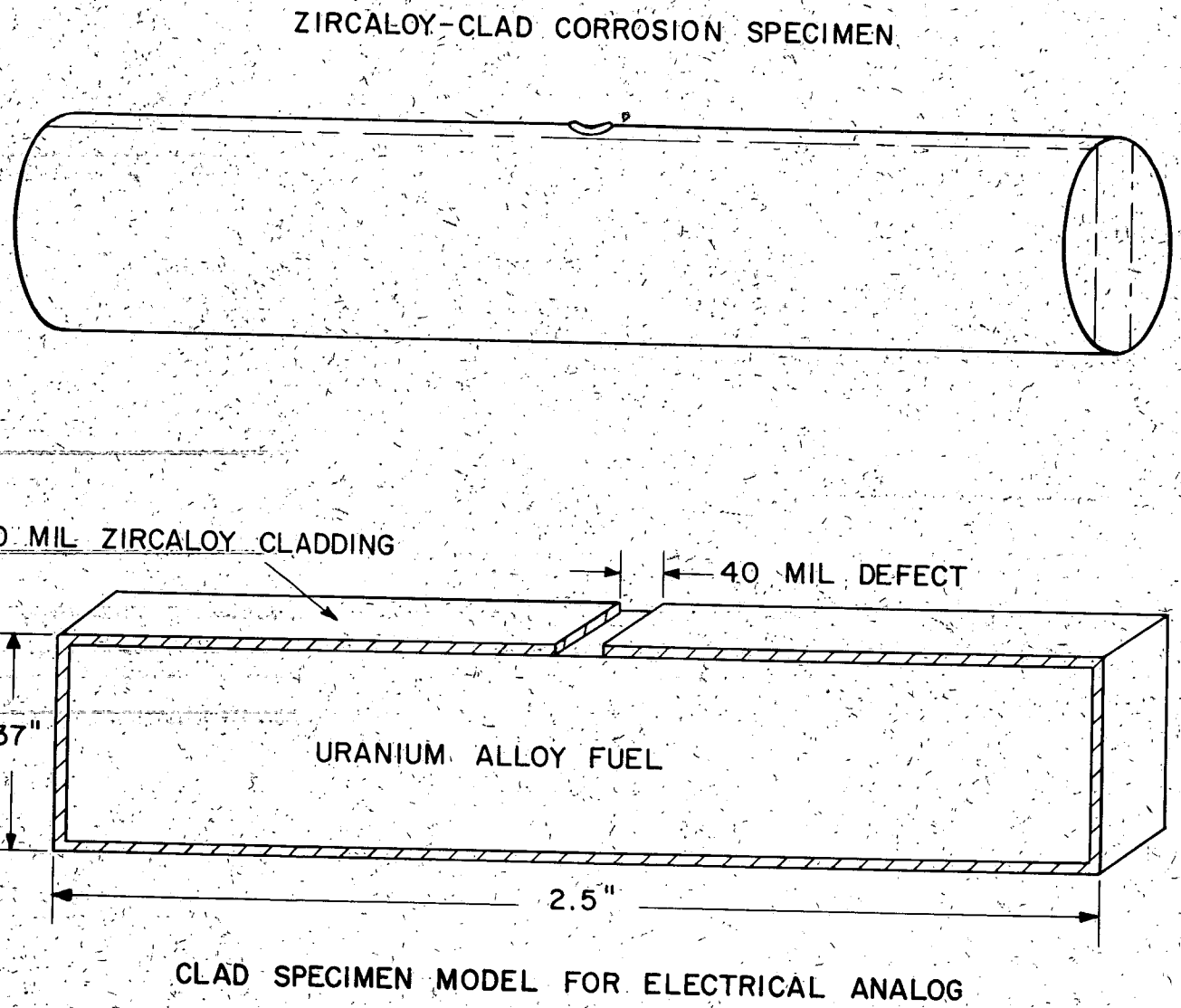

Fig. 64. Sketch illustrating section used to simulate a clad fuel rod with an electrical analog computor

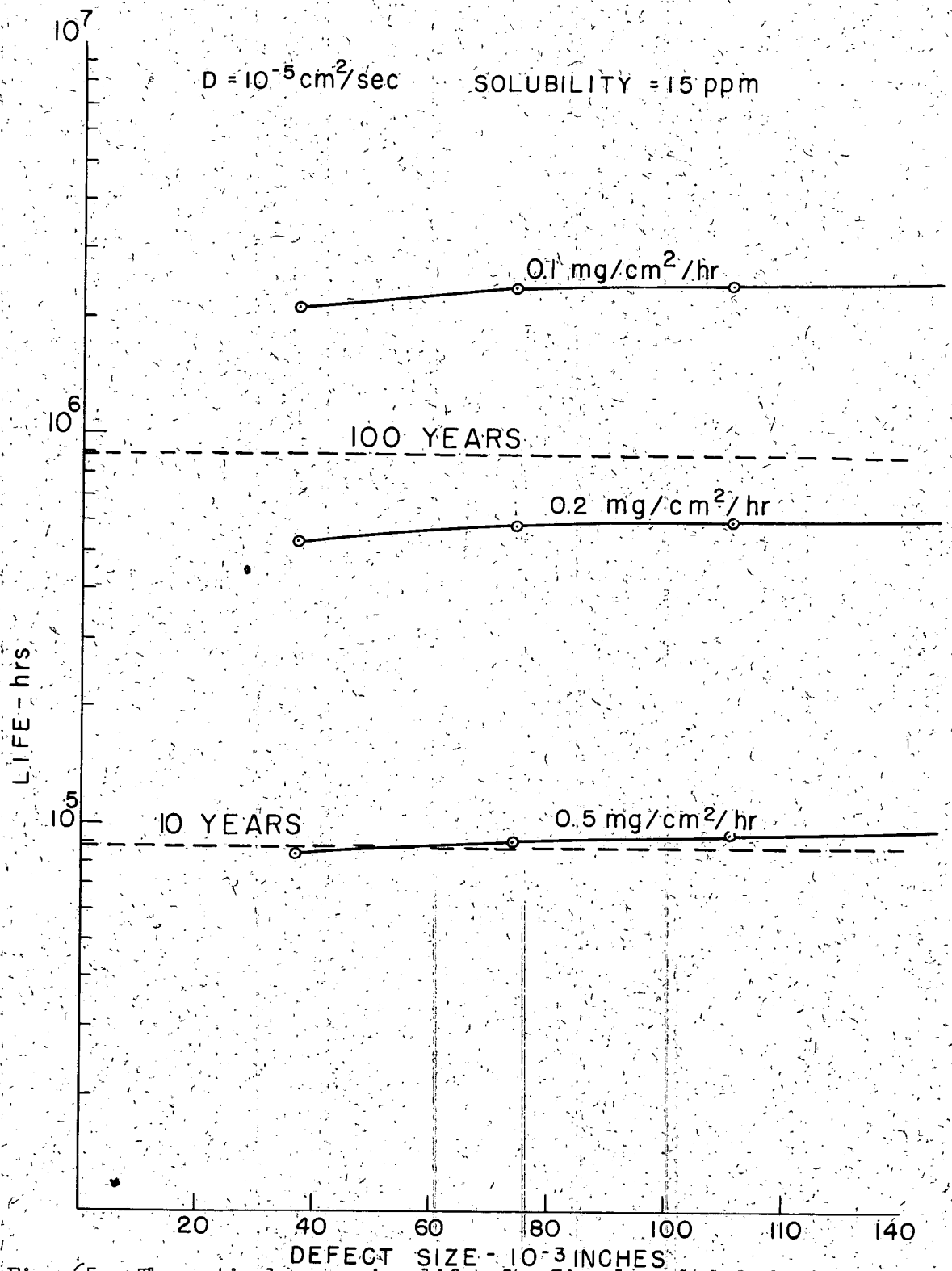

Fig. 65. Theoretical corrosion life of a Zircaloy-clad fuel element as a function of defect size and corrosion rate for a hydrogen diffusivity of D = 10^{-5} cm²/sec

Neg 17421-25

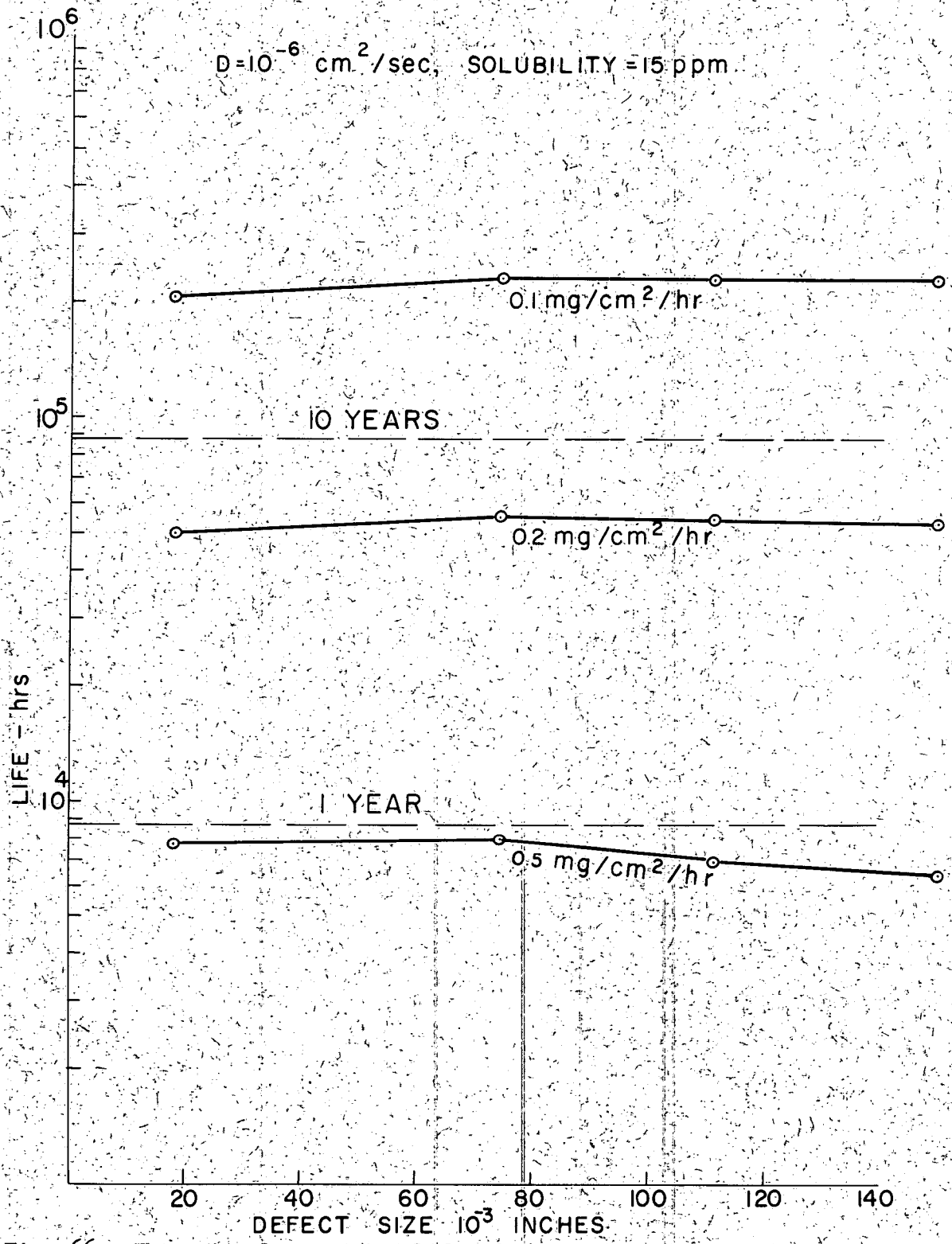

Fig. 66. Theoretical corrosion life of a Zircaloy-clad fuel element as a function of defect size and corrosion rate for a hydrogen diffusivity of $D = 10^{-6}$ cm^2/sec

Neg 17421-26

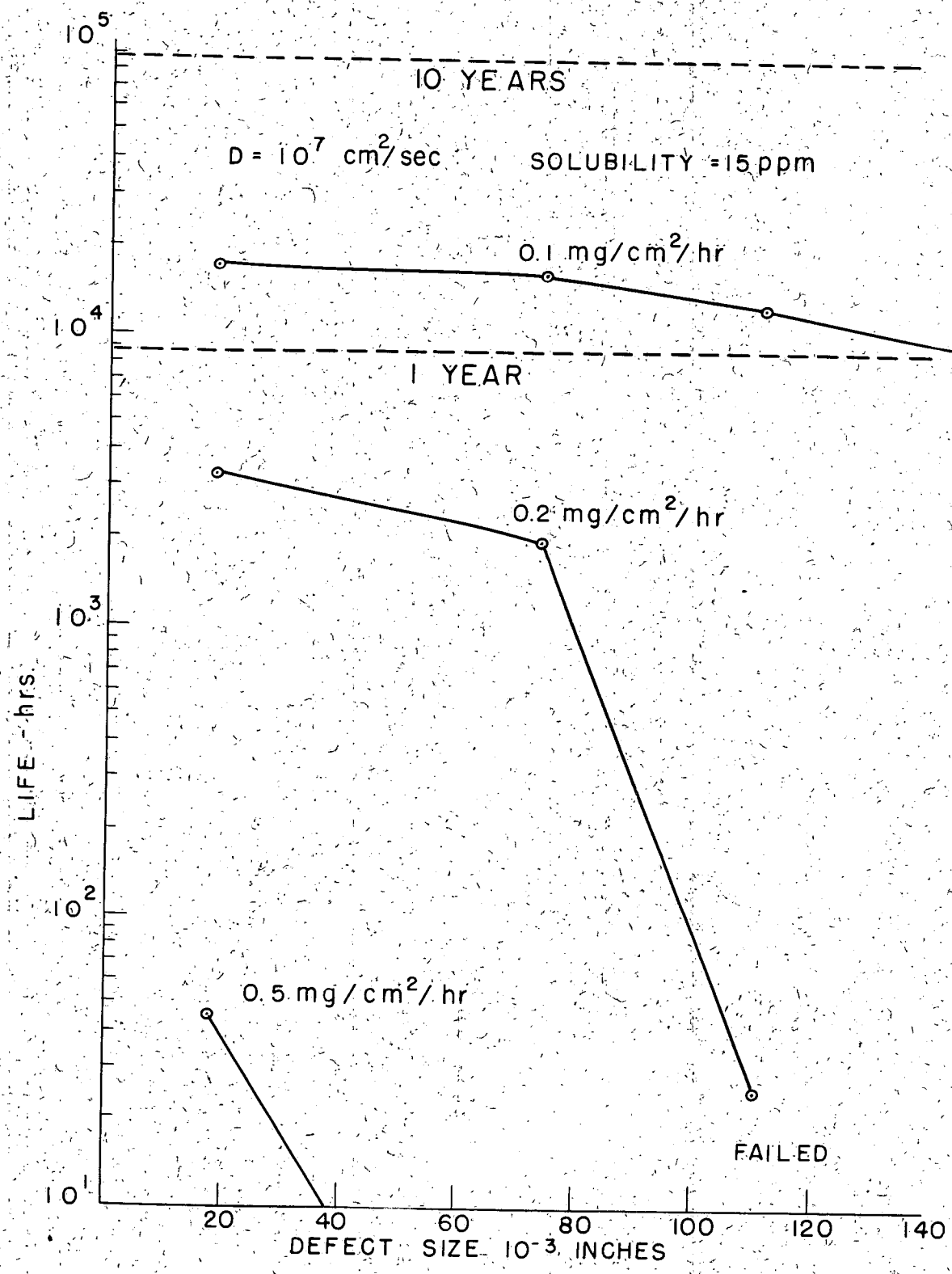

Fig. 67. Theoretical corrosion life of a Zircaloy-clad fuel element as a function of defect size and corrosion rate for a hydrogen diffusivity of $D = 10^{-7}$ cm^2/sec

Neg. 17421-4

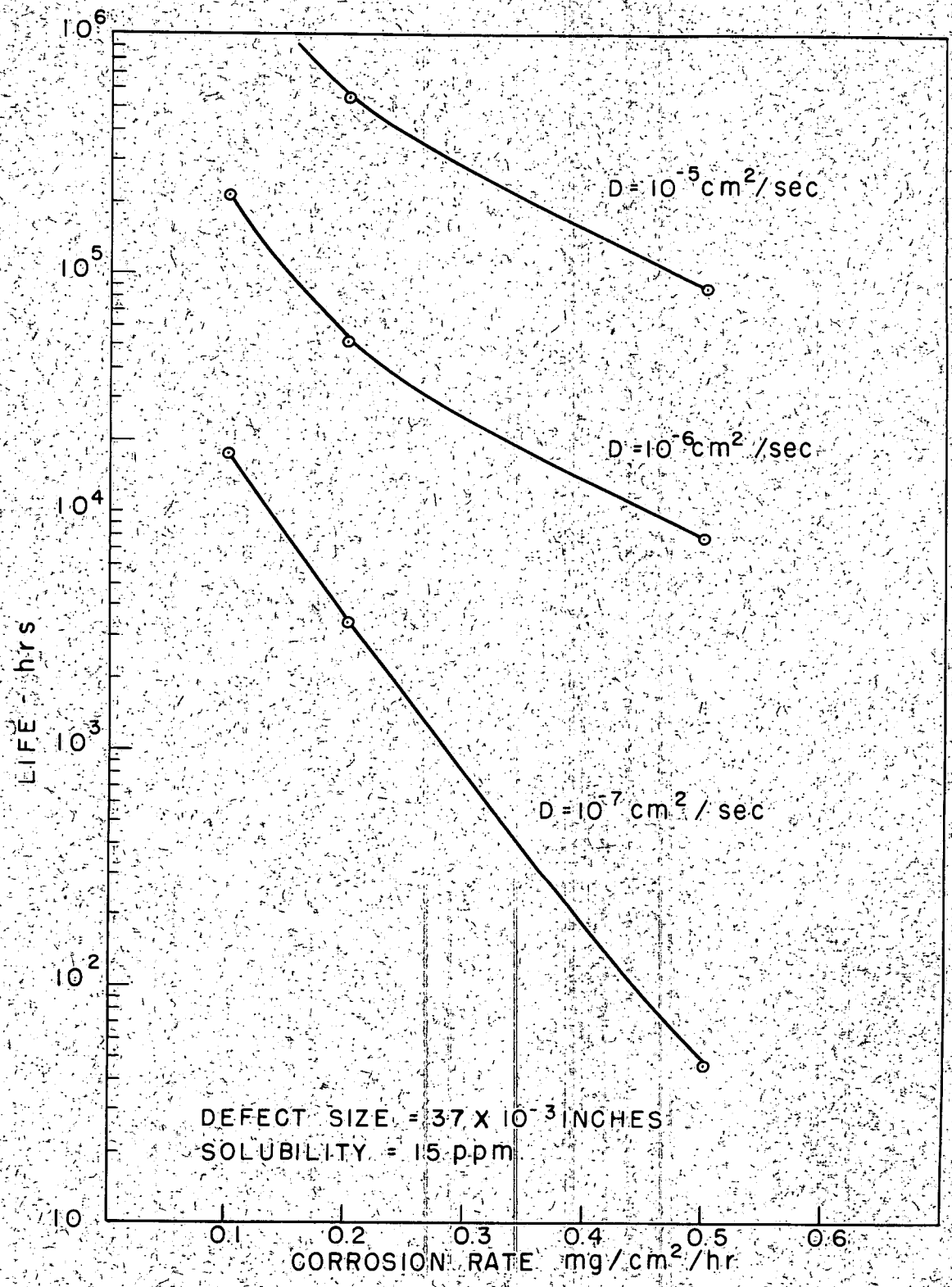

Fig. 68. Theoretical corrosion life of a Zircaloy-clad fuel element as a function of hydrogen diffusivity and corrosion rate
Neg 17421-3

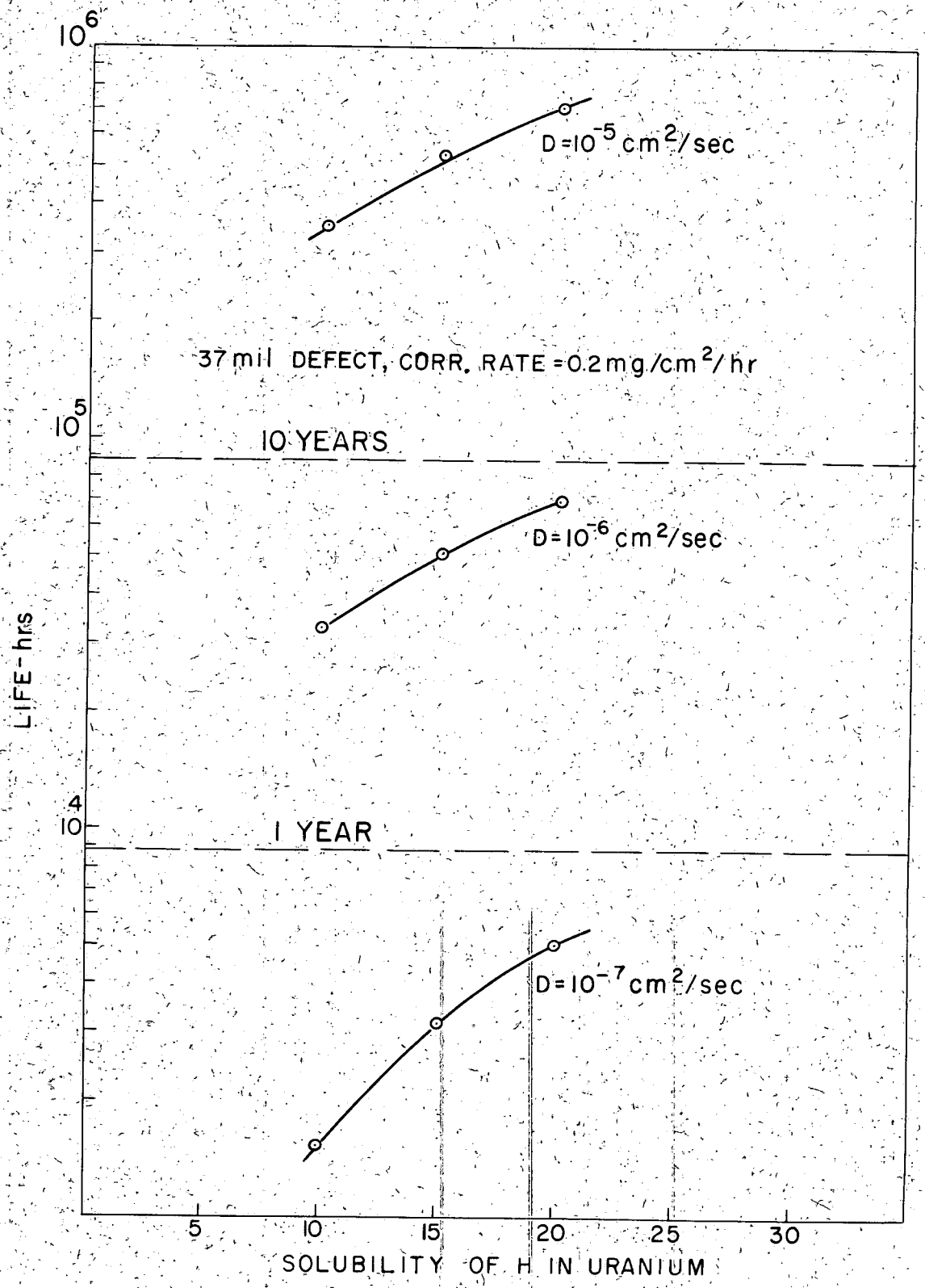

Fig. 69. The effect of hydrogen solubility upon the theoretical corrosion life of a Zircaloy-clad fuel element
Neg 17421-6

UNCLASSIFIED